109-008-7B55
MOTC-IOT-108-H2DA001h

水波時尺或時頻分析法之比較與應用 （2/4）

The Best Wavelet for Waves and Its Optimization— Wavelet Coherences versu Fourier Coherences

交 通 部 運 輸 研 究 所

中 華 民 國 109 年 2 月

109-008-7B55
MOTC-IOT-108-H2DA001h

水波時尺或時頻分析法之比較與應用 （2/4）

The Best Wavelet for Waves and Its Optimization— Wavelet Coherences versu Fourier Coherences

著 者：李勇榮

交通部運輸研究所

中華民國 109 年 2 月

國家圖書館出版品預行編目(CIP)資料

水波時尺或時頻分析法之比較與應用. (2/4) /
李勇榮著.-- 初版. --臺北市:交通部運研所,
民109.02
面 ; 公分
ISBN 978-986-531-087-5(平裝)

1.波動 2.數值分析

332.654 109000059

水波時尺或時頻分析法之比較與應用 (2/4)
The Best Wavelet for Water Waves and Its Optimization -- Wavelet Coherences versus Fourier Coherences
著 者：李勇榮
出版機關：交通部運輸研究所
地 址：台北市敦化北路 240 號
網 址：www.ihmt.gov.tw (中文版＞中心出版品)
電 話：(04)26587183
出版年月：中華民國 109 年 2 月
印 刷 者：
版(刷)次冊數：初版一刷 60 冊
本書同時登載於交通部運輸研究所港灣技術研究中心網站
定 價： 200 元
展 售 處：
交通部運輸研究所運輸資訊組•電話：(02)23496880
國家書店松江門市:10485 臺北市中山區松江路 209 號 F1•電話:(02) 25180207
五南文化廣場：40042 臺中市中山路 6 號•電話：(04)22260330

GPN：1010900160 ISBN：978-986-531-087-5(平裝)

109

水波時尺或時頻分析法之比較與應用(2/4)

交通部運輸研究所

GPN: 1010900160

定價:200 元

交通部運輸研究所自行研究計畫出版品摘要表

出版品名稱： 水波時尺或時頻分析法之比較與應用 （2/4）
The Best Wavelet for Water Waves and Its Optimization —
Wavelet Coherences versus Fourier Coherences

國際標準書號（或叢刊號）	政府出版品統一編號	運輸研究所出版品編號	計畫編號
ISBN: 978-986-531-087-5（平裝）	1010900160	109-008-7B55	108-H2DA001h

主辦單位：港灣技術研究中心
主管：蔡立宏
計劃主持人：李勇榮
研究人員：李勇榮
聯絡電話：04-26587183
傳真號碼：04-26571329

研究期間
自 108 年 01 月
至 108 年 12 月

關鍵詞：The Best Wavelet for Water Waves、Physical Optimization、Coherences

摘要：

本研究鑑取水波應用分析之最佳仔波函基，並探討其實際的物理優化，另以試驗水槽波流共關頻振現象充分驗証。此最佳仔波在離散領域是為半正交之樞點順適仔波；其在連續領域的對應仔波是為莫利仔波。此外我們亦將富立葉函基加入比較考量。此處所含蓋離散仔波函基類屬相當廣泛，具有函基屬性上的全面性或完整性含蓋。而鑑取手法，其統計方面取用多種熵值規範，多元性地比較熵值表現，並探討各類仔波轉換係數之累積機率密度函數。由這些比較，我們驗証此一最佳仔波表現除了遠較其它仔波突出，亦且明顯優於富立葉波譜函基者。再者，本研究進一步探討增進仔波分析與水波物理之真確相似性，透過連續仔波之載頻參數調適，應用變動時頻窗手法以模擬不同尺度水波演化情形。接著，我們比較使用這一最佳函基的仔波共關頻振與使用富立葉函基之波流共關頻振表現。由仔波共關頻振之絕對優越性足以驗証此處鑑取研究之目的。吾人深信： 至此，水波模擬之最適離散暨最適連續仔波已是定論。

出版日期	頁數	定價	本出版品取得方式
109 年 2 月	180	200	凡屬機密性出版品均不對外公開。普通性出版品，公營、公益機關團體及學校可函洽本所免費贈閱；私人及私營機關團體可按定價價購。

機密等級：
□限閱 □機密 □極機密 □絕對機密
（解密【限】條件：□ 年 月 日解密，□公布後解密，□附件抽存後解密，
□工作完成或會議終了時解密，□另行檢討後辦理解密）
■普通

備註：本研究之結論與建議不代表交通部之意見。

PUBLICATION ABSTRACTS OF RESEARCH PROJECTS
INSTITUTE OF TRANSPORTATION
MINISTRY OF TRANSPORTATION AND COMMUNICATIONS

TITLE:

The Best Wavelet for Water Waves and Its Optimization —

Wavelet Coherences versus Fourier Coherences

ISBN(OR ISSN)	GOVERNMENT PUBLICATIONS NUMBER	IOT SERIAL NUMBER	PROJECT NUMBER
978-986-531-087-5（pbk）	1010900160	109-008-7B55	108-H2DA001h

DIVISION: HARBOR & MARINE TECHNOLOGY CENTER
DIVISION DIRECTOR: Li-Hung Tsai
PRINCIPAL INVESTIGATOR: Yueon-Ron Lee
PROJECT STAFF: Yueon-Ron Lee
PHONE: 886-4-26587183
FAX: 886-4-26571329

PROJECT PERIOD
FROM Jan. 2019
TO Dec. 2019

KEY WORDS:
The Best Wavelet for Water Waves, Physical Optimization, Coherences

ABSTRACT:

The best wavelet, either in the discrete or in the continuous domain, for water wave simulations is named. The best basis in the discrete domain is the semi-orthogonal cardinal spline wavelet; the counterpart wavelet in the continuous domain is the Morlet wavelet. In the identification and verification processes, comprehensive basis categories of discrete wavelet groups are taken into account and inclusive entropy measures are adopted. In addition, cumulative probability distributions of transform coefficients of various wavelet groups are examined. Entropy statistics of transform coefficients under all criteria shows unambiguous jurisdiction for the comparisons; moreover, those statistics related to the Fourier basis is included in the comparisons. Results show the univocal superiority of the present best basis over any other bases, including the Fourier basis, for wind wave signals in the tank. Furthermore, the practical deficiency of the best wavelet regarding its energy description on water waves is illustrated and an optimization aiming for better physics is devised. Such a refinement is done through the adaptation of a carrier frequency parameter associated with wavelet time-frequency windows. At last, as a definitive proof of the present realization of the best basis, the wavelet coherences are compared to the Fourier spectral coherences for measurements of wave and aqueous flow fields in a wind-wave tank. The absolute superiority, as well as the outstanding and informative results, of wavelet coherences make the full vindication of the present study. It is believed that, concerning wavelets' applications to water waves, the best basis identified here is the last and ultimate word in wavelets.

DATE OF PUBLICATION	NUMBER OF PAGES	PRICE	CLASSIFICATION
Feb. 2020	180	200	□SECRET □CONFIDENTIAL ▪UNCLASSIFIED

The Best Wavelet for Water Waves and Its Optimization — Wavelet Coherences versus Fourier Coherences

Yueon-Ron Lee (李勇榮)

交通部運輸研究所港灣技術研究中心

ronlee@ms4.hinet.net

Revision: December 23, 2019
Printed: December 23, 2019

LIST OF CONTENTS

LIST OF FIGURES

LIST OF TABLES

ABSTRACT

The best wavelet, either in the discrete or in the continuous domain, for water wave simulations is named. The best basis in the discrete domain is the semi-orthogonal cardinal spline wavelet; the counterpart wavelet in the continuous domain is the Morlet wavelet. In the identification and verification processes, comprehensive basis categories of discrete wavelet groups are taken into account and inclusive entropy measures are adopted. In addition, cumulative probability distributions of transform coefficients of various wavelet groups are examined. Entropy statistics of transform coefficients under all criteria shows unambiguous jurisdiction for the comparisons; moreover, those statistics related to the Fourier basis is included in the comparisons. Results show the univocal superiority of the present best basis over any other bases, including the Fourier basis, for wind wave signals in the tank. Furthermore, the practical deficiency of the best wavelet regarding its energy description on water waves is illustrated and an optimization aiming for better physics is devised. Such a refinement is done through the adaptation of a carrier frequency parameter associated with wavelet time-frequency windows. At last, as a definitive proof of the present realization of the best basis, the wavelet coherences are compared to the Fourier spectral coherences for measurements of wave and aqueous flow fields in a wind-wave tank. The absolute superiority, as well as the outstanding and informative results, of wavelet coherences make the full vindication of the present study. It is believed that, concerning wavelets' applications to water waves, the best basis identified here is the last and ultimate word in wavelets.

摘要

本研究鑑取水波應用分析之最佳仔波函基，並探討其實際的物理優化，另以試驗水槽波流共關頻振現象充分驗証。此最佳仔波在離散領域是爲半正交之樞點順適仔波；其在連續領域的對應仔波是爲莫利仔波。此外我們亦將富立葉函基加入比較考量。此處所含蓋離散仔波函基類屬相當廣泛，具有函基屬性上的全面性或完整性含蓋。而鑑取手法，其統計方面取用多種熵值規範，多元性地比較熵值表現，並探討各類仔波轉換係數之累積機率密度函數。由這些比較，我們驗証此一最佳仔波表現除了遠較其它仔波突出，亦且明顯優於富立葉波譜函基者。再者，本研究進一步探討增進仔波分析與水波物理之眞確相似性，透過連續仔波之載頻參數調適，應用變動時頻窗手法以模擬不同尺度水波演化情形。接著，我們比較使用這一最佳函基的仔波共關頻振與使用富立葉函基之波流共關頻振表現。由仔波共關頻振之絕對優越性足以驗証此處鑑取研究之目的。吾人深信：至此，水波模擬之最適離散暨最適連續仔波已是定論。

Chapter 1

Introduction

1.1 Background

In wavelet's applications to water wave physics, it is quite often seen that a specific function basis is adopted for no reason at all. The results thus yielded are destined to be inconclusive and problematic, or even misleading and erroneous — mathematics does not need to be liable to physics. Mathematics provides the tools without any precondition while physics needs proper instrumentation and should be reasonable. Moreover, the usefulness of a particular data analysis methodology is highly case dependent; there simply exists neither a full-fledged analyzing function basis nor an all-purpose numerical scheme for all sorts of signals and applications.

Chronically, from the somewhat traditional and well established spectral perspective to the more recent wavelet viewpoints, we have the following instrumentations:

- Fourier transform;
- Short time Fourier transform or windowed Fourier transform;
- The Gabor's analytical signal procedure and the relevant Hilbert transform;
- Various time-frequency transforms associated with individual distributions or kernels, such as Wigner Distribution, Page distribution, Choi-Williams distribution, etc. [9];

- The continuous wavelet transform or the integral wavelet transform;

- The discrete wavelet transform.

It is noted that, unlike the discrete and continuous Fourier transforms, which are basically identical in both function bases and formulations, the discrete wavelet transform and the continuous wavelet transform are two essentially different categories with regard to the following two aspects. First, they generally use completely different function bases; Second, they involve relatively quite independent mathematical formulations.

In the following descriptions let assume the analytical target to be a one-dimensional time series signal and let outline the most basic attributes for individual analytical methodologies.

The Fourier transform yields another one-dimensional data in frequency domain. The transform correspondence is one to one. And the correspondence is a time domain variable to a frequency one.

For short time Fourier transform, it yields somewhat localized frequency contents by capping the signal with a window. And, when the capping window is shifted along the time line, it provides time-dependent spectral information. Through such multiple processes the transform correspondence is from the one dimensional time variable to the two dimensional time and frequency variables.

For Gabor's analytical signal procedure, it is based upon the Hilbert transform, which is basically the inverse Fourier transform of a one-sided spectrum that is formed through the chopping off the part of negative frequency. here the independent variable in the two corresponding transform domains is both time. And the procedure yields instantaneous frequency distribution and amplitude envelop curve along the time line [9, 17]. Ideally, the instantaneous frequency and amplitude should be independent with each other (since they are of two completely different physical units) but in reality they are intertwined and sometimes twine in an unimaginable way. Moreover, the interaction is extremely serious when the relative rate of variation of amplitude is significant. And the symptoms intro-

duced here manifest its Fourier transform relevance. Thusly, insurmountable uncertainty involved is always a concern [17].

As for various time-frequency transforms associated with individual distributions (or kernels), they also provide time-varying frequency contents that are conceptually identical to the short time Fourier transform, except that the involved analyzing kernels are related to individual distribution kernels rather than the Fourier kernel of short time Fourier transform. For these transforms they always have their individual pros and cons; none is perfect.

For the discrete wavelet transforms, a one-dimensional time series yields directly another one-dimensional coefficient series that contains the information that covers both "time" and "scale". The correspondence is one independent variable to a variable that mixes two independent variables into one in one transform process. But here, for almost all of the discrete wavelets, the "scale" is generally quite different from the sinusoidal frequency and normally not even possible to be assigned to a "representative frequency". And this causes tremendous difficulties in physics apprehension. Besides, we rarely see a complex discrete wavelet in water wave applications. The dual-tree complex discrete wavelet transform may still provide a quantity different from the general concept of sinusoidal "frequency".

As to the continuous wavelet transform, the one-dimensional time series yields two-dimensional coefficients that contain information varying both in time and in scale. But now, due to its loosen theoretical requirement and hence its flexibility in design, it is possible to bring in a physically meaningful "representative frequency" rather than just "scale". The numerical implementation is a multi-process scheme conceptually similar to the short time Fourier transform, except its core differences in the design of the capping windows of varying sizes and its better localization for the fulfillment of the requirement of the wavelet "resolution of identity". Again, every time point has a component scale distribution and every scale may play a role at a specific time.

1.2 Local and transient effects

It is well known that Fourier transform is suitable for characterizing stationary signals and not quite satisfactory for analyzing transient local phenomena. The reasons can be illustrated by the following properties of the transform.

- Any Function cannot be both time- and band-limited. If a function is limited (finitely supported) in one domain, then the independent variable of its corresponding function in the other domain stretches the entire real line (**R**). In real world situations, however, signals are almost always limited in time and space; meanwhile, hardware's capability is generally band-limited. This simply implies that there is not going to be a function basis that perfectly matches theory to practice. A slight variation of the Fourier transform is the short time Fourier transform, which is just the Fourier transform of the windowed signal, i.e., the original signal capped with or multiplied by a window function. In short time Fourier transform this property of mutual exclusivity in time and frequency localizations is indicated by the Balian-Low theorem, which basically states that if the window function $g(t)$ of a Gabor type frame

$$g_{m,n}(t) = e^{-2\pi imt} g(t-n), \tag{1.1}$$

  in which $m, n \in \mathbf{Z}$, is well localized in time, then the associated Fourier transform window can not be well localized in frequency. The point here sounds a bit abstract, but, in reality, this is conceptually equivalent to the following points.

- The Gibbs phenomenon states that, if there is a jump in signal, then the overshoots, occurring at both sides of the discontinuity when the inverse Fourier transform is implemented, can never disappear and remain at constant. This amounts to say that it takes quite many a spectral component to make up a sharp transient feature and that a local variation affects a broad range of the spectrum just as the Fourier transform of the delta function (more precisely, delta distribution) covers the whole

frequency axis.

- Fourier basis functions are periodic and extend bi-infinitely; signals thus studied are better to be periodic and sampled infinitely. The unavoidable side effects for not fulfilling these requirements are many: frequency leakages, smoothing errors, edge effects due to data truncations, aliasing due to under-sampling or non-periodicity (figure 1.1 (TFW–WP BB) is actually a case of under-sampling, where a linear chirp is sampled at a rate half of the Nyquist frequency), and, uncontrollable spectral variance due to the finite resolution or histogram processing.

Overall, the syndromes associated with the above listed items can be referred to the non-stationary effects.

1.3 Windowed transforms

Except the fourier transform all the transforms mentioned in the preceding section can be classified as a form of windowed transform (either in time or in frequency).

Both short-time Fourier transform and wavelet transform try to remedy Fourier basis's deficiencies in characterizing transient phenomena by analyzing the set of localized signals. For the short time Fourier transform this can easily be executed by varying m and n in equation 1.1. For the wavelet transform this can be illustrated through the use of the Morlet wavelet by varying its translation and dilation variables.

Both transforms yield local spectral information – more precisely, local scale information, if the term "frequency", "Hz", or "spectrum" is strictly reserved for sinusoidal functions. However, due to the Balian-Low theorem mentioned above, the waveform associated with short time Fourier transform can never be truly local in time since in reality the frequency domain of discrete Fourier transform is always band-limited by obeying the Nyquist law. In this regard, wavelets can be of exactly local; at least, they must have suitable or better decaying property such that they contain no zero-frequency component.

Let us further outline a few specific properties pertaining to individual transform:

- Both short time Fourier transform and wavelet transform are windowed transforms. In short time Fourier transform there exist two quite distinctive operations. The first operation is applying a suitable time-window to the signal; the second operation is performing the Fourier transform for the capped signal. The corresponding inverse transform (or reconstruction process) of the short time Fourier transform is naturally associated with a frequency-window and involves two similar distinctive operations too. However, in wavelet transform these two distinctive steps are not clearly observable — rather than using the very distinctive "window (either time- or frequency-window)" and "Fourier basis function (i.e., sine or cosine function)", the "window" and the "basis function" are synthesized in an inseparable specific form called "wavelet". In fact, one can clearly solidify this notion by comparing the Gabor type frame (equation 1.1) with the Morlet wavelet when the window function $g(t)$ of equation 1.1 is assumed to be a Gaussian bell. The intention for either the combined operation or synthesized operation is completely the same: to provide a mechanism (or kernel) for projecting a signal into modulated or oscillating wave constituents.

- The time-frequency windows in short time Fourier transform keep rigid for different scales since the window function $g(t)$ in Equation 1.1 does not depend on m, i.e., their widths (usually referring to time) and heights (usually referring to frequency) do not change for all frequencies. In wavelet transform, the windows are adjusted to different scales, but the sizes (or areas) of different windows are still fixed, i.e., each window's height and width are inversely proportional and the product remains constant (either for discrete wavelet transform or continuous wavelet transform). The concept of fixed size windows is illustrated by the fixed area of the gray blocks in the phase planes shown in figures 1.1 (TFW–WP BB) and 1.2 (TFW–WP BL), where the discrete wavelet packet transforms are performed for a chirp signal using different bases originating from the same seeding mother wavelet. In the figures, since the bases are orthonormal, all time-frequency windows do not overlap. As for the con-

tinuous wavelet transform, various time-frequency windows severely tangle with each others. And we generally do not show the actual sizes and shapes of various windows — rather, each window is represented by a point (or a small area depicting the time-frequency resolution) having coordinates corresponding to its centroids in the time and frequency axes.

- The function basis of the short time Fourier transform is the unique orthonormal Fourier basis comprised of sine and cosine functions; whereas, for wavelet transform, apart from the very loose constrain that the basis function (or the mother wavelet) satisfies the admissibility condition (for continuous wavelet transform) or stability condition (for discrete wavelet transform), there is virtually no restriction on the choice of basis functions. The coefficients of short time Fourier transform, which represent local Fourier spectral information, still have the exact meaning of "frequency". In wavelet transform, wavelet coefficients refer to specific scales rather than "frequencies". Here, we generally suffer from their physical interpretability due to the following reasons: (1) No unique basis — the analyzing function or mother wavelet can be designed in a plenty of ways, and the basis functions related to the mother wavelet can be either dependent or independent (orthogonal or non-orthogonal); (2) Scale does not have unit — together with the first point, it severely hampers out ability to directly perceive the wavelet's size and physical shape; and, (3) No fixed algorithm to implement wavelet transform — many techniques and various adaptations exist, such as, the treatment using flexible time-frequency windows for continuous wavelet transform [16], multi-voice [12] or multi-wavelet [10, 11, 33] frames, and discrete wavelet transform using different dilation factors other than the most often seen value of 2 [3]. Generally speaking, these varieties may not be as disturbing in certain application fields (such as data transmission or signal decomposition and reconstruction) as they are for our studies focusing on the water wave physics.

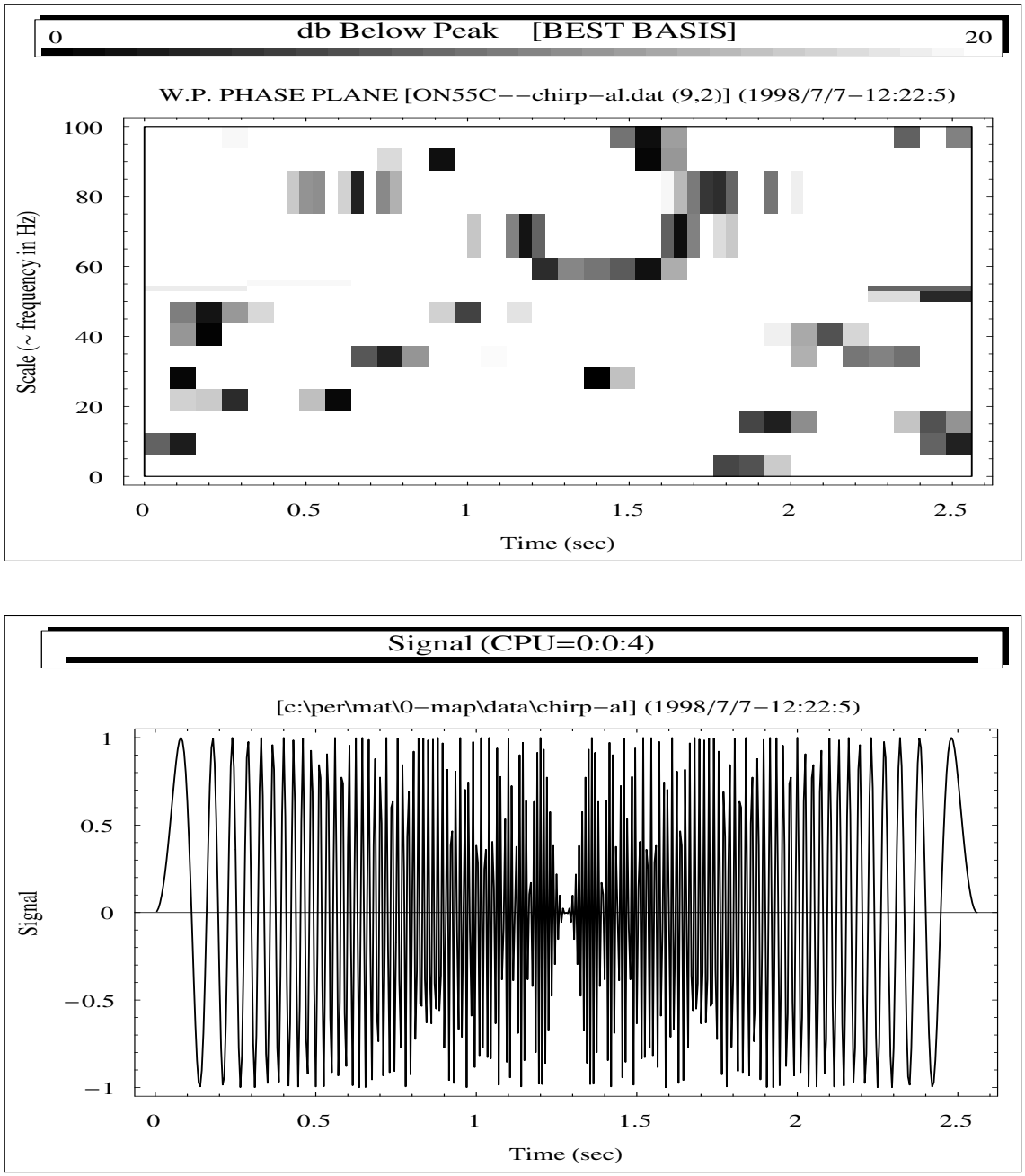

Fig 1.1 (TFW–WP BB) The time-frequency window distribution (or phase plane) of a wavelet packet's best basis (`top`) for a linear chirp signal that is sampled under an aliasing condition (thus the symmetric frequency distribution (`bottom`) is yielded). Here the wavelet packet is associated with a Coiflet of 30 convolution weights and the basis refers to the best basis rather than basis associated with the best level as to be shown in the next figure. The original signal, if not under-sampled, has linear instantaneous frequency distribution form 0 to 100 Hz in the full span of time. Note the non-symmetric distribution and and the scattering of windows. These phenomena reflect the composite frequency bands of a mother wavelet and inherent quarks that may arise, as well as the shift-non-invariant transform property.

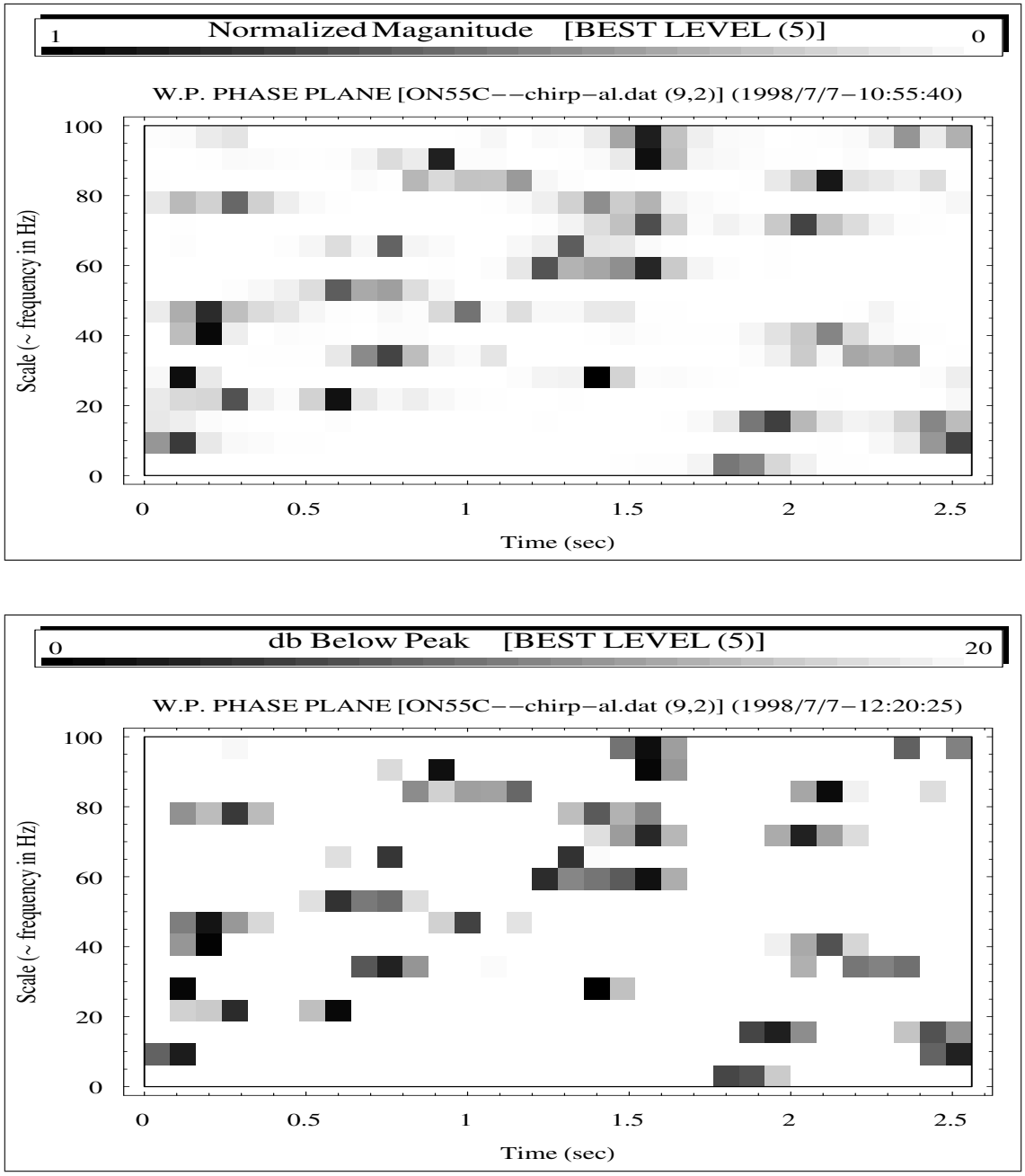

Fig 1.2 (TFW–WP BL) Choosing an appropriate wavelet basis is a dilemma to be resolved first. Here are shown two different wavelet packet phase plane representations associated with the same Coiflet and the same aliasing signal as the preceding figure. The distributions are now based on wavelet packet's best level, which occurs at transform level 5 for such a signal. The top sub-figure is in logarithmic measure and the bottom is in linear measure. In view of the fact that a single orthonormal mother wavelet can yield many different wavelet representations, and the fact that there are basically infinitely many wavelet bases, as well as the fact that we may use different graphic renderings; we are easily trapped in the quandaries of wavelet analyses.

- We note that the present scope focuses on the $L^2(\mathbf{R})$ Banach space, i.e., the Hilbert space, since some of the statements here may not apply to other function spaces or classes [12, 29]. Nevertheless, most of the intricacies that differentiate different spaces are only of analytic interest up until now (e.g., on the existence of multiresolution analysis (MRA), on the regularity and differentiability of wavelets and its associated scaling functions). From the practical point of view, it is far enough to restrict to the Hilbert space, i.e., a space of functions with finite "energy" contents.

1.4 The objectives

There are basically infinitely many wavelet function bases to choose from in any data analyses or in any applications. Nevertheless, it is not uncommon to see that a particular wavelet is chosen without given any usage specificity. The arising problems thusly quite often exceed the problems they want to solve, and the provided results in most cases are shoddy and misleading, or even erroneous. A mathematical existence does not always accommodate a reasonable physical nicety. And this is particularly true for wavelets' employment in our field concerning water wave physics.

The foothold to use localized transforms in our water wave applications can be stated quite simply, as well as intuitively — if we perceive our signal as composed of waves which are limited both in life span and in covering distance, i.e., constituent components are evolving with time and in space, then it is natural to adopt wavelet as our analyzing function. Furthermore, in addition to waves' modulation nature, if we also acknowledge, even for regular waves, that intrinsic instability due to nonliner effects may exist and that interactions and boundary conditions are everywhere to be observed, then it is still quite possible that, for stationary signals, wavelet decomposition can provide better descriptions of physics than can the Fourier decomposition. Besides, another advantage of using wavelets is the possible flexibility in adapting their wave forms to our desires; this is related to the modifications of time-frequency windows for better physical implications.

In this study the subject matter can essentially be separated into three main independent parts — the identification, the optimization, and the vindication. And the contents can basically be divided into six main core constituents.

1. In the first constituent we mainly focus on the characterizations of discrete wavelet categories. And the covered discrete wavelet categories should be quite comprehensive — in the sense that they have included all the extreme analytical properties in wavelet designs. And it is the author's belief that if you ever find an individual wavelet you have great chance to assign it into one of these categories, and if not, you have great reason to say that its properties fall within (or between) the covered characterizations and thus its possible usefulness (or destiny) trapped accordingly. The relevant characterizations and intrinsic properties for all the categories are extensively illustrated through the depictions of their mother and farther wavelets, the translations and dilations of wavelets, the zoom-ins or blowups of any kind of wavelets, the linear phase filtering features. Physical counterparts of analytical aspects are provided when possible.

2. In the second constituent, we work on the identification of optimum discrete wavelet basis specifically for studies of water wave related signals, and signals obtained from wind-wave-tank experiments are used. Here inclusive entropy criteria are adopted for both the whole comprehensive sets of wavelets and the Fourier basis.

3. In the third constituent we mainly focus on exploring the analytical essence of the behavior of any wavelet function basis concerning its performance or fitness in our water applications, in other words, what is the mathematical factor that leads to the different statistical performances based on the entropy. And this is related to the study of the phase distribution of a wavelet characterizing function (the $m_0(\xi)$ function in a later chapter) for each individual basis.

4. In the fourth constituent we mainly focus on the identification of the continuous counterpart wavelet of the optimum discrete basis, i.e., a continuous wavelet trans-

form corresponding to the multiresolution analysis of the semi-orthogonal cardinal spline dual wavelet. Here we address why there is the need of a continuous transform both mathematically and physically; that is to say, what are the advantages and disadvantages of discrete and continuous wavelet transforms concerning their applications to water waves.

5. In the fifth constituent we address what can be done to improve the physical relevance between the basis functions in the continuous domain and the wave constituents of our signals. Here the topics include: the demand of better physics in modeling the energy phenomenon; the uncertainty relationship and the degrees of freedom for adaptivity; the physics of the "carrier frequency" and the time-frequency windows of flexible size and shape; and finally the proof of the existence of admissability condition under such an adaptation.

6. In the sixth constituent we make the comparisons between the wavelet coherences based upon the best wavelet and the spectral coherences based upon the Fourier bases. The absolute superiority of wavelet coherences is shown and the reasons are delineated.

1.5 Summary

In summary, the study is to put forward an optimal wavelet basis that is both mathematically and physically right for water wave analyses; moreover, to prove it beyond doubt. ❖

Chapter 2

The Wavelet Categories and Their Characterizations

2.1 Introduction

In almost all lab or model experiments various modeling or scaling laws can at best be partially satisfied. The situation is further complicated for a multi-scale and multi-dimensional phenomenon in a multi-factor system.

In the introduction chapter we noted the problems of transient effects that attested to diversified scales. Moreover, for water wave experiments, it is acknowledgeable that there may exist significant distortions concerning the coupling mechanisms targeted. For example, a limitation in space and time in the tank, on the one hand, introduces the lack of scale diversification that may hinder the development of certain mechanisms and impose restrictions upon the evolutions of certain interactions; on the other hand, introduces serious boundary and initial conditions that may act as exploitations of factual considerations. With these understandings, as well as the cognizance regarding the inadequacy of the Fourier spectral approach in our applications as discussed earlier, it is understandable that, if the modeling of the proposed physics is at all possible, the deployment of an optimized analyzing scheme using sensitive and appropriate basis functions is desired. Specifically speaking, we shall select among a broad array of functional bases the most appropriate one for our signals and describe the proper analyzing method. Akin to such

an attempt, it warrants to give more systematical descriptions of different properties of various categories of wavelet function bases.

Herein comprehensive categories of discrete wavelet are studied. Their comprehensiveness is essentially reflected by the inclusions of all the extreme and opposite analytical properties in wavelet designs. That is to say, the characterization of a particular wavelet not seen or not named here should fall between or within the basis properties covered here.

2.2 Program and workbench developments

The wavelet programming and all relevant numerical characterizations were developed from the ground up using mainly the **Asyst** programming language [18]. The programs not only cater comprehensive wavelet bases but also provide broad characterizations of their relevant functions and intrinsic properties. The code is written with the mind of being flexible, friendly, and versatile. Accuracy and error-free requirements are highly abided by. And it is followed that keyboard inputs should be minimized and manual input of original and intermediate data should not be allowed. In addition, several add-in programs and auxiliary applications are integrated. Overall, they mainly consist of the following.

- The Postfix language — The Postfix add-in to the **Asyst** core programming enables the real-time, as well as direct, generation of high quality Adobe Encapsulated Postscript figures. The process secures the proper labeling and correct legends. And it is confidently guaranteed that the statements or analyses deriving from the figures make no mistakes. Besides, the automation exceeds the condition that the generation of quality figures as many as one wishes is surely possible, and that the elimination of the painful task of plotting seemly countless figures when making parametric alterations or test cases is certainly true. Using a commercial graphical application software can never archive such functionalities, moreover, it is basically

error-prone.

- The on-screen real time display of PCX format figures — The Encapsulated Postscript figures are mainly for quality printing and created in the background. A real-time and interactive monitor display is desirable and essential. This should greatly enhance the debugging efficiency and make possible the writing of a huge and complex code that is user-friendly, easy to maintain, as well as flexible, interactive and accurate.

- The data spreadsheet interface — The output or input of data to or from the Excel or Lotus-123 compatible worksheets is integrated. In cases that articulated or complex figures are desired or post-processing and supplementary analysis are needed such an interface is readily convenient and trouble free.

- The **Mathematica** programming language — This coding is mainly for the streamlined generation of various high quality graphical renditions for the two-dimensional or three-dimensional time-scale data, such as the modulus and phase information derived from the **Asyst** programs. There is no manual intervention when commuting between the **Asyst** outputs and the **Mathematica** inputs.

- The LaTeXmacros and packages — In addition to the utilization of various existing LaTeXpackages, a vast amount of LaTeXcodes and macros were also written for the following purposes: the systematic displays and printouts of numerous all sorts of figures for analyzing, reasoning, and comparing; the eye-pleasant code listings for programs and somewhat easy debugging; the casual generations of printouts, papers, reports, etc., for archiving and proof-reading; the facilitation for efficient management and pain-free integration of different case studies.

- The **WinEdt** macro programming language — The language is specifically used to develop a non-fallible workbench. Hundreds of these macros were written and integrated. The workbench provides a working platform or shell environment for

writing the codes of various programming languages, as well as provide various add-on operations, such as file management, various format operations, code compiling, cloud backups (these were developed in the `Windows 2000` or pre `XP` era when handsets and cloud concept were unfamiliar to the general public), etc. Lots of attention were paid to the accomplishment of an environment that is pleasant, efficient, easy and safe. With this workbench all the code pieces, subroutines, and component files are managed and displayed in a way of being scientific, organized and reflexive. Moreover, various tasks can be integrated and streamlined. Without such a workbench the editing and debugging, as well as the whole work, must be extremely painful and exhausting and the present study is surely inconceivable.

2.3 Wavelet basis categories

The Riesz wavelet bases tested here can basically be divided into four categories: orthonormal (ON), semi-orthogonal (SO), bi-orthogonal (BO), and orthonormal wavelet packets bases. For the orthonormal category it is divided into several different subgroups: Daubechies wavelets (both the most and least asymmetric), Coiflets, Meyer wavelet, and Battle-Lemarié wavelets.

No detail accounts of these wavelets will be given; only the main criteria and core features of each categories will be briefed. Let first state the related notations and conventions needed for the context that follows. Let a function or a signal be denoted by $f(t)$; the two-scale scaling function of a Riesz basis be $\phi(t)$; the associate mother wavelet be $\psi(t)$ and its dyadic wavelets be $\psi_{j,k}(t) = \sqrt{2^j}\,\psi(2^j t - k)$, where $j, k \in \mathbf{Z}$ and k stands for translation and j for dilation. The concept of translations and dilations are illustrated in figures 2.1 (Wavelet T&D-1) through 2.6 (Wavelet T&D-6).

The space V_j (formed by $\psi_{j,k}$, $k \in \mathbf{Z}$ for a given j) in the multiresolution ladder are nested in $\cdots \subset V_{-1} \subset V_0 \subset V_1 \cdots$, and the finest and the coarsest scale space, say, for a 1024-point signal, are V_{10} and V_0, respectively; the number of filter coefficients or

the number of convolution weights be N if the associated wavelet is finitely supported (support length equals to $N-1$); the dual wavelet and dual scaling function, if exist, be $\widetilde{\psi}(t)$ and $\widetilde{\phi}(t)$; the inner product be $\langle \cdot, \cdot \rangle$; and the Kronecker delta be $\delta_{j,k}$, $j, k \in \mathbf{Z}$, which is equal to 0 for $j \neq k$ and 1 for $j = k$.

Up until now, all practical wavelets of discrete transform are associated with the theory of multiresolution analysis (MRA) [2, 12, 25, 26]. For Riesz wavelets there always exist dual wavelets except for orthonormal wavelets, which are self-dual. Any discrete wavelet transform involves two convolution operations: one yields detail information; another yields smooth information [31]. Convolutions can either be implemented in a direct way in the time domain for compactly supported wavelets or in an indirect way in the frequency domain. We list the basic properties (restricted to real-valued wavelets) and give the symbols of representation for various categories and subgroups as follows.

2.4 Orthonormal wavelets

The orthonormal wavelets covered here include the following categories: Daubechies most compactly supported wavelets (denoted as ONxxA); Daubechies least asymmetric wavelets (ONxxS); Coiflets (ONxxC); Meyer wavelet (Meyer); Battle and Lemarié wavelet (B&L). Here in all the subsequent annotation x is an integer related to support length (physically, the span of mother wavelet curve).

$$\psi = \widetilde{\psi}, \tag{2.1}$$

$$\phi = \widetilde{\phi}, \tag{2.2}$$

$$\langle \psi_{j,k}, \widetilde{\psi}_{l,m} \rangle = \delta_{j,l}\delta_{k,m}, \tag{2.3}$$

$$f(t) = \sum_{j,k} \langle f, \psi_{j,k} \rangle \psi_{j,k}, \tag{2.4}$$

One MRA ladder (single set of frame bounds),

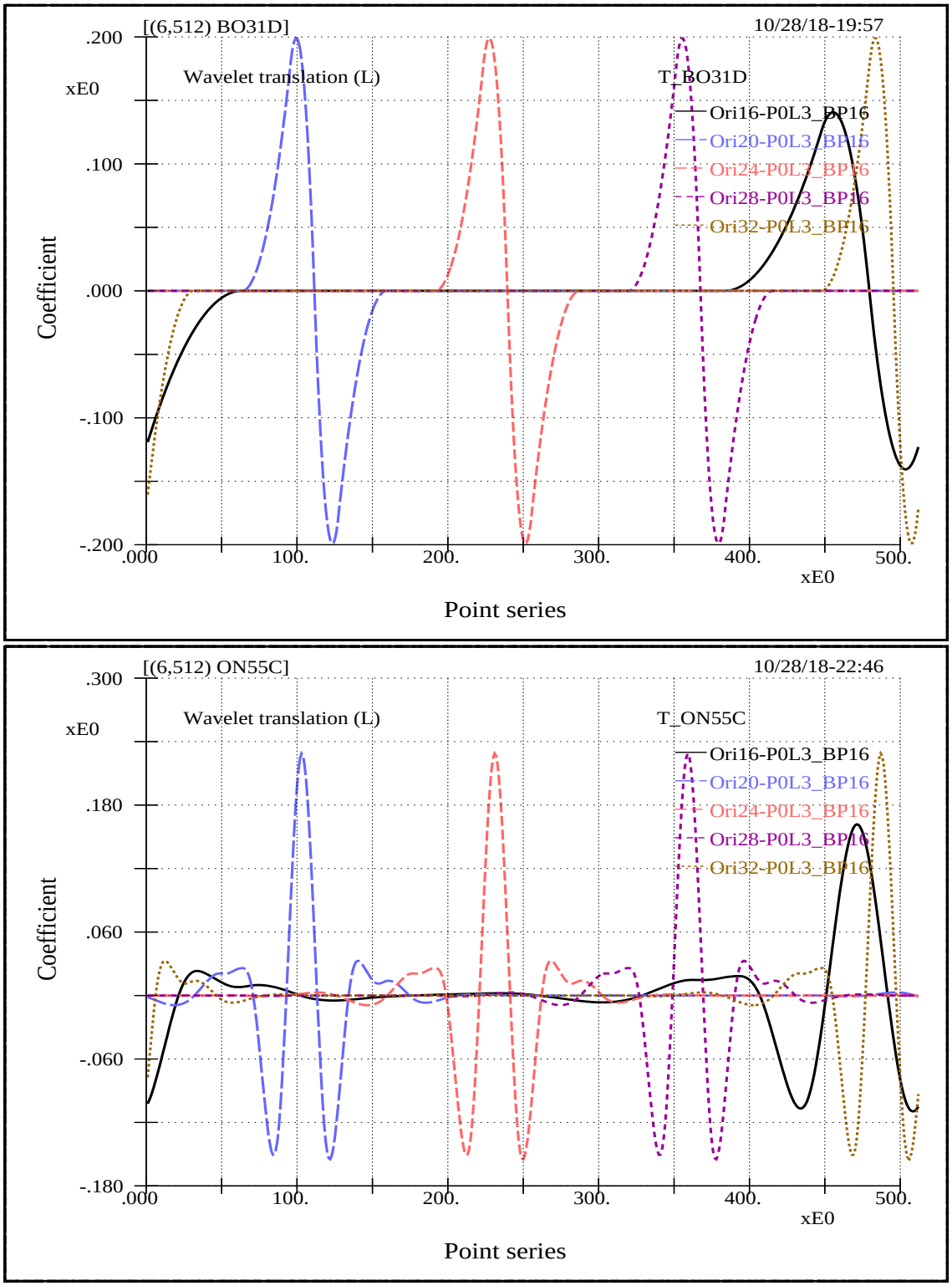

Fig 2.1 (Wavelet T&D-1) Wavelet's time-scale constructs – The time-scale concept of wavelet analysis is associated with two variables, i.e., the translation and the dilation. Here the concept of translation and dilation on the scales of transform level 3 is shown for two different wavelets (BO31D `(top)` and ON55C `(bottom)`). Individual curves are the inverse transforms of unit value at points 16, 20, 24, 28, and 32 that are situated upon level 3.

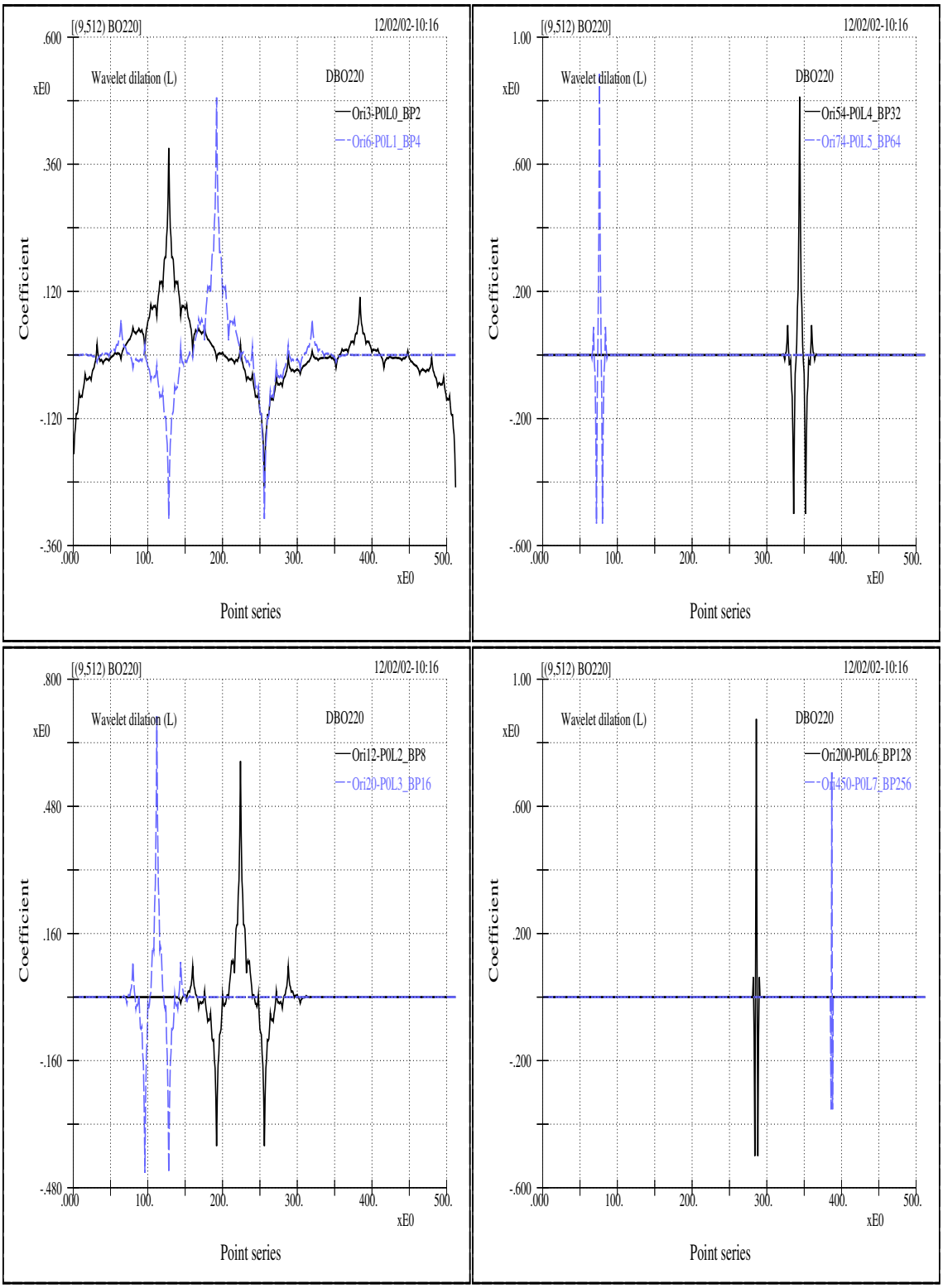

Fig 2.2 (Wavelet T&D-2) Wavelet's time-scale constructs for a bi-orthogonal wavelet – Here the concept of dilation and the fractal nature across scales of wavelet are shown for scales from transform level 0 to level 7 for the BO22O wavelet. Each curve corresponds to an individual scale and specific location as labeled in the sub-figures.

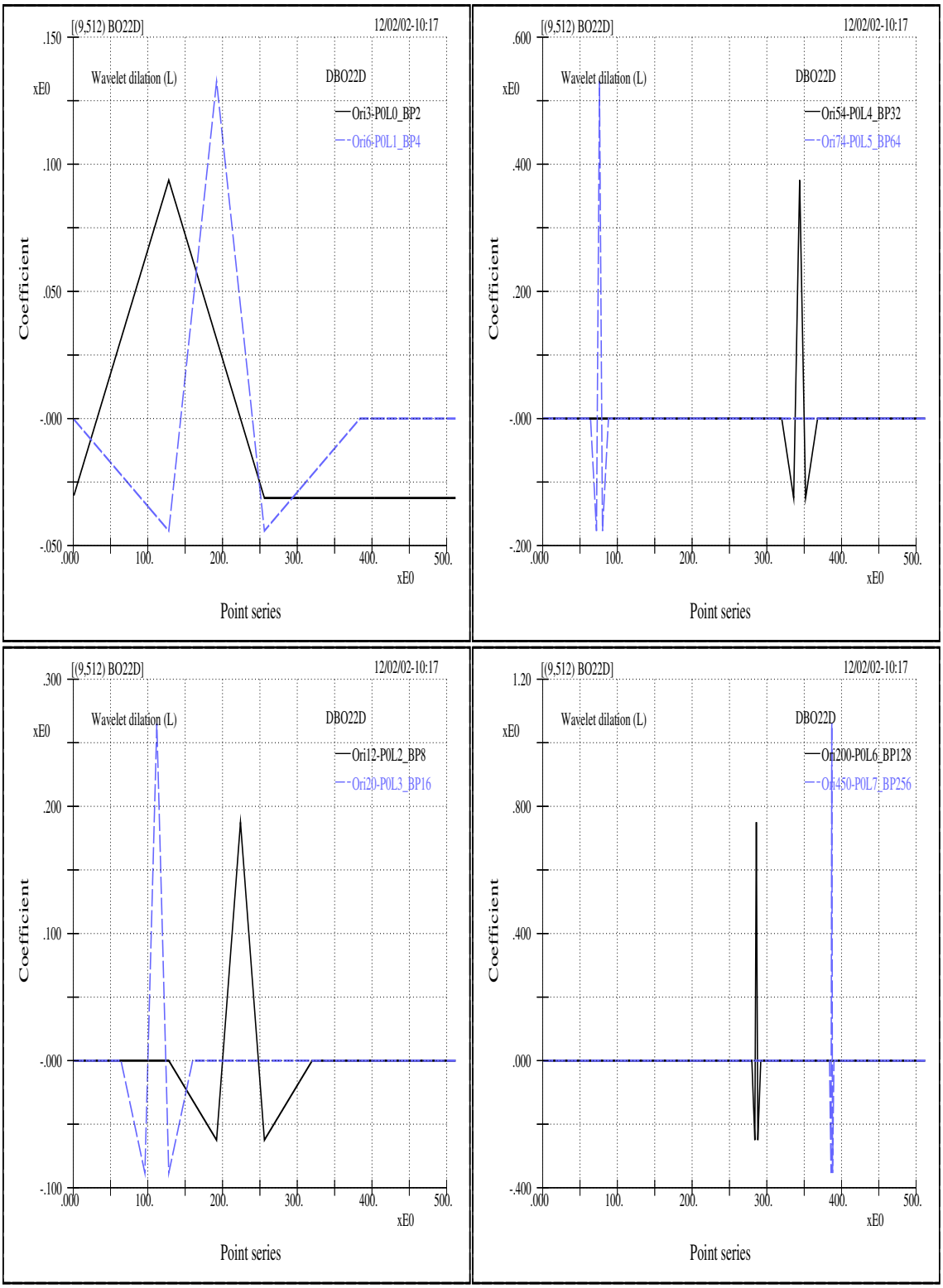

Fig 2.3 (Wavelet T&D-3) The fractal nature across scales of the dual wavelet (BO22D) and its dilation constructs are shown here. The dual wavelet refers to the wavelet used in the preceding figure (BO22O). Each wavelet curve corresponds to an individual scale (from scale level 0 to level 7) and its specific translation location as labeled in individual sub-figure.

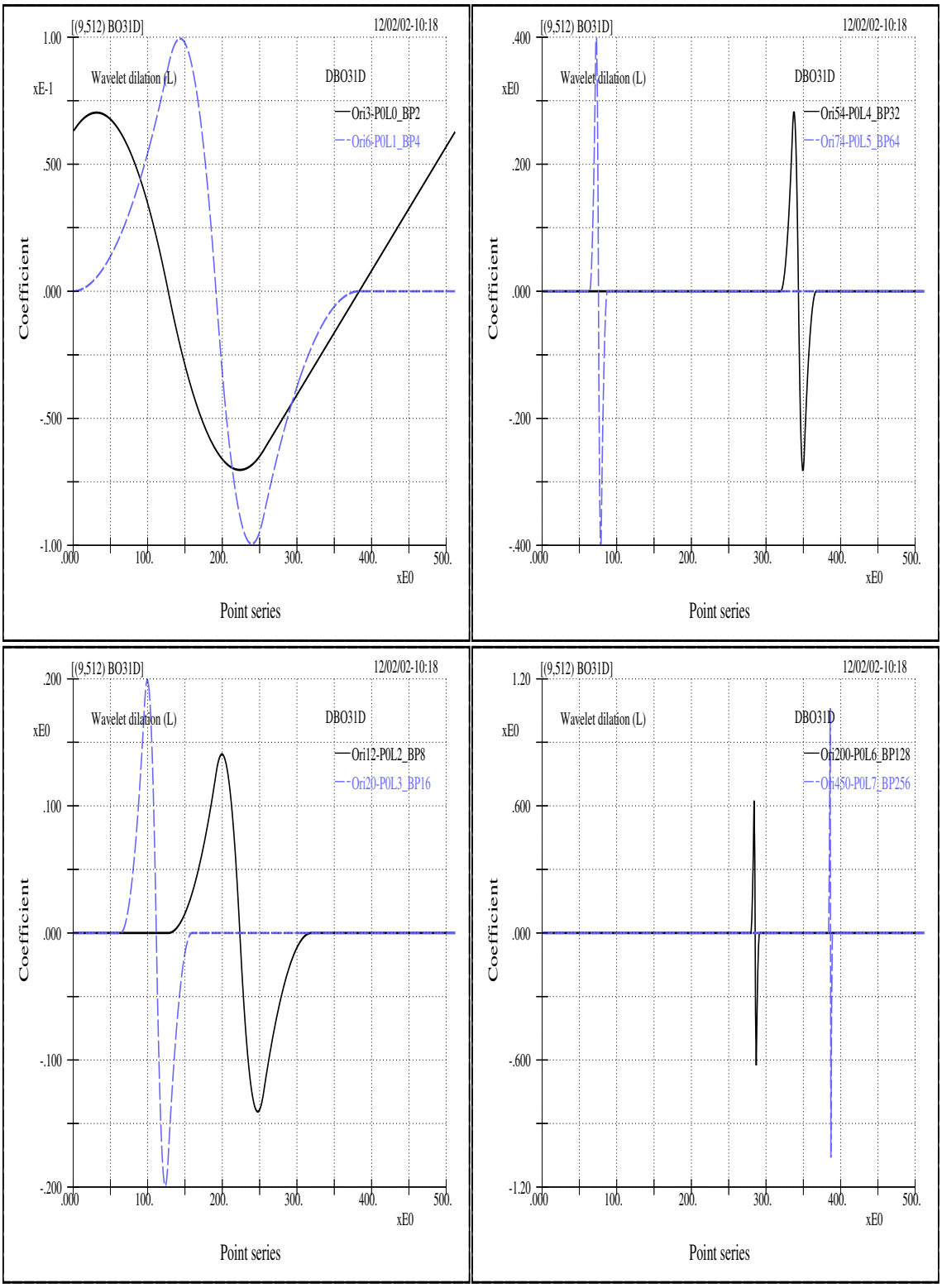

Fig 2.4 (Wavelet T&D-4) The wavelet dilation concept and smoothly fractal nature from scale level 0 to level 7 for the dual BO31D wavelet. Each wavelet curve corresponds to an individual scale and its specific time location as labeled in individual sub-figure.

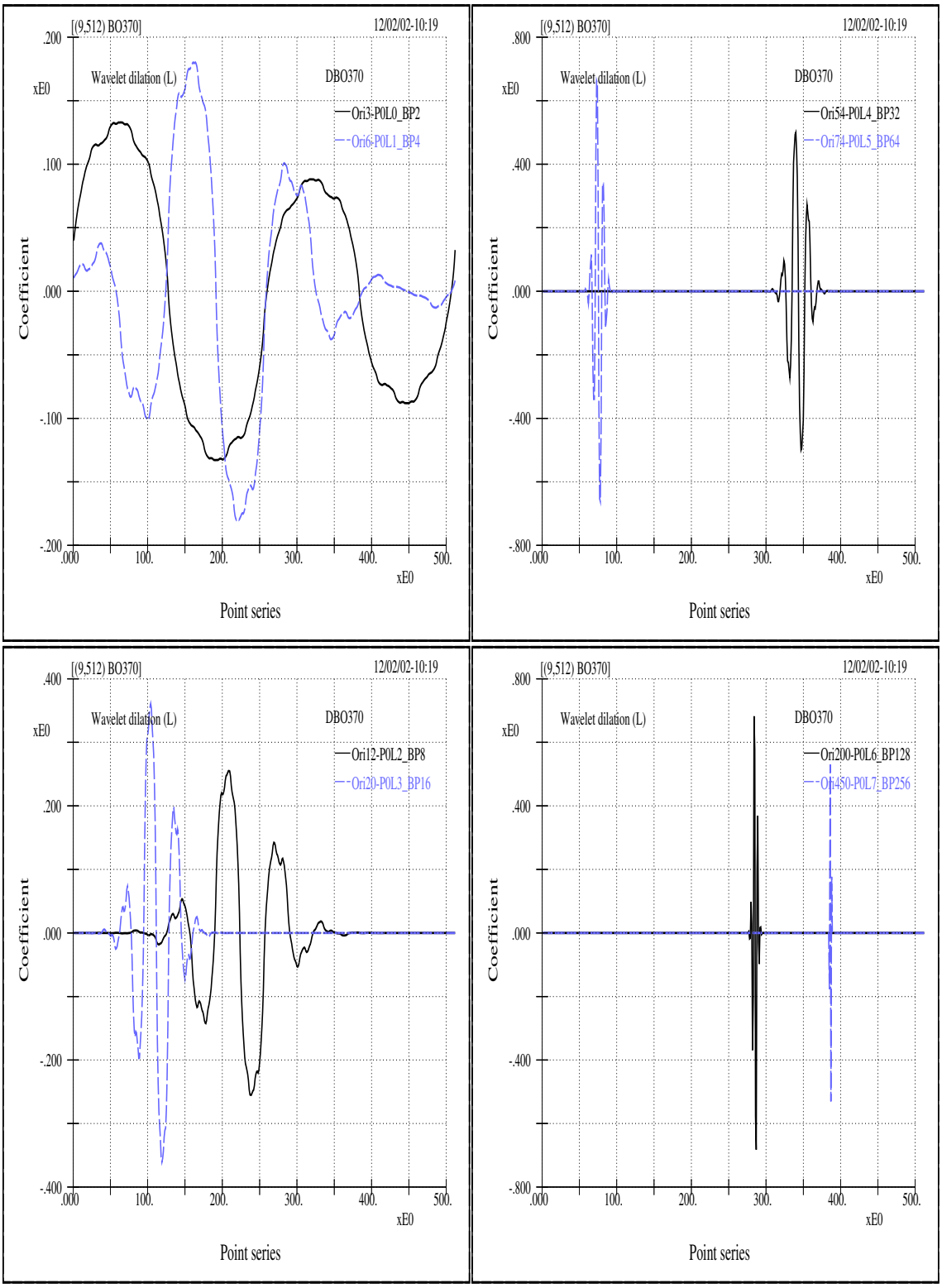

Fig 2.5 (Wavelet T&D-5) The wavelet dilation concept and the fractal nature from scale level 0 to level 7 for the BO370 wavelet. Each wavelet curve corresponds to an individual scale and its specific time location as labeled in individual subfigure.

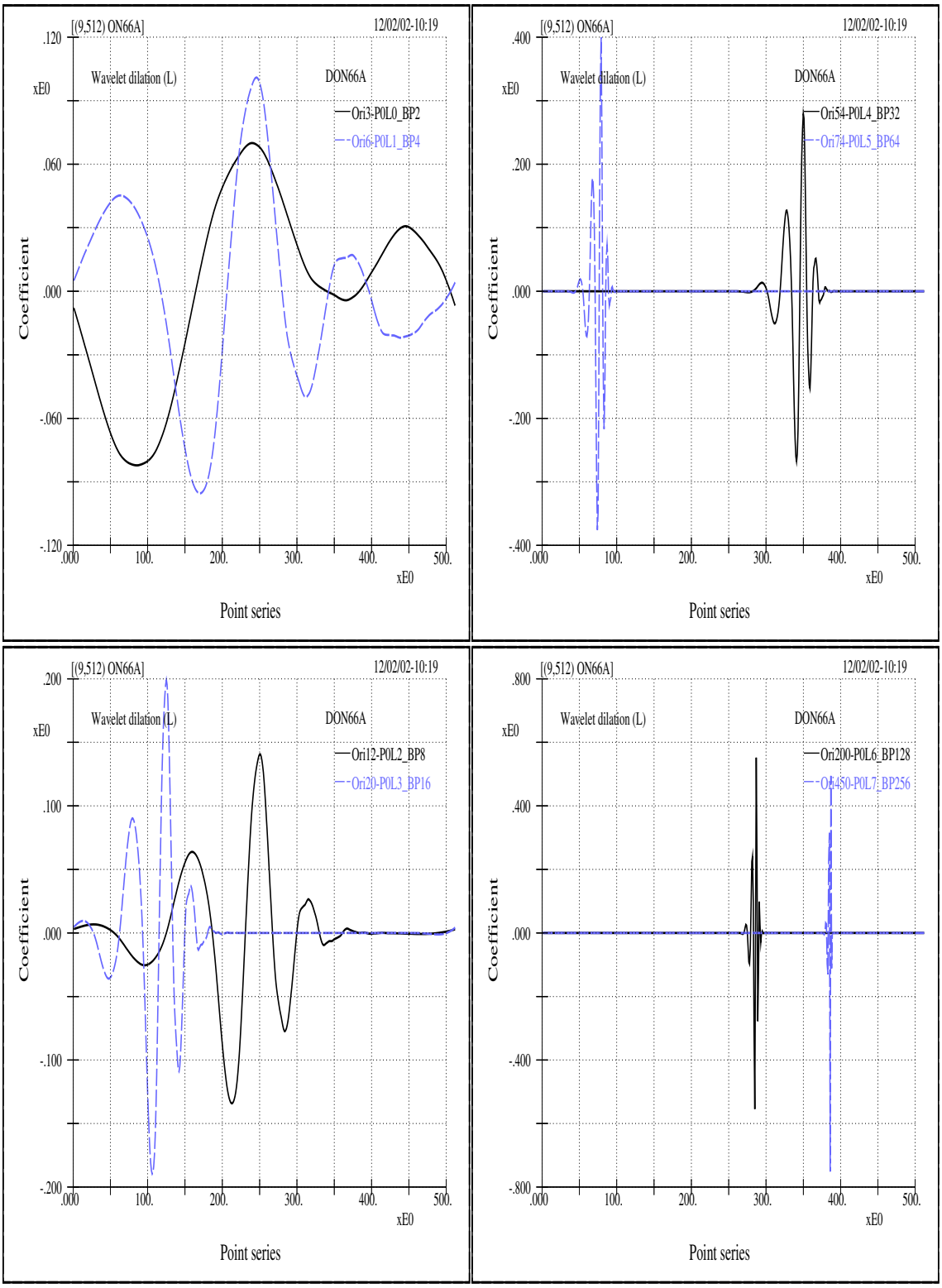

Fig 2.6 (Wavelet T&D-6) The wavelet dilation concept and the fractal nature for the ON66A wavelet, which belongs to the most asymmetric category. Each wavelet curve corresponds to an individual scale (from level 0 to level 7) and its specific time location as labeled in individual sub-figure.

One filter pair (one smooth and one detail).

2.4.1 Daubechies most compactly supported wavelets (ONxxA)

The wavelets in this group have maximum number of vanishing moments for given compatible support width. Or stated otherwise, they are the most compactly supported wavelets for given compatible number of vanishing moments. The famous most compactly supported continuously distributed wavelet belongs to this group and has only four filter coefficients. These wavelets are quite asymmetry (so, the "A" in ONxxA). The mother and farther wavelets for the group corresponding to the originating points of 12 (boundary point based on level 2) and 6 (boundary point based on level 3), respectively, for this group are shown in figures 2.7 (MW–ONxxA) and 2.8 (FW–ONxxA). The vanishing moments and the number of filter coefficients are, respectively,

$$\int_{-\infty}^{\infty} t^l \psi(t) dt = 0, \quad l = 0, 1, \cdots, x, \tag{2.5}$$

$$N = 2x, \tag{2.6}$$

where x is the integer number in ONxxA. The minimum number of x is 2.

2.4.2 Daubechies least asymmetric wavelets (ONxxS)

For a given support width, these wavelets, in contrast to those of the ONxxA subgroup, are the most symmetric ones (so, the "S" in ONxxS, but still not symmetric). They have the same representations of vanishing moments and number of filter coefficients as those of ONxxA. But the known minimum number of x is 4. The mother and farther wavelets for this group corresponding to the same originating points as the previous ones are shown in figures 2.9 (MW–ONxxS) and 2.10 (FW–ONxxS).

2.4.3 Coiflets (ONxxC)

The Coiflets have vanishing moments for both ψ and ϕ; therefore, from Taylor expansion point of views [12], they have high compressibility for fine detail information (i.e., a great portion of the fine scale wavelet coefficients are relatively small); and henceforth, they have simple quadrature rule to calculate the fine smooth information (i.e., the calculation of the inner product of a function and the fine-scale scaling functions is more efficient). Since every discrete wavelet transform involves both smoothing and detailing operations, there may exist some advantages from these two properties for certain applications such as applications that do not stress lossless of signal contents or perfect reconstructions [10, 34]. Their vanishing moments and number of filter coefficients are

$$\int_{-\infty}^{\infty} t^l \psi(t) dt = 0, \quad l = 0, 1, \cdots, x, \tag{2.7}$$

$$\int_{-\infty}^{\infty} \phi(t) dt = 1, \tag{2.8}$$

$$\int_{-\infty}^{\infty} t^l \phi(t) dt = 0, \quad l = 1, \cdots, x, \tag{2.9}$$

$$N = 6x. \tag{2.10}$$

For this group the mother and farther wavelets are shown in figures 2.11 (MW–ONxxC) and 2.12 (FW–ONxxC).

2.4.4 Meyer wavelet (Meyer)

The Meyer wavelet (denoted as Meyer or ME in figures) is the wavelet with most compact support in frequency domain (here, if without any specific assignment, "finitely supported" refers to time domain). Therefore, due to contrast properties between the two Fourier domains, the wavelet is infinitely differentiable in time domain, i.e., has an infinite Lipschitz regularity C^{∞} and does not have exponential decay. And the support length $N \to \infty$. The associated mother and farther wavelets corresponding to the same

originating points are shown in figure 2.13 (MFW–Meyer).

2.4.5 Battle and Lemarié wavelet (B&L)

The Battle and Lemarié wavelet (denoted as B&L or LE in figures) of m^{th} order is constructed from the orthonormal scaling function derived by applying the standard orthonormalization trick to the m^{th} order cardinal B-spline N_m [4, 6]. For $m = 1$, it is exactly the Haar wavelet. The latter is the only finitely supported wavelet in this group (also the case of BO11O=BO11D to be mentioned below) and is also a non-continuously distributed wavelet with the most compact support. All other wavelets in this group are infinitely supported. These wavelets have an exponential decay and possess C^{m-2} regularity. The mother and farther wavelets for the Battle-Lemarié wavelet are shown in figure 2.14 (MFW–B&L). Compared to the curves of Meyer wavelet (figure 2.13 (MFW–Meyer)), they look quite identical even though their constructions, or derivations, or formula involved (including Lipschitz regularity and decay property) are completely different.

2.5 Semi-orthogonal wavelets (SOxO and SOxD)

The semi-orthogonal wavelets are inter-scale, but not inner-scale, orthogonal. Their scaling functions are cardinal B-spline N_m and have finite two-scale relations. Although there are two distinctive (independent) filter pairs (one for the decomposition and the other for the reconstruction), there is only one MRA V_j-ladder. It was shown by Chui [6, 7] that the cardinal B-spline wavelet of an order higher than $m = 3$ is almost a modulated Gaussian (but a modulated Gaussian is not a wavelet). Therefore only the fourth order Cubic B-spline wavelet ($m = 4$) is tested. It has the following characterizations.

$$\psi \neq \widetilde{\psi}, \tag{2.11}$$

$$\phi = \widetilde{\phi}, \tag{2.12}$$

$$\langle \psi_{j,k}, \psi_{l,m} \rangle = \langle \widetilde{\psi}_{j,k}, \widetilde{\psi}_{l,m} \rangle = \delta_{j,l}, \tag{2.13}$$

$$f(t) = \sum_{j,k} \langle f, \psi_{j,k} \rangle \widetilde{\psi}_{j,k} = \sum_{j,k} \langle f, \widetilde{\psi}_{j,k} \rangle \psi_{j,k}, \tag{2.14}$$

$$N = 3x - 1 \quad \text{for SO}x\text{D}, \tag{2.15}$$

$$N \to \infty \quad \text{for SO}x\text{O}. \tag{2.16}$$

One MRA ladder ,

Two filter pairs ,

The mother and farther wavelets of the fourth order and the associated dual wavelets are shown in figures 2.15 (MFW–SO0) and 2.16 (MFW–SOD).

2.6 Bi-orthogonal wavelets (BO$x\,y$O and BO$x\,y$D)

The wavelets in this category are constructed also by Daubechies, and are sometimes called non-orthogonal wavelets. As is well known all real-valued orthonormal compactly supported wavelets, except the Haar wavelet, are not symmetrical. However, from the point of view of reconstructing a signal from its partially truncated wavelet coefficients, the symmetry is a desired property of the filter when a more natural perception or smoother variations is important. There is a very practical implication here: if non-symmetrical function bases are used, then a small change in the wave form causes significant variations of scale information. In other words, to have minor impacts to the data analysis, it is desirable to have bases as symmetrical as possible. Moreover, when considering that random errors, or noise, or uncontrolled factors are present, we should be able to comprehend the significance of this property. In fact many of the figures given in this study indicate such a feature. The symmetry can be achieved by sacrificing orthogonality; if this is the case one has dual pairs for both wavelets and scaling functions. It is obvious that conditions for semi-orthogonal cases are more general than those of orthogonal ones,

and the bi-orthogonal cases are even more general. This situation is clearly indicated by the additional freedom of dual scaling function, as is reflected by the two parameters x and y in the notations of BOxyO and BOxyD. Nevertheless, the wavelets in this category involve only one pair of independent filters for both decomposition and reconstruction even though there involve two different MRA ladders that are associated with their own individual sets of Riesz bounds. This is quite opposite to the case of semi-orthogonal wavelets where they involve one MRA ladder but with two filter pairs.

$$\psi \neq \widetilde{\psi}, \tag{2.17}$$

$$\phi \neq \widetilde{\phi}, \tag{2.18}$$

$$\langle \psi_{j,k}, \widetilde{\psi}_{l,m} \rangle = \langle \phi_{j,k}, \widetilde{\phi}_{l,m} \rangle = \delta_{j,l}\delta_{k,m}, \tag{2.19}$$

$$f(t) = \sum_{j,k} \langle f, \psi_{j,k} \rangle \widetilde{\psi}_{j,k} = \sum_{j,k} \langle f, \widetilde{\psi}_{j,k} \rangle \psi_{j,k}, \tag{2.20}$$

$$N = 2y + x - 1 \quad \text{for BO}xy\text{O and } x \text{ odd}, \tag{2.21}$$

$$N = 2y + x - 2 \quad \text{for BO}xy\text{O and } x \text{ even}, \tag{2.22}$$

$$N = 2y + x - 1 \quad \text{for BO}xy\text{D and } y \text{ odd}, \tag{2.23}$$

$$N = 2y + x - 2 \quad \text{for BO}xy\text{D and } y \text{ even}. \tag{2.24}$$

Two MRA ladders,

One filter pair,

The mother and farther wavelets for this group and the associated dual wavelets are shown in figures 2.17 (MW–BOxy0) through 2.20 (FW–BOxyD).

2.7 Wavelet packets

The wavelet coefficients derived from an orthonormal wavelet decomposition can be further decomposed by using either the set of filter coefficients (called two-scale sequence in Chui [6]) associated with the original wavelet, or different sets of filter coefficients associated with other orthonormal wavelets. Therefore, basically there can be infinitely many wavelet packet decompositions. These further decompositions are of a tree-like refinement process and are called the wavelet packet transform. The wavelet packet coefficients give better frequency resolutions with longer time supports. There are no simple formulas to describe the tree-like decompositions, but a schematic plot help elucidate the mechanism shown in figure 2.21 (WP Tree). The branch patterns and the number of branches can be chosen in any way so long as there is no repeat occurrences within any column under the stretch of the coefficients. That is to say, any column, wide or narrow, must have one and only one contribution from all levels (rows). Due to the tree-like process the computational works are dramatically increased.

Figure 2.22 (WP forms) depicts the wave forms of two wavelet packets based upon ON22A and associated with the same location point 100 at different scale levels 2 and 5. It demonstrates the typical bundled shape of distribution of wavelet packets as compared to wavelet.

For this category we have two criteria for selecting our best basis. One is still called the "best basis"; another "best level basis". Take for example, for a 1024-point signal, the finest level occurs at $j = \log_2 1024 = 10$ and there are 2^{10} different choices of bases. And within these 2^{10} choices the one which yields the minimum entropy is called the "best basis". And if we enforce the restriction that all wavelet packets be at the same level j, then we have 10 levels (0 to 9) to choose from; the level that yields minimum entropy is called best level basis. The indexes of a wavelet packet coefficient, i.e., the subscript and superscript of U labeled in the figure determine the time of occurrence of that coefficient and also indicate the associated support length and frequency resolution, i.e., the shape

and location of the coefficient's time-frequency window within the phase plane. Concepts regarding the wavelet packet transform can be seen in figure 1.1 (TFW–WP BB). Again we also see the effects of non-symmetrical filtering. One specific feature is that the areas of all individual windows are all equal.

2.8 Wavelet nature

Wavelets are fractal in nature, that is to say, no matter how detail we zoom into the wavelet curve its blowups all show similar characterization, and this is related to the wavelet differentiability, regularity, support length, and decaying property.

The **Asyst** program is written to be able to blow any wavelet constructions, such as mother and father wavelets, wavelet bases and wavelet packet bases at any point on any level. A few examples are shown in figures 2.23 (BU–BO2yO) to 2.30 (BU–BO35O).

Her we note that wavelets with fancy analytical properties are often of bizarre wave forms and not of our choice for studying water wave related physics — either judging from they entropy values to be given in the next chapter or form their stability conditions.

Moreover, this blowup exercise hints the behaviors of several numerical and theoretical aspects of wavelet analysis, such as the edge effects, the possible differences of function curves due to finite resolution, and the convergent or error propagation property.

Figures 2.29 (BU–BO31O) and 2.30 (BU–BO35O) show the blow-ups of bi-orthogonal wavelet BO31O and BO35O, respectively. Relevant data for BO31O is: Origin of wavelet curve: level 2, position 12 (i.e., element U_2^{12} in figure 2.21 (WP Tree)); Blow-up point: 150; data length: 512. Each sub-figure shows successive blow-up scale of 2^6. Here the blow-ups diverge rapidly, i.e., the wavelet fails to identify itself numerically in the refinement cascade. Relevant data for BO35O is: Origin of wavelet curve: level 2, position 12 (i.e., element U_2^{12} in figure 2.21 (WP Tree)); Blow-up point: 225; data length: 512. Each sub-figure shows successive blow-up scale of 2^6. Here the blow-ups converge but go with peculiar inclinations. Figure 2.28 (BU–WP-ON) also exhibits the grouping or bundling tendency, as

well as the fractal behavior, of wavelet packets. A few more specific or intrinsic properties and their implications might be noted in the legends of individual figures.

2.9 Summary

The purpose of this chapter is to give an idea of the comprehensiveness of the wavelet categories covered here and to provide the basic understanding of wavelet intrinsic properties as well as their possible implications in applications for water waves. It is hoped that these numerous figures suffice the robustness of the study. ❖

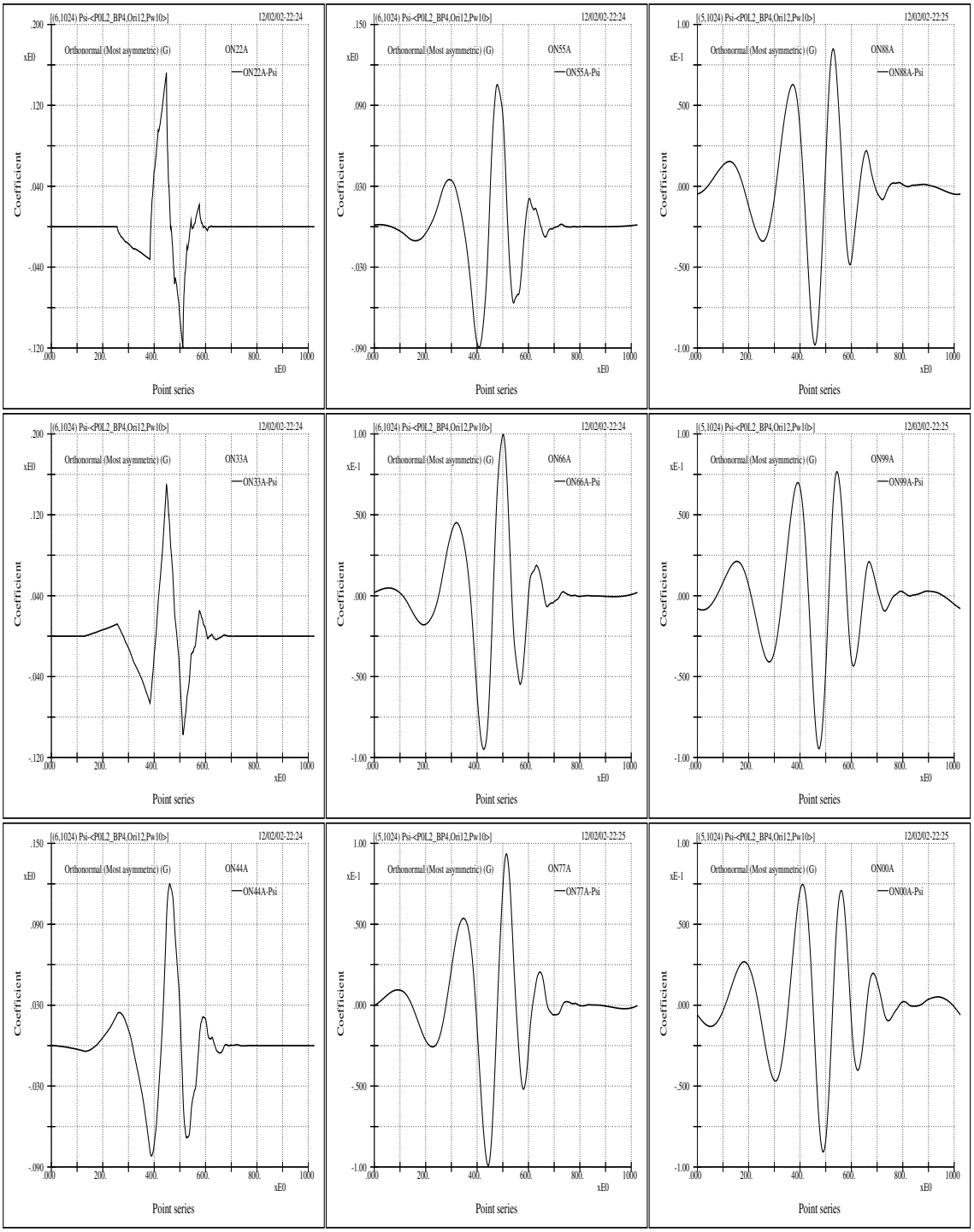

Fig 2.7 (MW–ONxxA) Any discrete wavelet transform is inherently associated with the pairing of a mother wavelet and a father wavelet (conventionally denoted as ψ and ϕ respectively). Such a pairing also links to the union of the constructs of "detail information" and "smooth information". Here the mother wavelets of the most asymmetric orthonormal group ONxxA are shown. These curves are the inverse transforms of a unit value located at point 12 for a 1024-point data. They are the constructs of the "detail information". It is noted that the "detail information" for these sub-figures is associated with a level greater than 3. That is to say the separation point between "smooth information" and "detail information" is located at point 8.

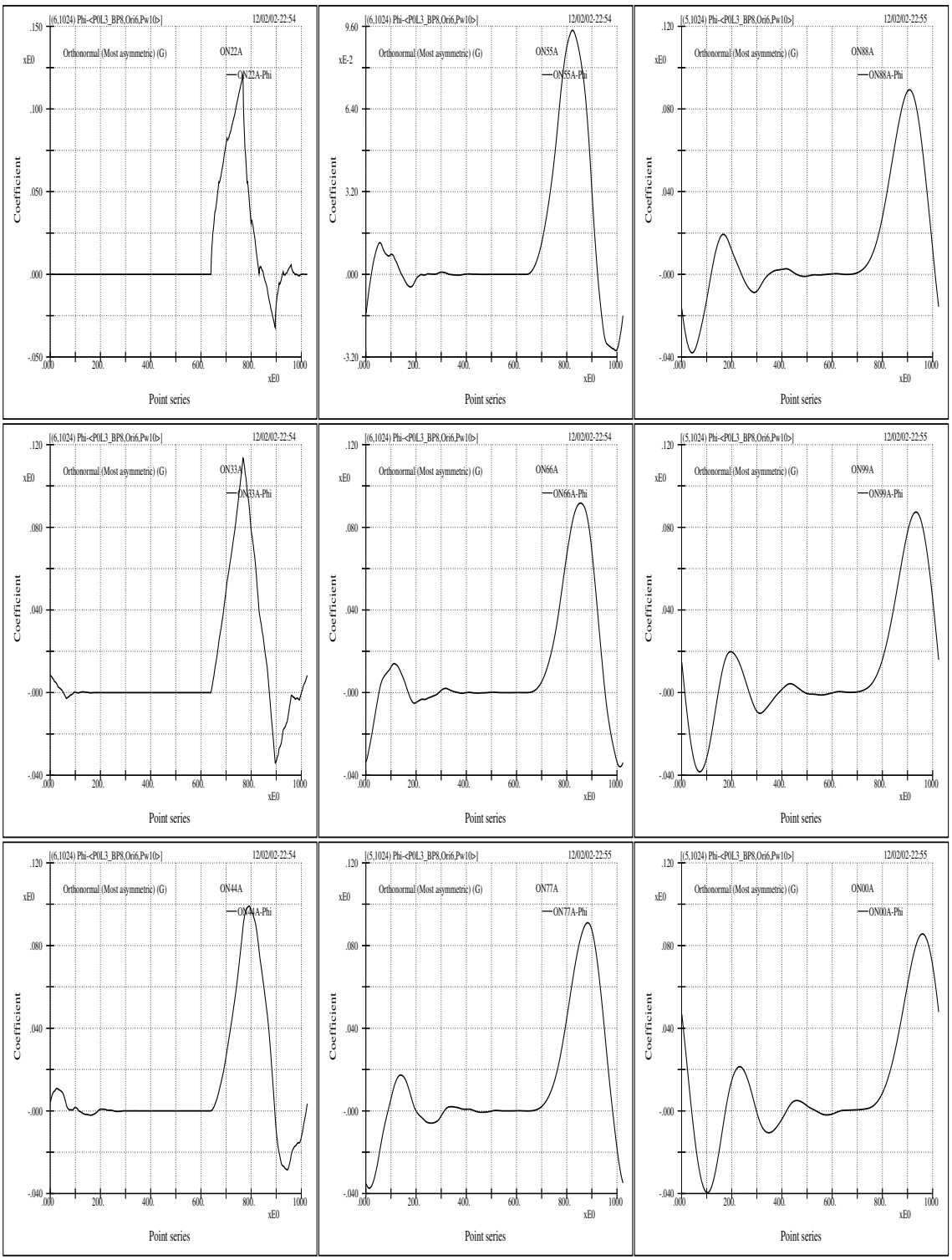

Fig 2.8 (FW–ONxxA) Here the father wavelets of the most asymmetric orthonormal group ONxxA are shown. They are the constructs of the "smooth information" corresponding to the "detail information" shown in the previous figure. These curves are the inverse transforms of a unit value located at point 6 for a 1024-point data. It is noted that the "smooth information" for these sub-figures is associated with a level less than or equal to 3. Again, the separation point between "smooth information" and "detail information" is located at point 8.

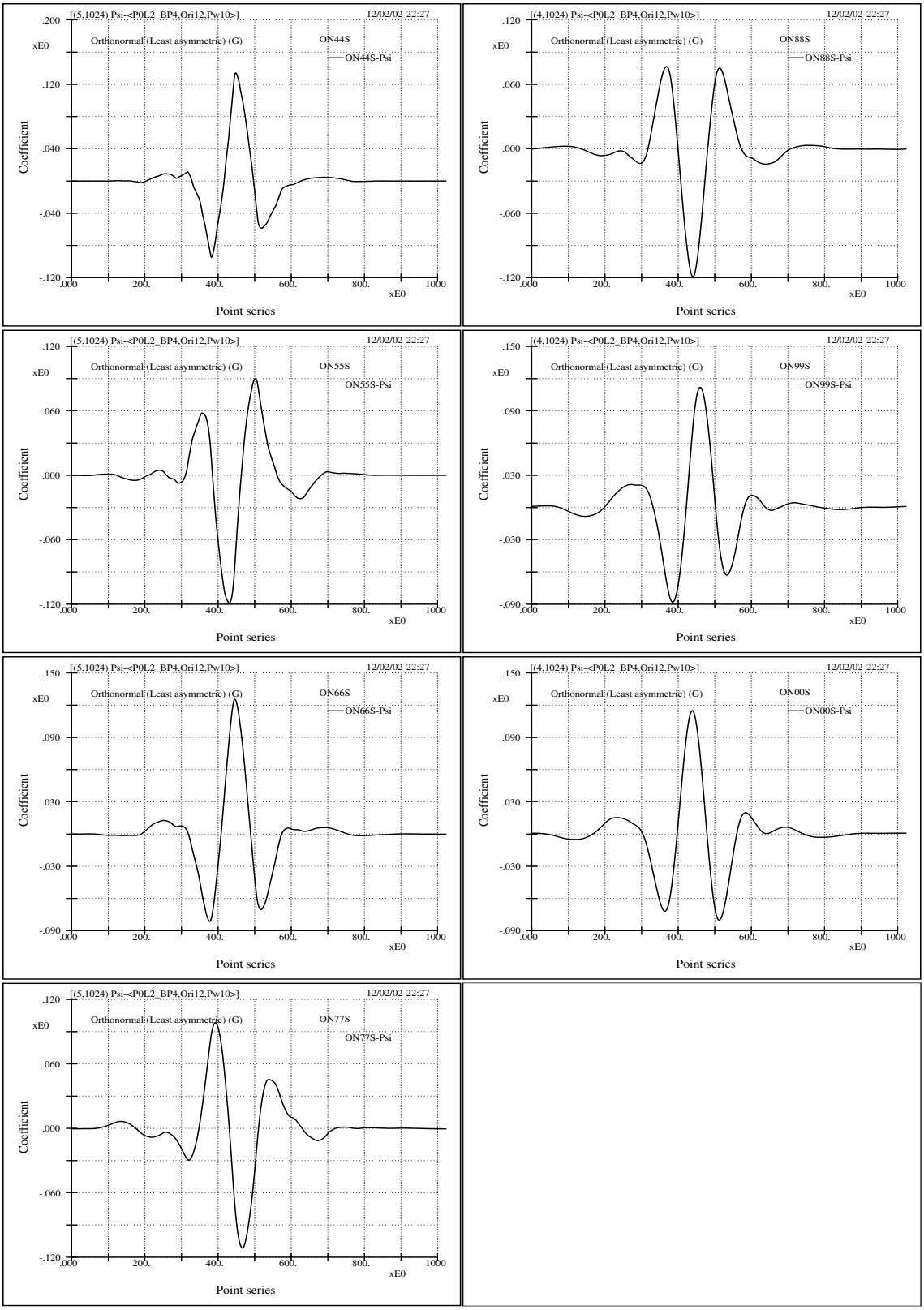

Fig 2.9 (MW–ONxxS) The mother wavelets of the most symmetric orthonormal wavelet group ONxxS are shown here. Each curve is the inverse transform of a unit value located at point 12 (at a scale level greater than 3) for a 1024-point data. Again, the separation point between "smooth information" and "detail information" is chosen at point 8.

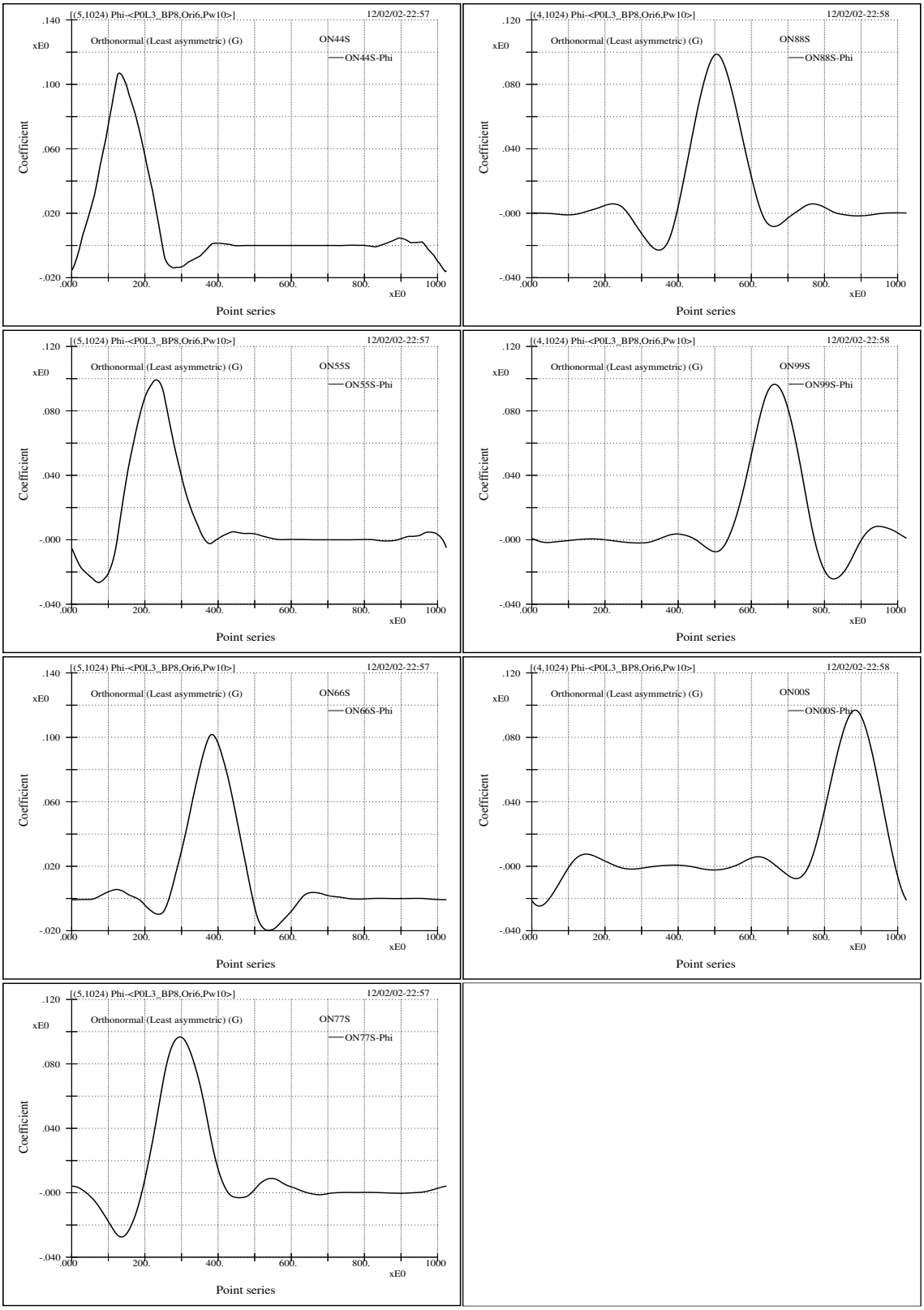

Fig 2.10 (FW–ONxxS) The father wavelets of the most symmetric orthonormal wavelet group ONxxS are shown here. Each curve is the inverse transform of a unit value located at point 6 (at a scale level less than or equal to 3) for a 1024-point data. Again, the separation point between "smooth information" and "detail information" is chosen at point 8.

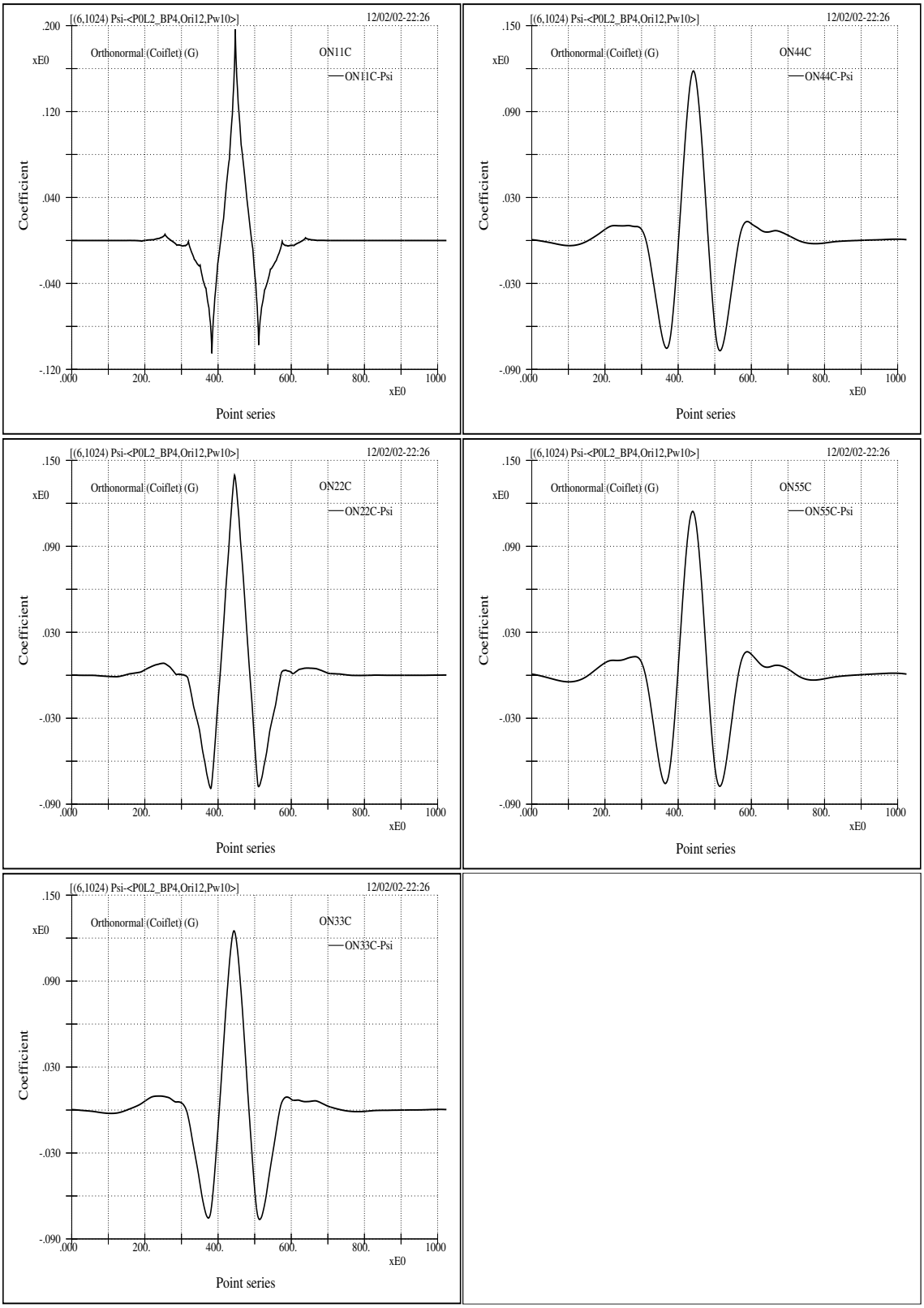

Fig 2.11 (MW–ONxxC) The mother wavelets of the orthonormal Coiflet wavelet group ONxxC are shown here. Each curve is the inverse transform of a unit value located at point 12 (at a scale level greater than 3) for a 1024-point data. The same separation point between "smooth information" and "detail information" is chosen at point 8.

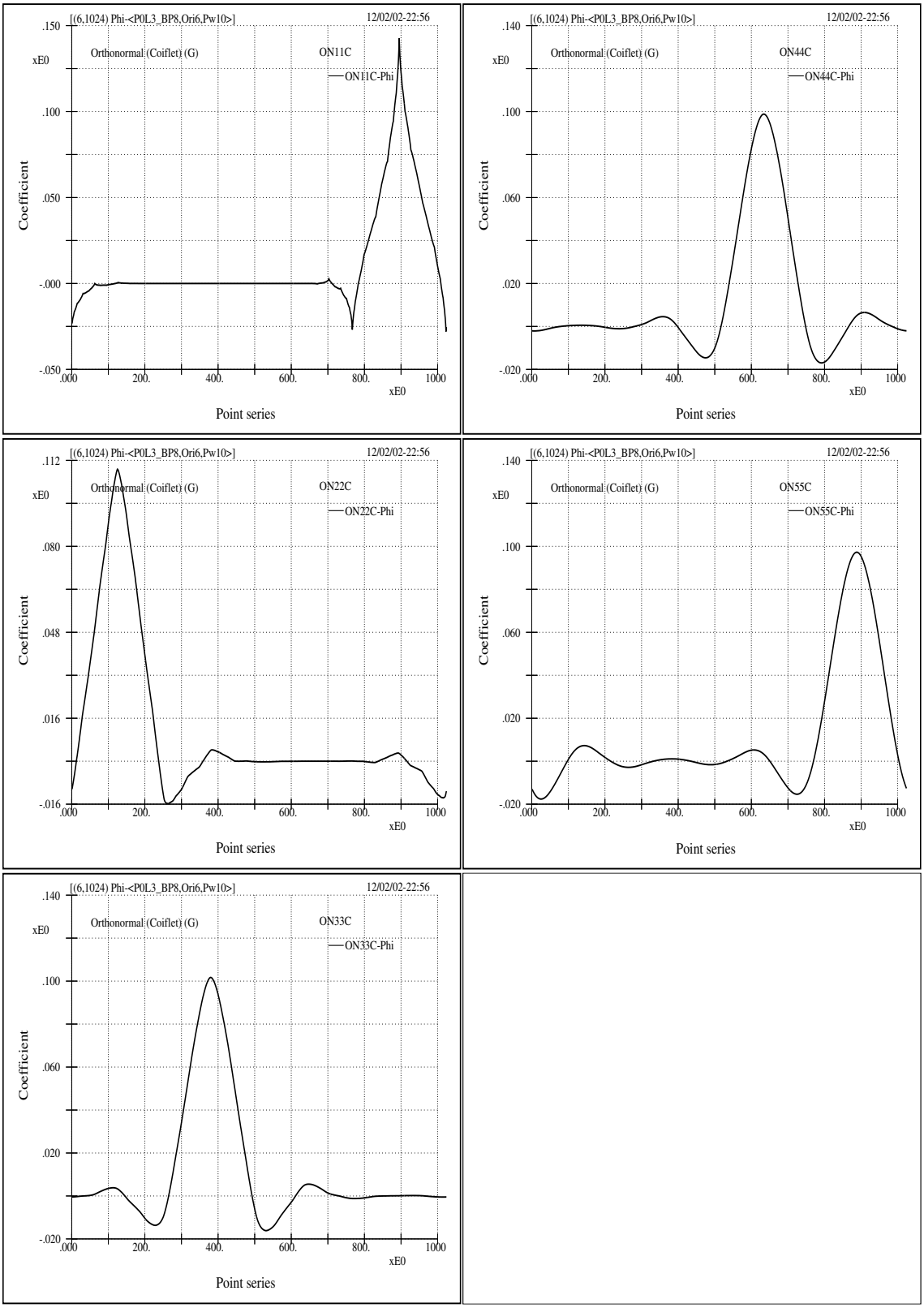

Fig 2.12 (FW–ONxxC) The father wavelets of the Coiflet wavelet group ONxxC are shown here. Each curve is the inverse transform of a unit value located at point 6 (at a scale level less than or equal to 3) for a 1024-point data. Again, the separation point between "smooth information" and "detail information" is chosen at point 8.

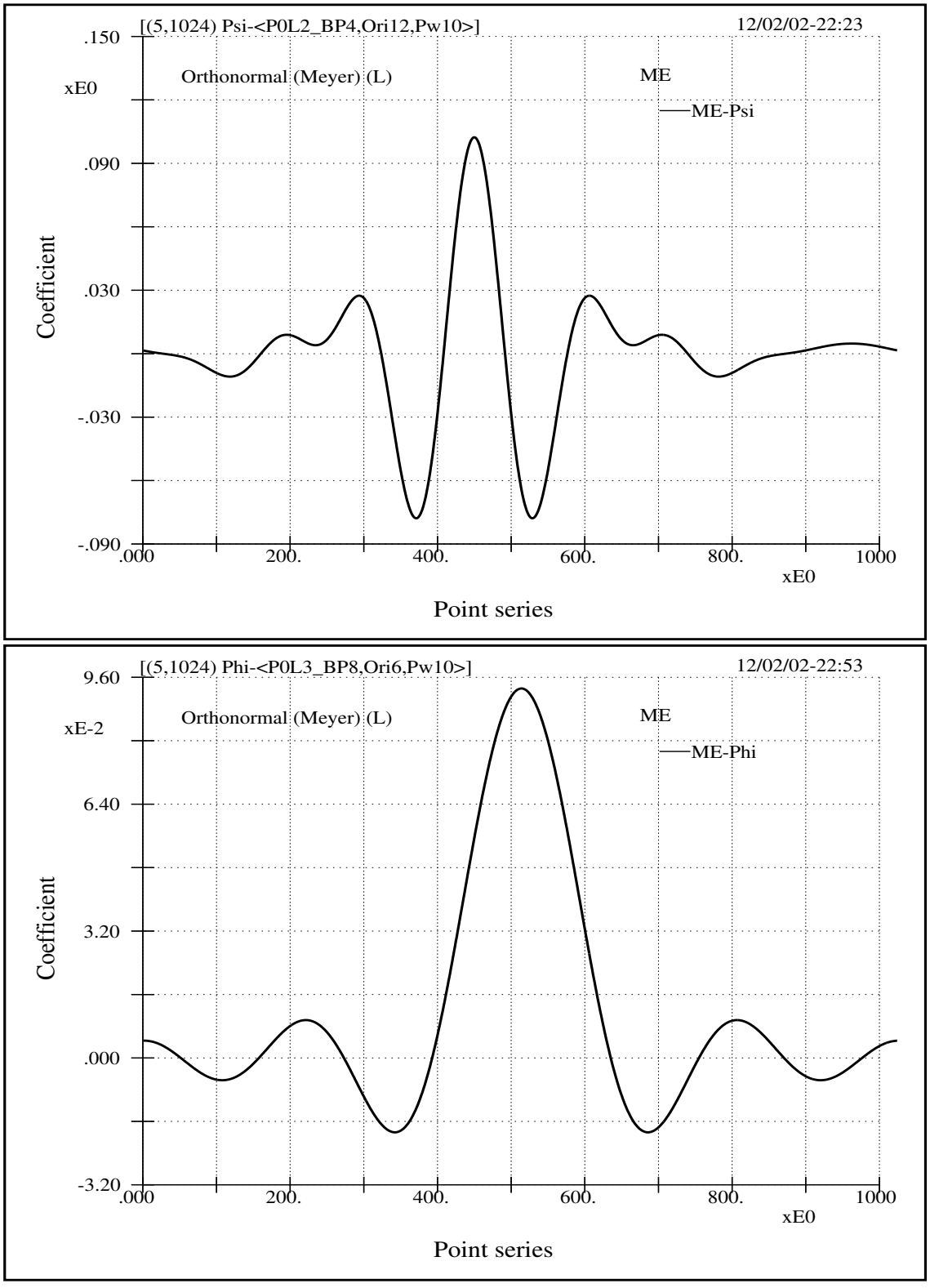

Fig 2.13 (MFW–Meyer) The mother (`top`) and farther (`bottom`) wavelets of the Meyer wavelet corresponding to the point location at 12 and 6, respectively, based upon the separation boundary point of 8 on level 3. It is noted that this figure is to be compared to the next one.

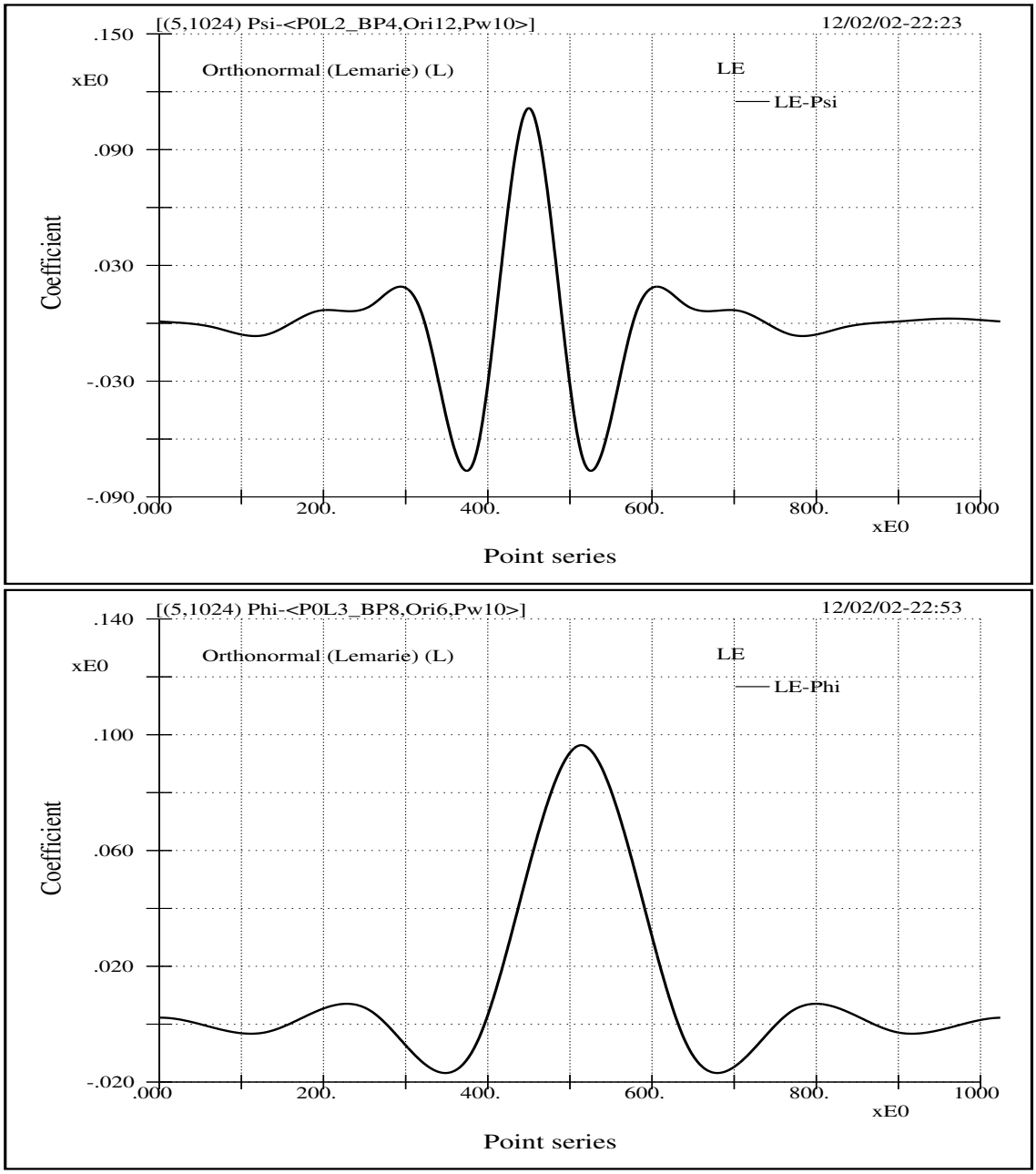

Fig 2.14 (MFW–B&L) The mother (top) and farther (bottom) wavelets of the Battle and Lemarié wavelet corresponding to the point location at 12 and 6, respectively, based upon the separation boundary point of 8 on level 3. Comparing the wavelet functions shown here with those shown in the preceding figure (figure 2.13 (MFW–Meyer)), we note the following interests. Firstly, these two different wavelets have quite similar looks, but they are associated with quite distinctive theoretical constructions and analytic properties, such as regularity, differentiability, rate of decay, support length, etc. Secondly, many intricate and complicate aspects among the discrete Riesz wavelet bases may have difficulty in their realization of practical usages, that is to say, mathematical complexity generally does not reflect our concerns about physical applications. Thirdly, water wave analysis concerns about physics, but a pure data analysis concerns only about mathematics. The important question is what is to be chosen to yield the most appropriated physics.

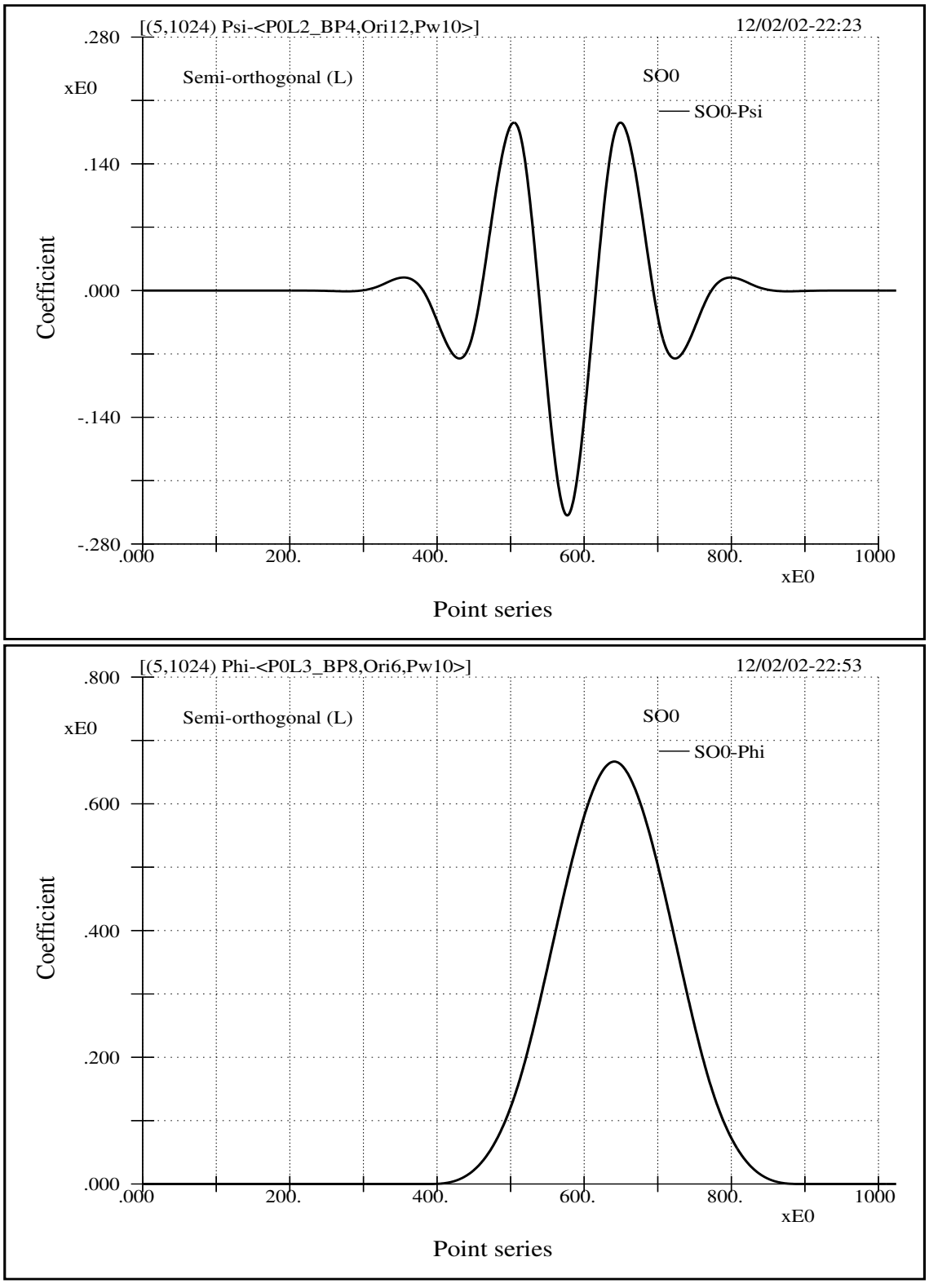

Fig 2.15 (MFW–SO0) The mother (`top`) and farther (`bottom`) wavelets of the semi-orthogonal wavelet designed by Chui (SO0) [6, 7]. The curves correspond to the same location points of 12 and 6. It will be shown that this wavelet possesses very important properties pertaining to the optimal modeling of water waves.

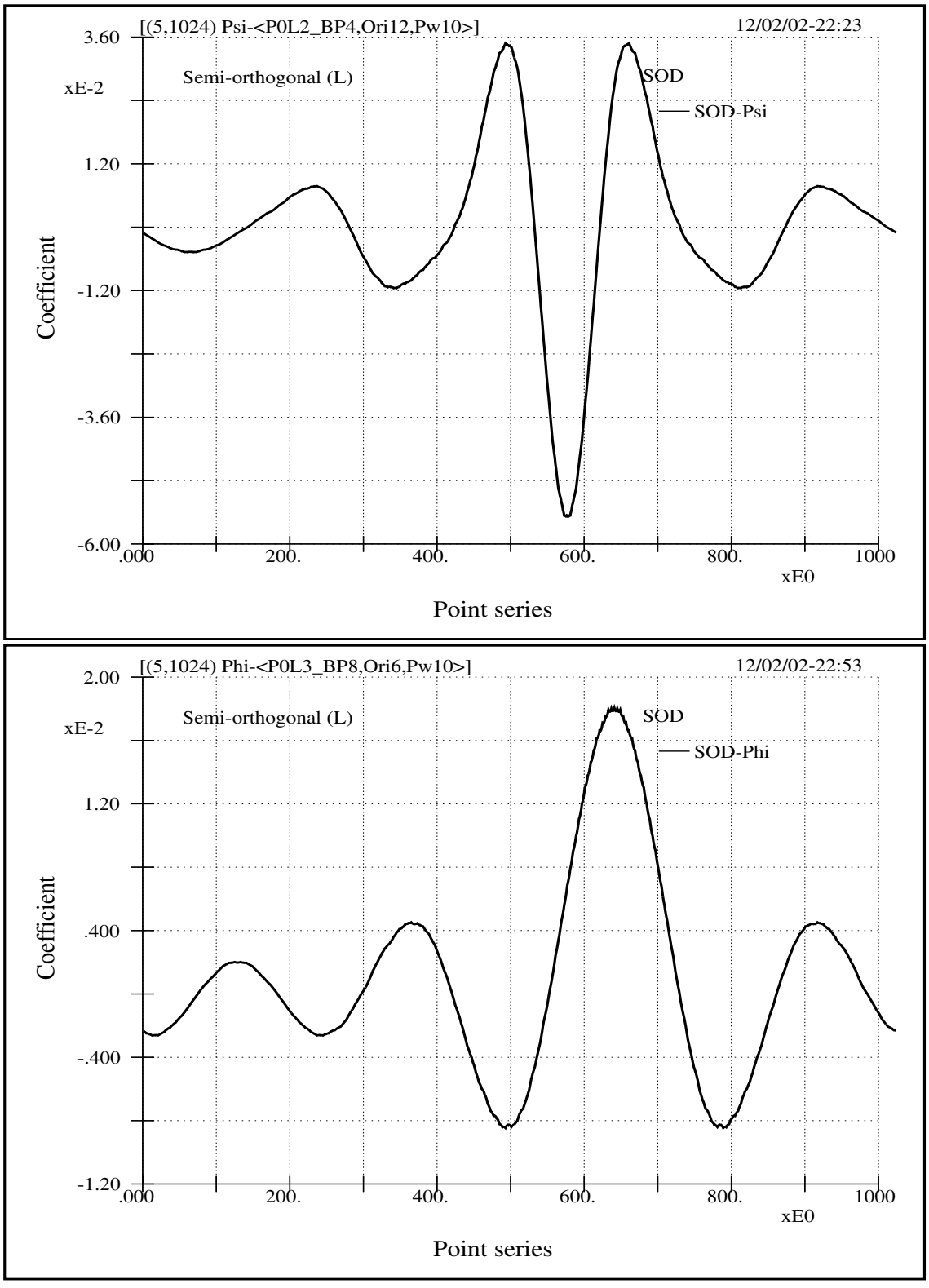

Fig 2.16 (MFW–SOD) The mother (`top`) and farther (`bottom`) wavelets of the dual of Chui's semi-orthogonal wavelet (i.e., SOD, the dual wavelet of the wavelet SO0 used in the preceding figure). Again, the curves correspond to the same location points of 12 and 6.

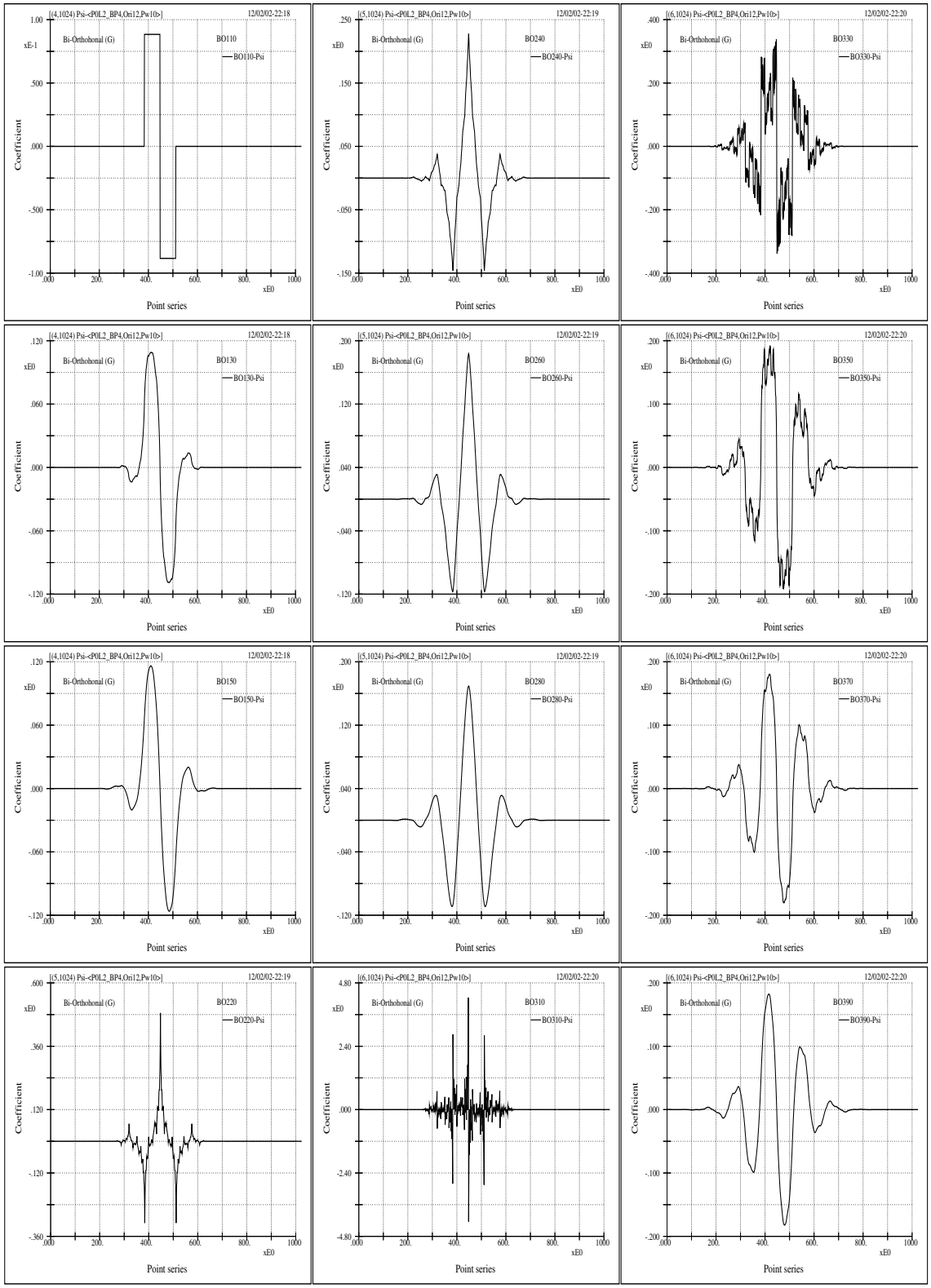

Fig 2.17 (MW–BOxy0) The mother wavelets of the bi-orthonormal wavelet group BOxyO are shown here. Again, the separation point between "smooth information" and "detail information" is chosen at point 8. And the inverse transforms are associated with location point 12. The fractal complexity of the curves depends on the configuration of the numbers of x and y.

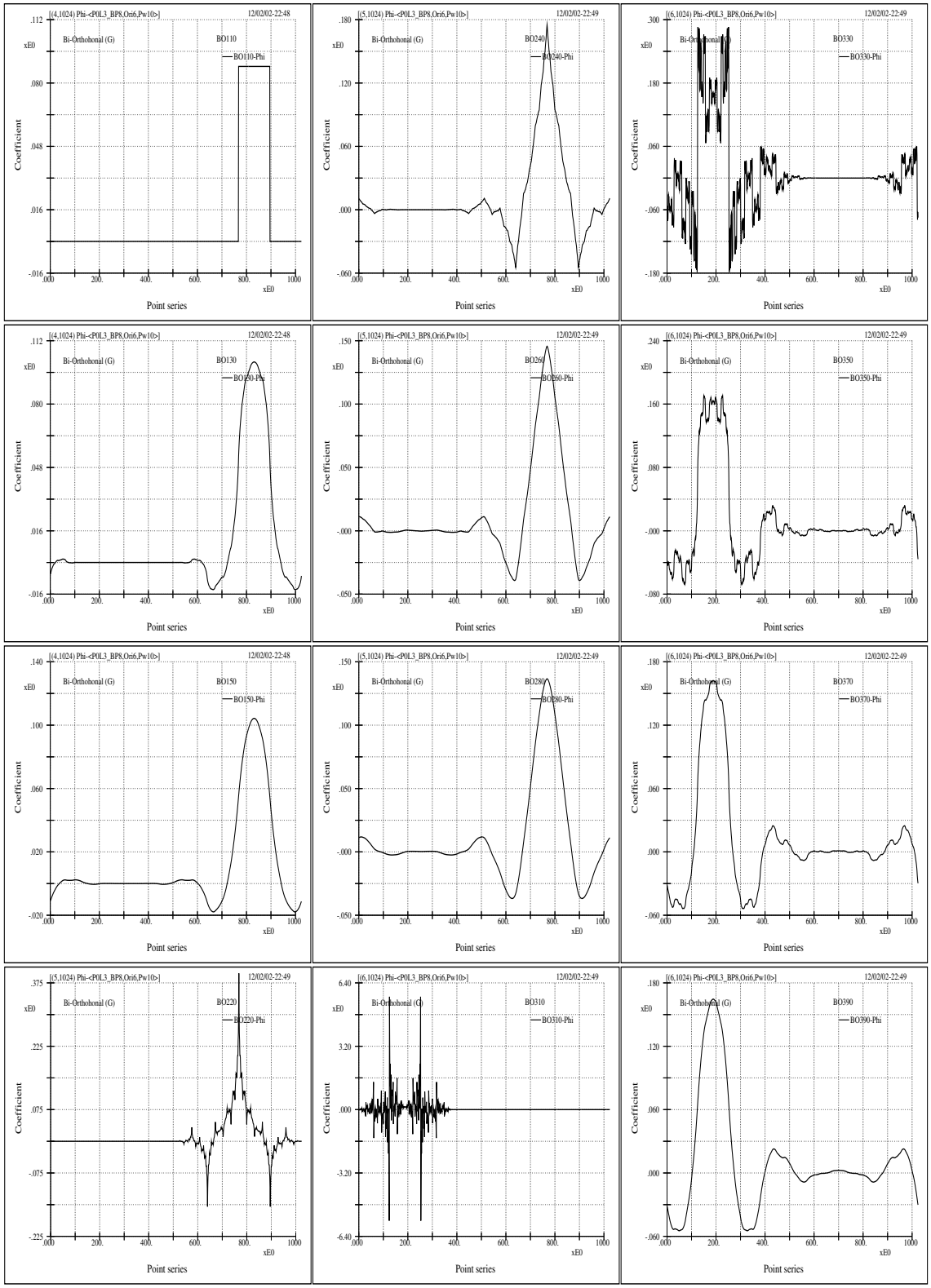

Fig 2.18 (FW–BOxy0) The farther wavelets of the same bi-orthonormal wavelet group BOxyO. The same separation point between "smooth information" and "detail information" is chosen at point 8. And the inverse transforms are associated with location point 6. Again, the fractal complexity of the curves depends on the configuration of the numbers of x and y.

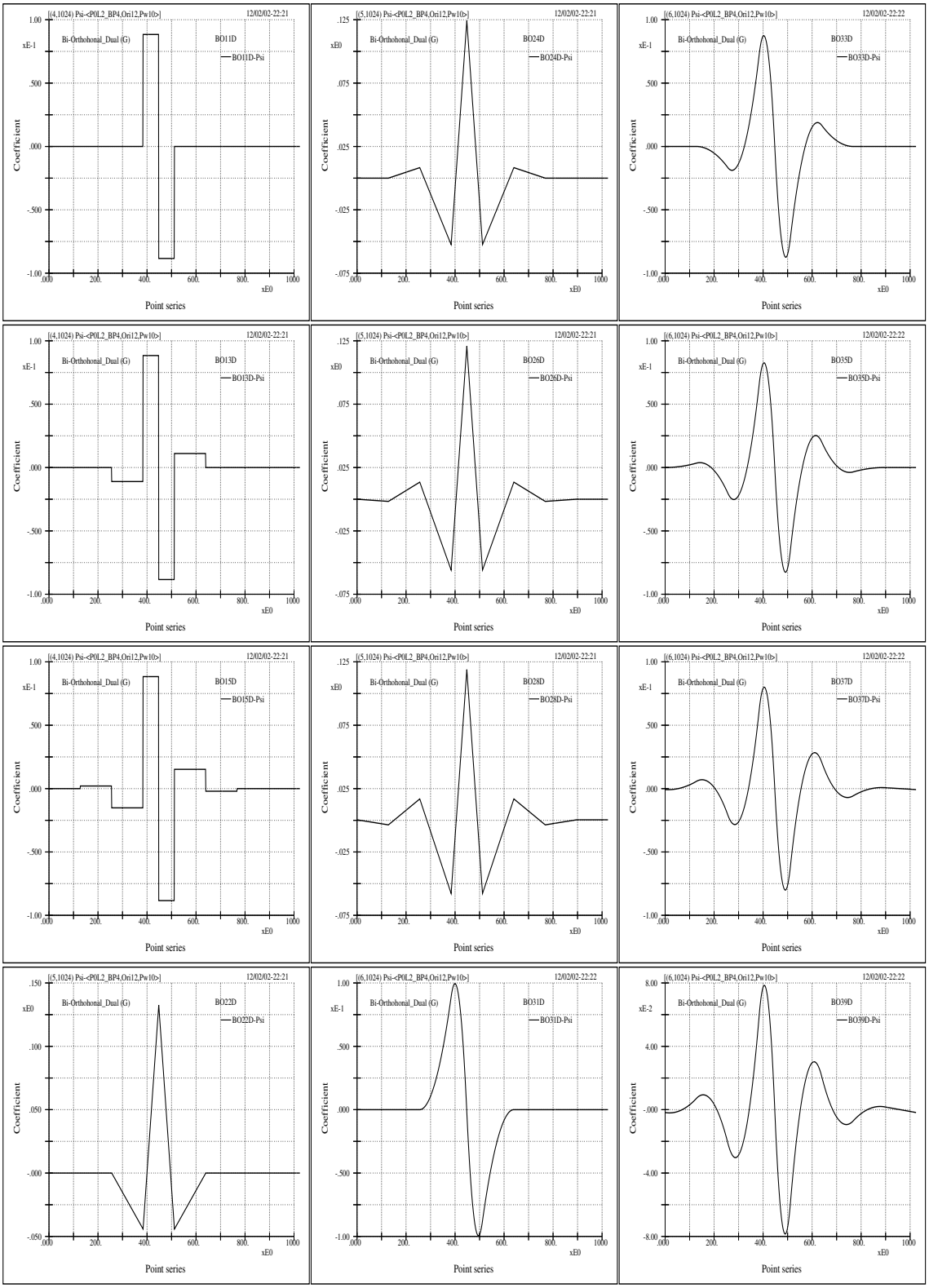

Fig 2.19 (MW–BOxyD) The mother wavelets of the dual bi-orthonormal wavelet group BOxyD. These curves are originating from the same point at 12. The fractal complexity of these dual wavelets shows much less extreme.

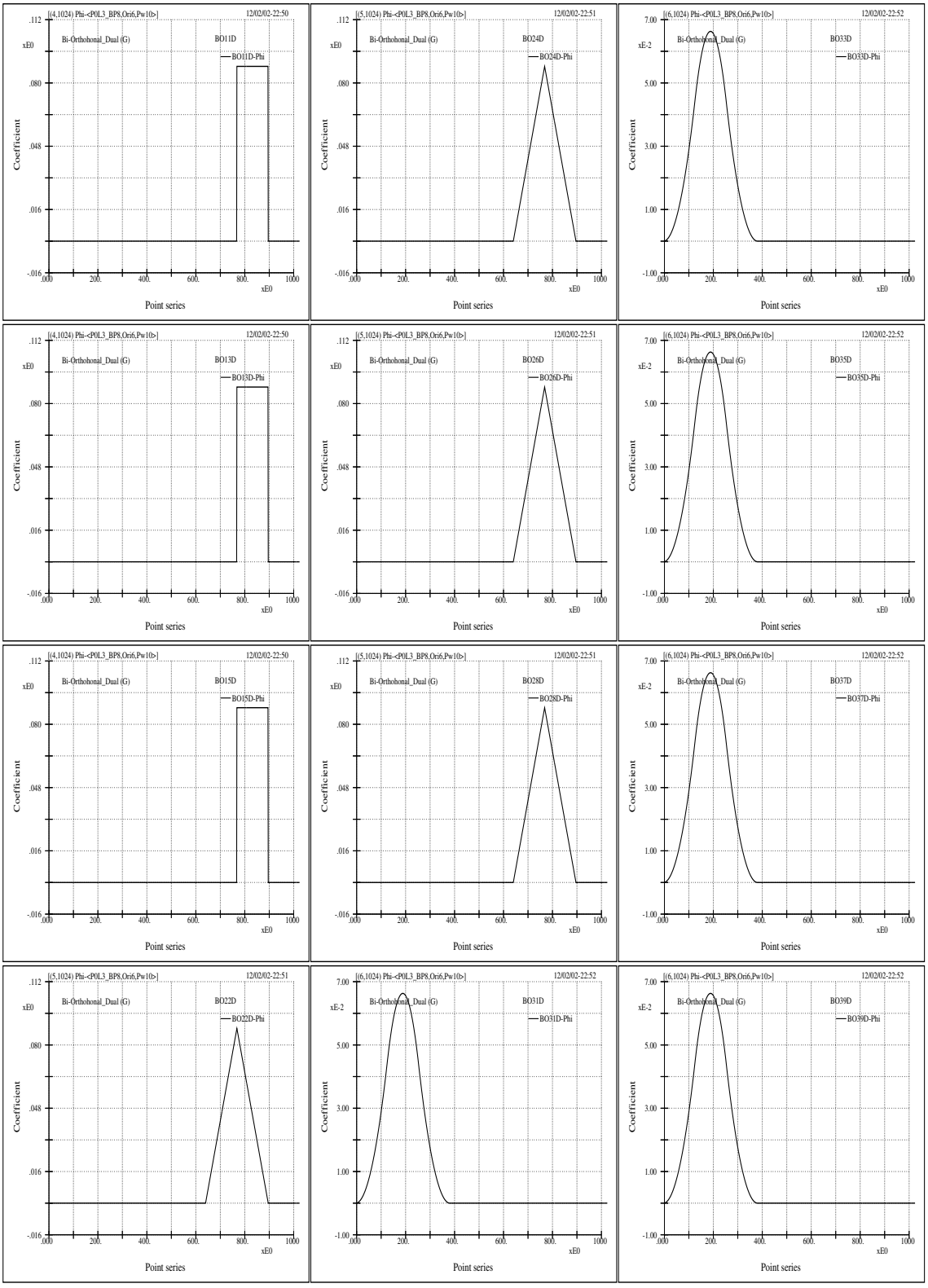

Fig 2.20 (FW–BOxyD) The farther wavelets of the dual bi-orthonormal wavelet group BOxyD originating from the same point at 12. The fractal complexity of both the mother and the father wavelets of these dual are much less extreme.

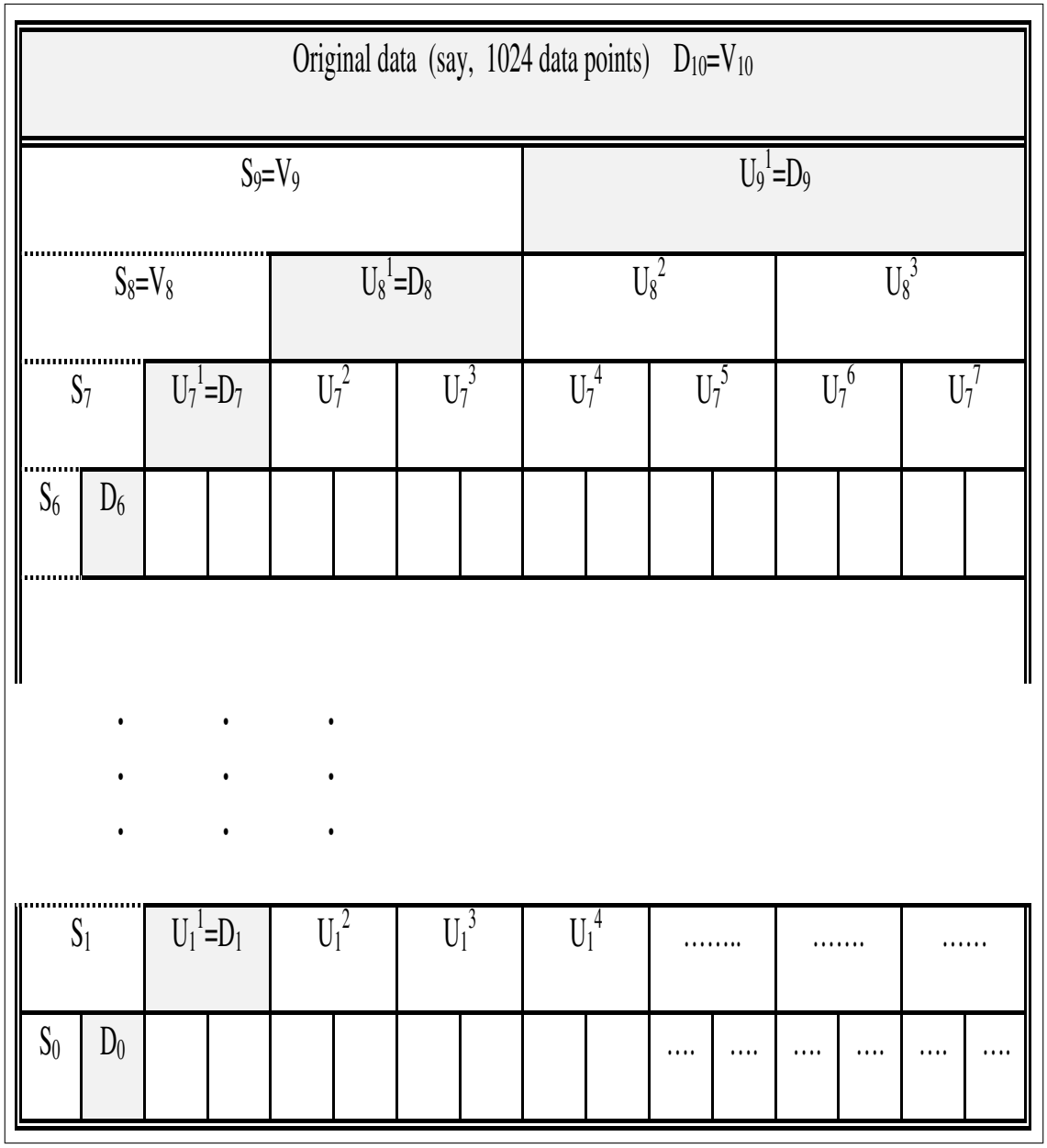

Fig 2.21 (WP Tree) The wavelet packet transform can be represented by this schematic representation of the tree-like structure of decomposition associated with orthonormal wavelets. Different branch compositions yield different transforms. Besides, a sub-root branch can be associated with either the same or different wavelet. The constructs are basically unlimited. Here the schematic notations S (or *V* in the text) and D stand for smooth and detail information, respectively. The U with superscript larger than 1 stands for further decomposition of D by wavelet packets. And all subscripts of U and D mean scale levels. Besides, the superscript of U means relative location of a specific frequency band within its compatible subscript (or scale level).

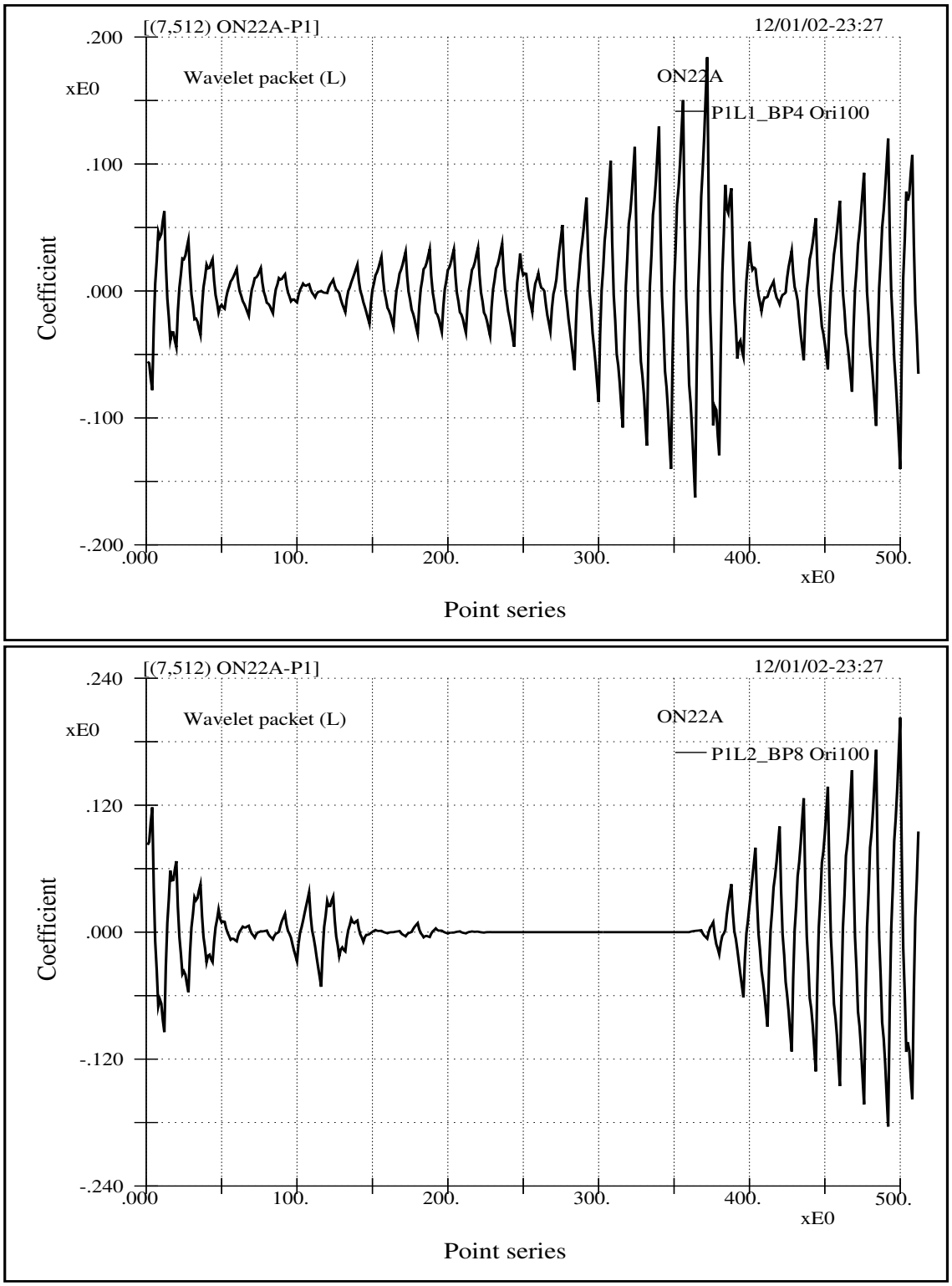

Fig 2.22 (WP forms) This figure depicts the wave forms of two wavelet packets based upon ON22A and associated with the same location point 100 at different scale levels 2 and 5, with boundary point at 8 and 64, respectively. It demonstrates the typical bundled shape of distribution of wavelet packets as compared to wavelet.

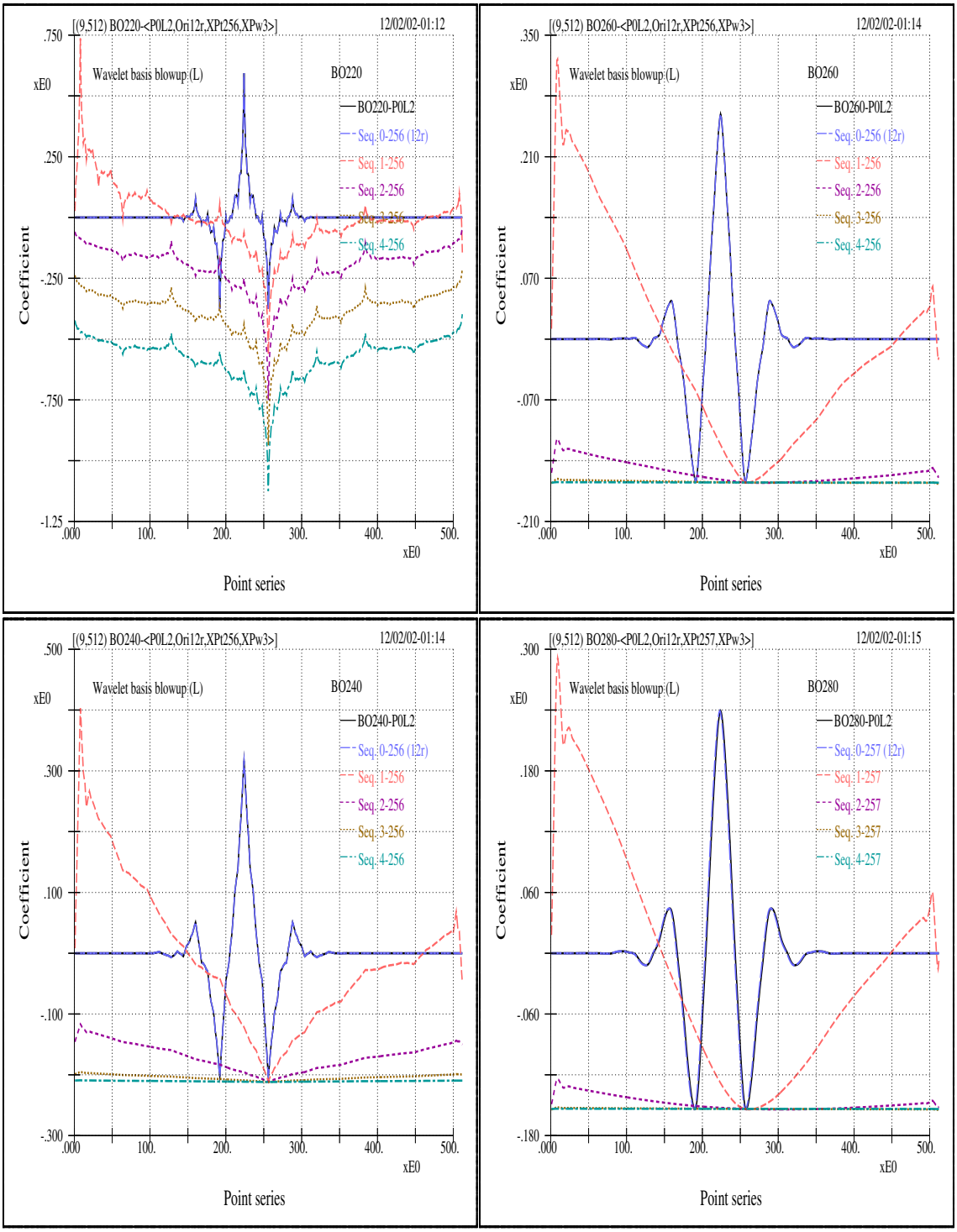

Fig 2.23 (BU–BO2yO) Wavelet's fractal nature across scales is demonstrated in various previous figures, but here the property is more appropriately shown by blowing up the wavelet at any fixed point. The curves shown here are the blowups of wavelets related to the bi-orthogonal group BO2yO. The scale interval between adjacent blowups is 2^3. The location of the blowup point is labeled in individual sub-figure (such as point 256 or 257). The scale level (which defines the boundary point between smooth and detail information) and the unit value originating point for individual wavelet to be exploded are also indicated in the sub-figures (such as L4 and Ori12).

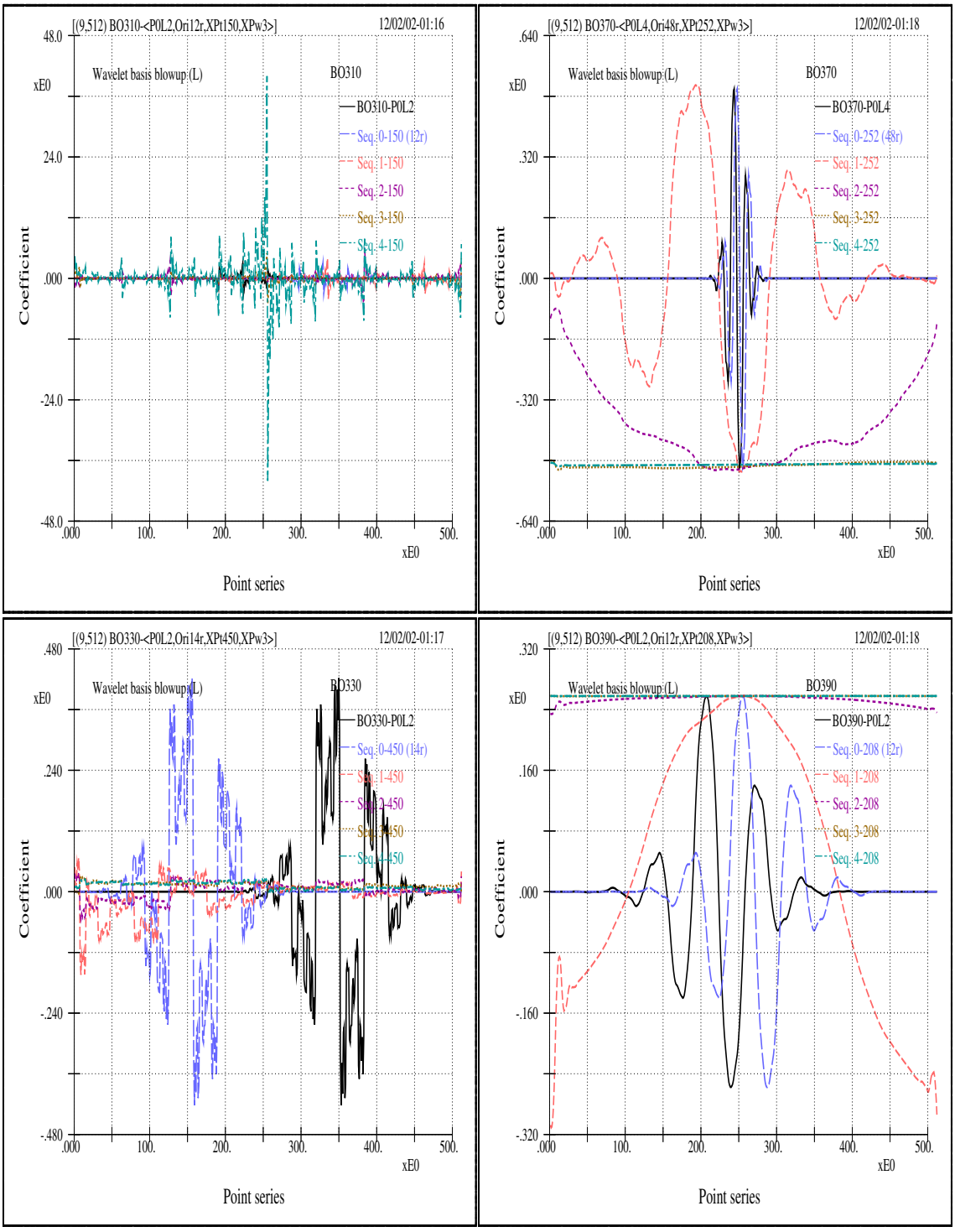

Fig 2.24 (BU–BO3yO) The blowups of wavelets related to the bi-orthogonal group BO3yO. The scale interval between adjacent blowups is 2^3. The location of the blowup point is labeled in individual sub-figure (such as point 150, 450, 252 and 208). The scale level and the unit value originating point for individual wavelet are indicated in the sub-figures (such as L2, L4 and Ori12, Ori14, Ori48, Ori12).

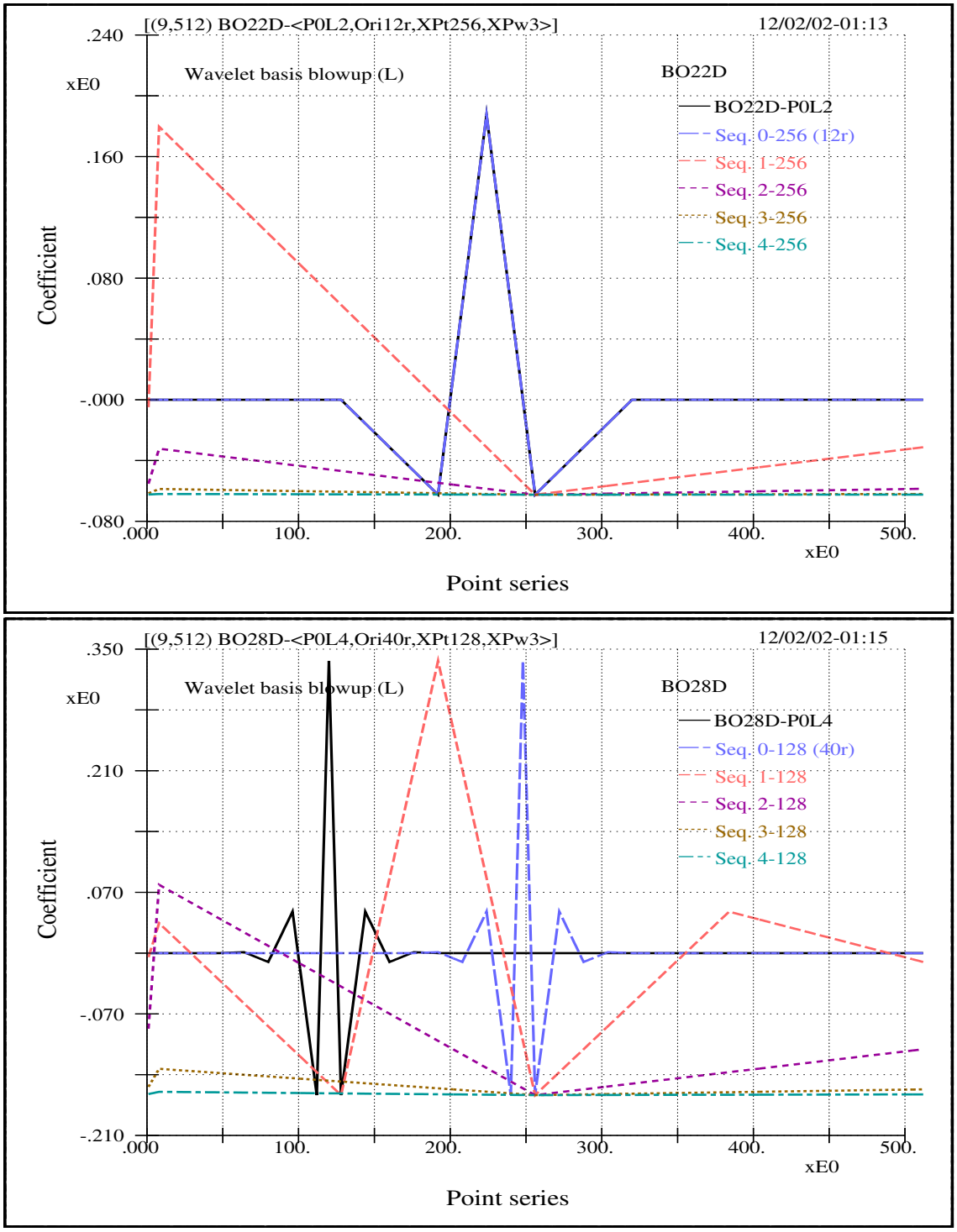

Fig 2.25 (BU–BO2yD) The blowups of wavelets related to the dual bi-orthogonal group BO2yD. The scale interval between adjacent blowups is 2^3. The location of the blowup point is labeled in individual sub-figure (such as point 256 or 128). The scale level and the unit value originating point for individual wavelet are indicated in the sub-figures (such as L2, L4 and Ori12, Ori40). In reference to the next figure, it is noted that the number of convolution weights play a part in the modeling entropy. And a too brief number of convolution weights generally yields quite unrealistic wave form.

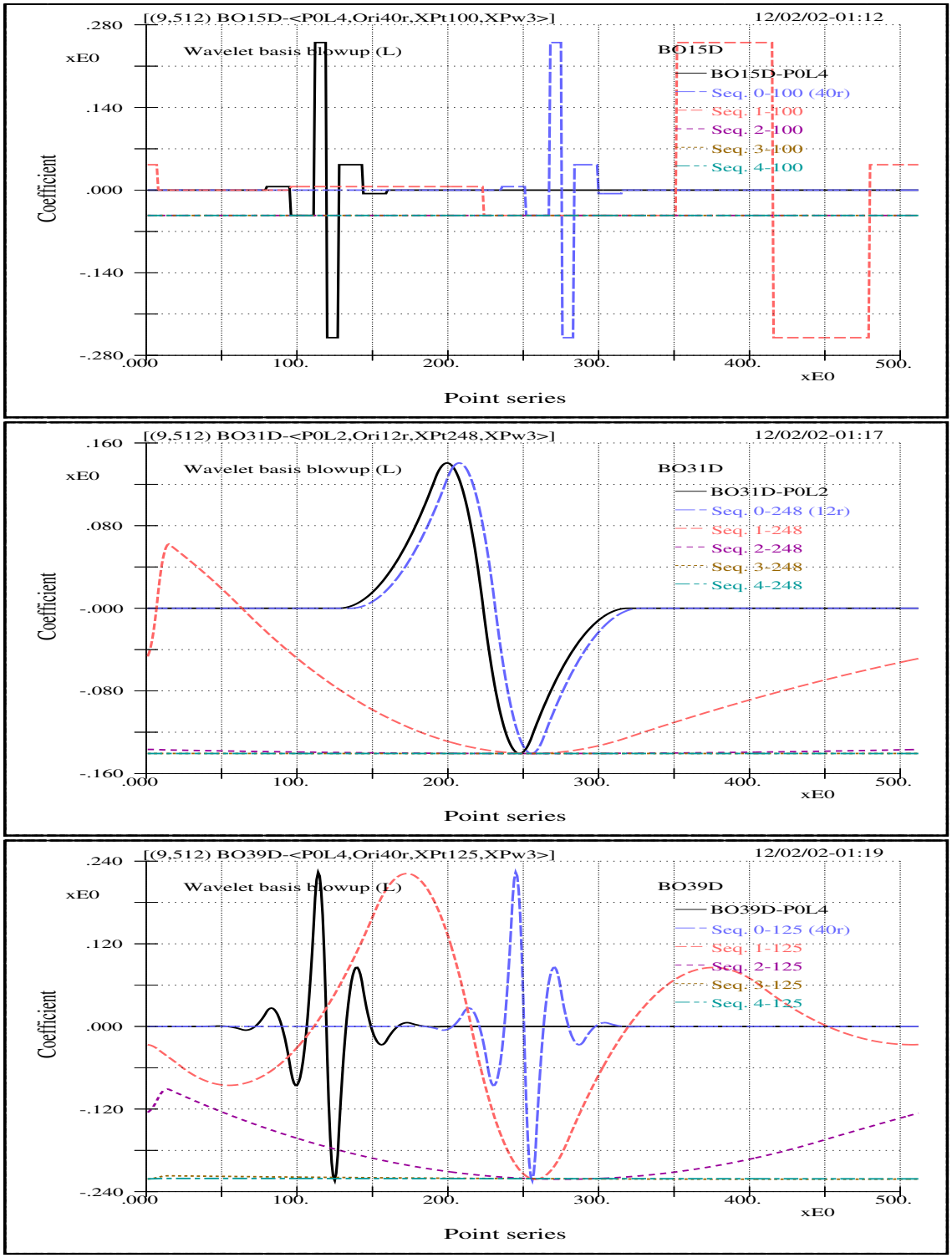

Fig 2.26 (BU–BO3yD) The blowups of wavelets related to the dual bi-orthogonal group BO3yD. The scale interval between adjacent blowups is 2^3. The location of the blowup point is labeled in individual sub-figure (such as point 100, 248, 125). The scale level and the unit value originating point for individual wavelet indicated in the sub-figures (such as L2, L4 and Ori12, Ori40). It is hinted here: comparing with the curve distributions of their counterpart group BO3yO, it is not hard to realized that the dual wavelet yields better modeling entropy as will be shown in later chapter.

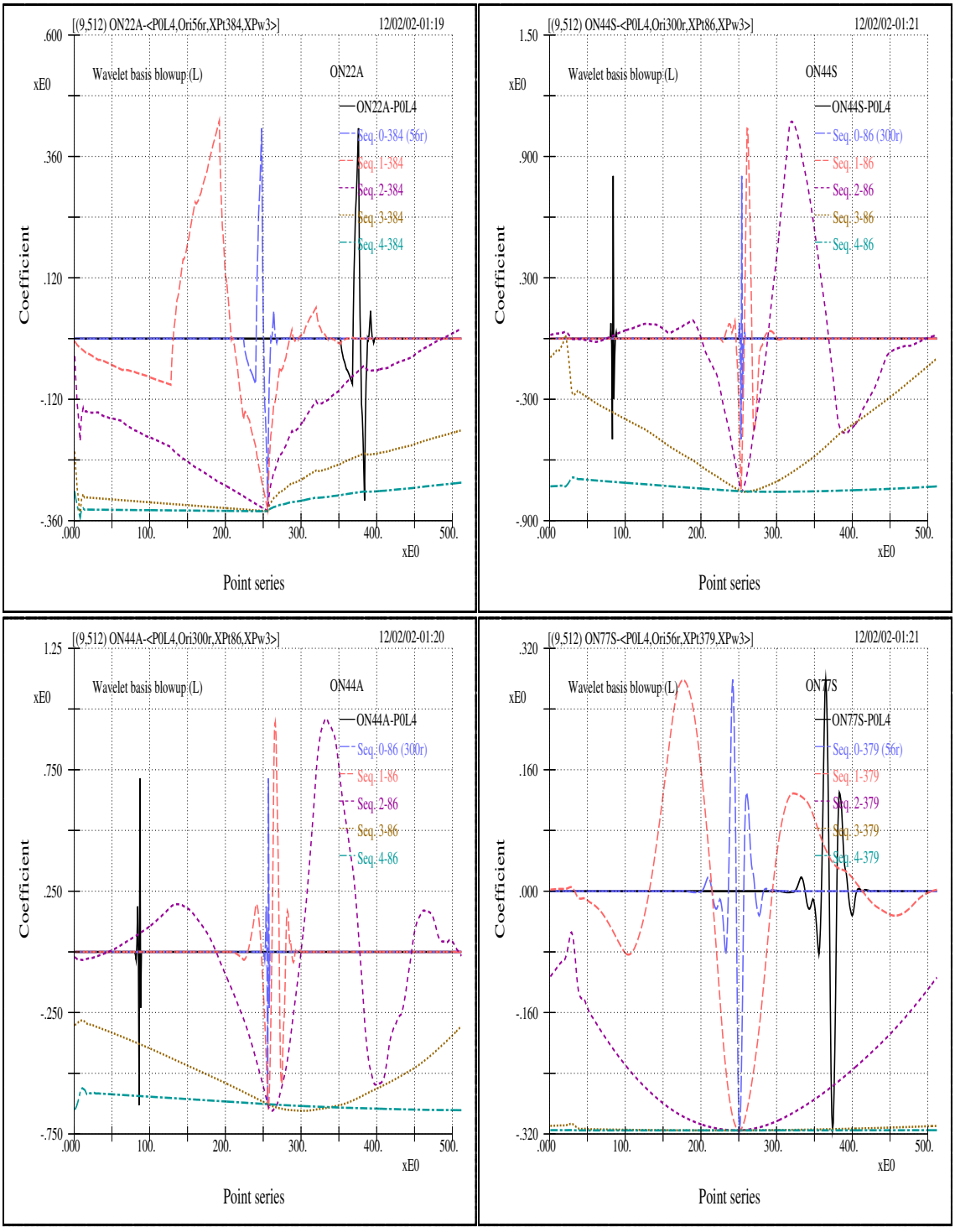

Fig 2.27 (BU–ONxAS) The blowups of wavelets related to the most asymmetric and the most symmetric orthogonal groups ONxxA and ONxxS. The scale interval between adjacent blowups is 2^3. The location of the blowup point is labeled in individual sub-figure (such as point 384, 86, 379). The scale level and the unit value originating point for individual wavelet indicated in the sub-figures (such as L4 and Ori56, Ori300). Again, it is noted that a too brief number of convolution weights yields quite unrealistic wave form.

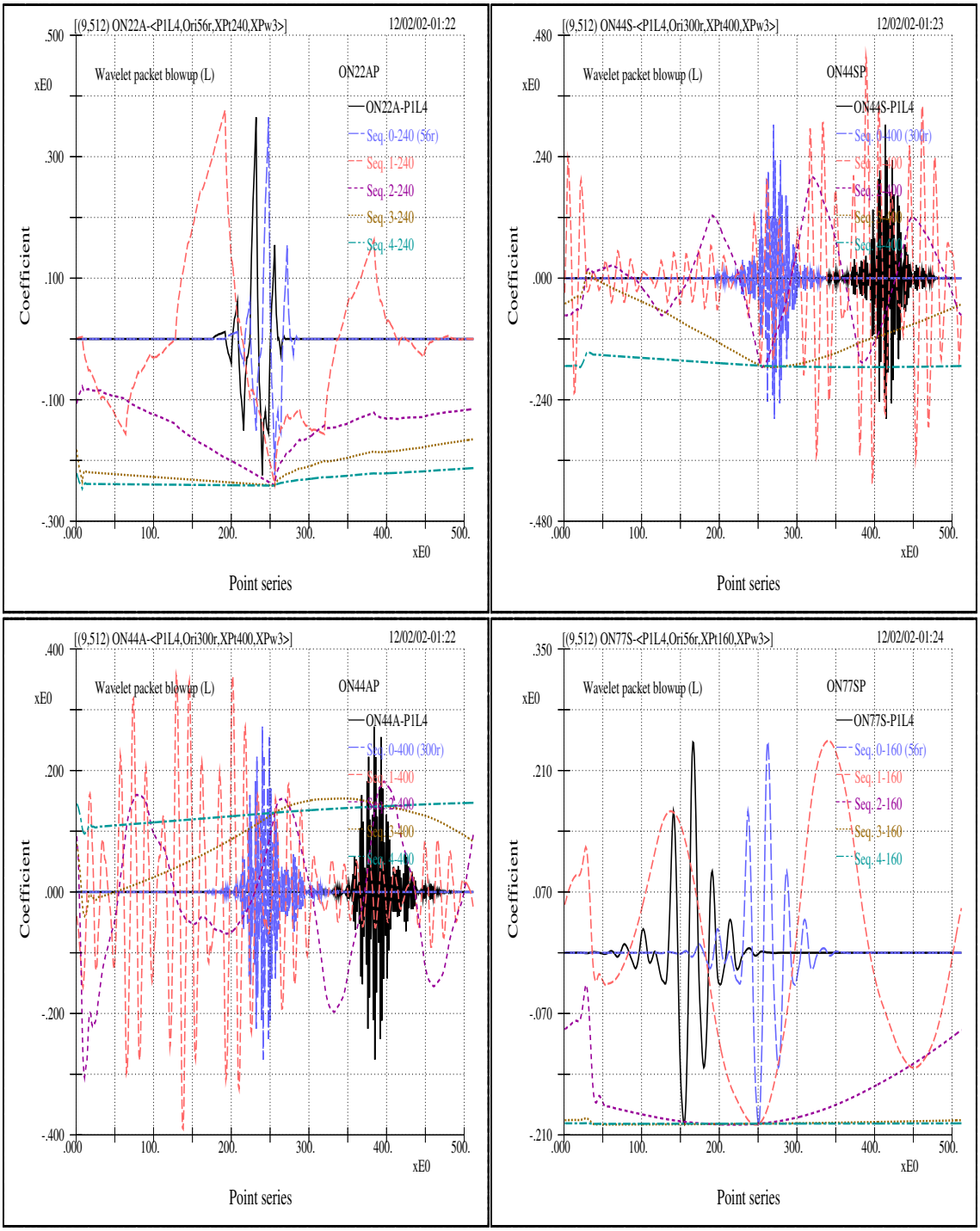

Fig 2.28 (BU–WP-ON) This figure shows the wavelet packet blowups related to the most asymmetric and the most symmetric orthogonal groups ONxxA and ONxxS. In reference to the preceding figure, it is easily comprehended that wavelet packet transform is even more unrealistic for modeling water waves. This is one, and an intuitive and visceral one, of the reasons why in the later chapter we don't bother calculating the entropy of any wavelet packet. Again, the scale interval between adjacent blowups is 2^3. The location of the blowup point is labeled in individual sub-figure (such as point 240, 400, 300, 56). The scale level and the unit value originating point for individual wavelet indicated in the sub-figures (such as L4 and Ori56, Ori300).

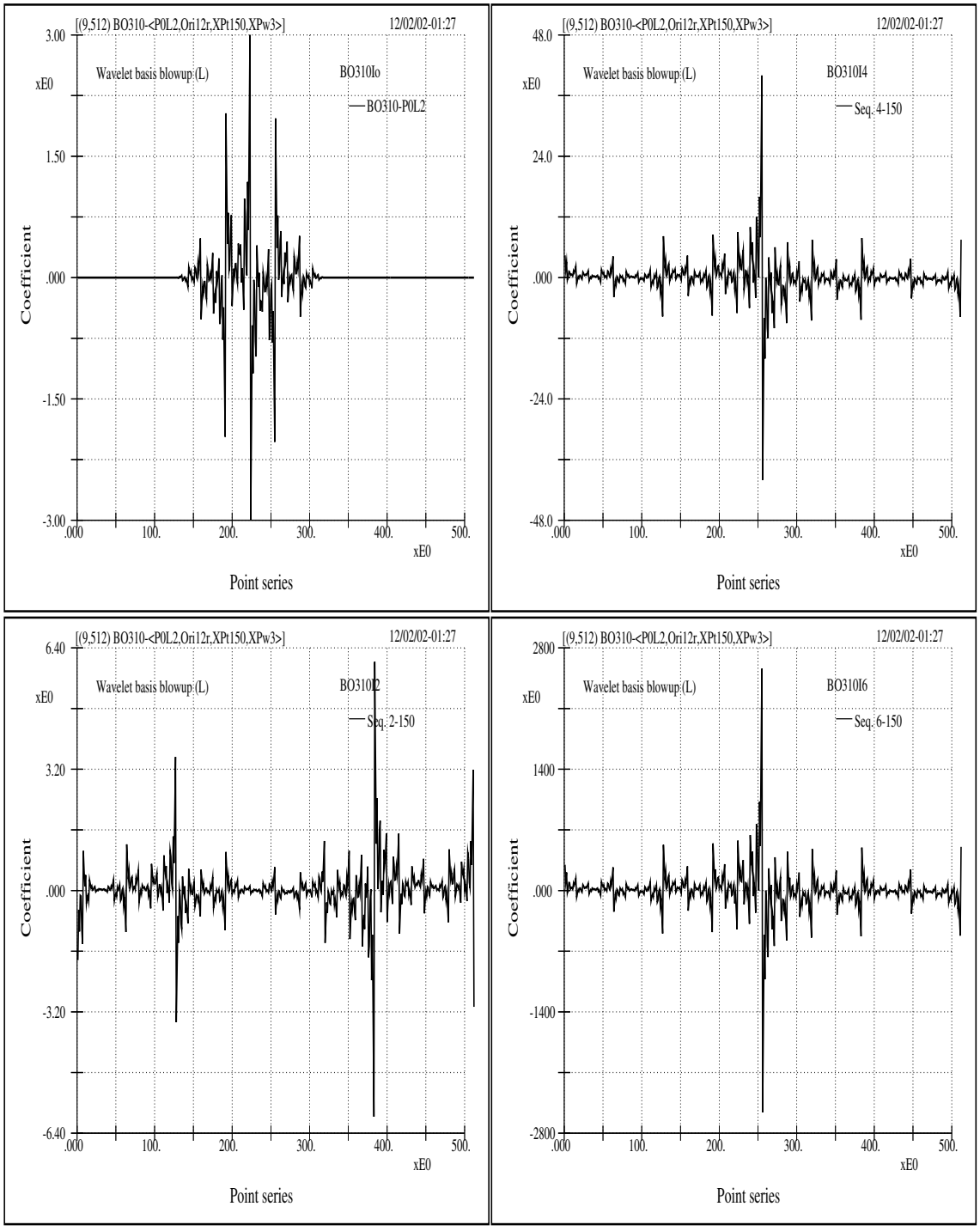

Fig 2.29 (BU–BO31O) The successive blowups of the bi-orthogonal BO31O wavelet at point 150 for scale level L2 and unit value originating point Ori12. Here the scale interval between adjacent sub-figures is 2^6. Note the vast difference in the ordinate axis. The phenomenon is related to the numerical demand of precision that is associated with a too brief number of convolution weights, as well as with its wavelet category.

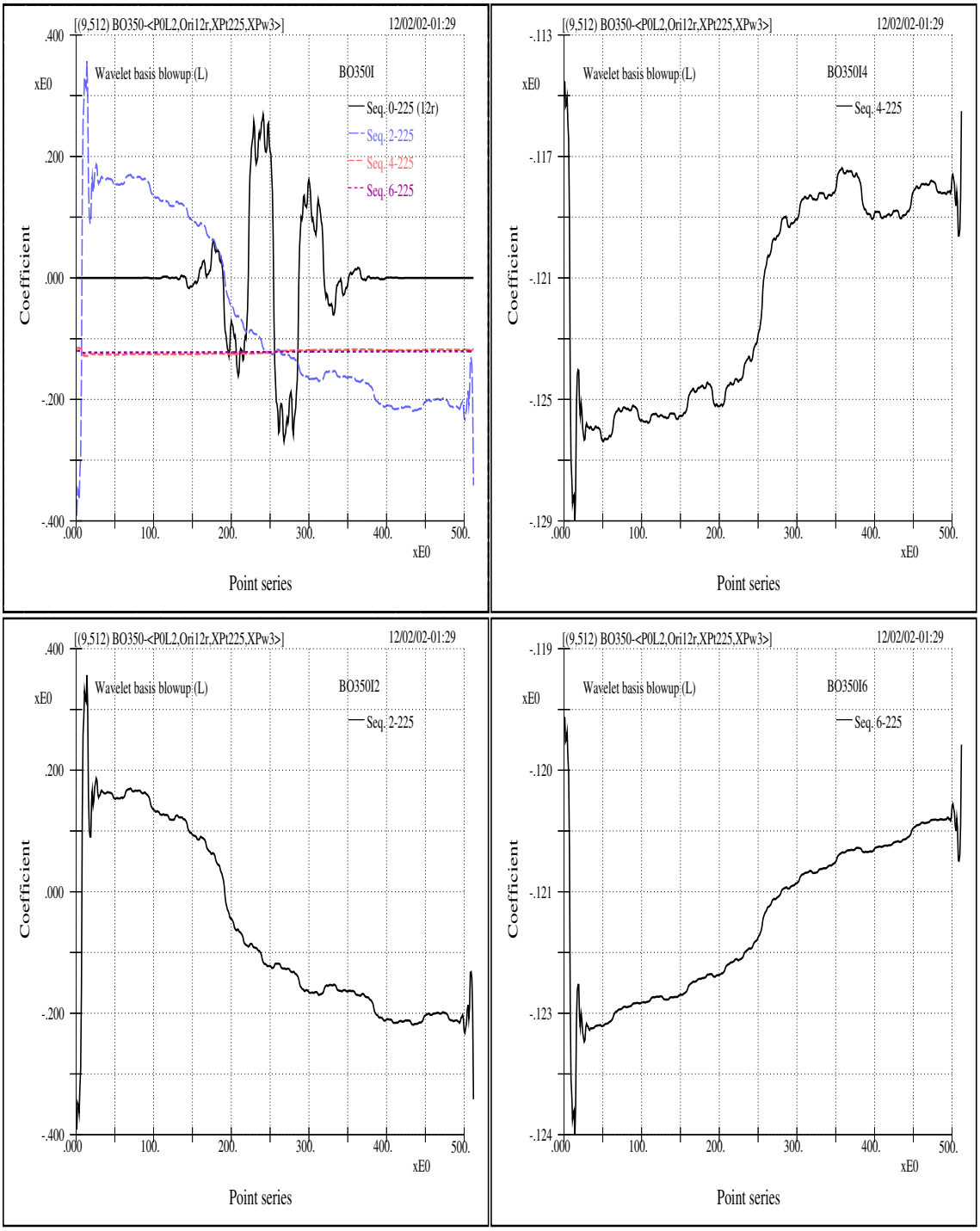

Fig 2.30 (BU–BO35O) The successive blowups of the bi-orthogonal BO35O wavelet at point 225 for scale level L2 and unit value originating point Ori12. Here the scale interval between adjacent sub-figures is 2^6. Note the completely opposite inclination of the distribution curve between adjacent sub-figures. Again, the phenomenon is related to a brief number of convolution weights, as well as the wavelet category. Overall, here it is hinted that there are many fancy wavelets but, for water wave physics, fancy sometimes is only an illusion.

Chapter 3

The Entropies and the Best Discrete Wavelet Basis

3.1 Entropy's physical pertinence

In studying the physics of certain phenomena using wavelets one of the most intriguing questions is how to choose the analyzing wavelet(s). The concern here is quite in contrast to those studies where they are mainly numerically or analytically oriented. For example, in coding of images or acoustic signals the goals are straightforward: the maximum compression with minimum handling, the highest effectiveness with lowest distortion, and the most distinctiveness with lest aberration; under such circumstances mathematical relevance between signal and wavelet can be materialized much more explicitly than physical pertinence needs to be unfolded for our applications.

By and large from this point of view, for our interests in characterizing the physics of water-wave related phenomena, it seems, at first, that the aspiration is not on 'efficiency" or "compactness". However, with the understanding that, on the one hand, the compactness of a transform result means the closeness between signal components and analyzing basis functions, and that, on the other hand, the conception that basis function forms which do not look like our signals (or signal components) are obscured from intuitive perceptions of physics; it is naturally justified to seek the wavelet that provides the most efficient or most economical representations for our signals. Still, at the end we are

bringing back to the concept of entropy — the most efficient representation — different disciplines but with the same objective.

The exploits in this chapter are mainly numerical experiments on measuring the "distances" between our signals and various Riesz wavelet bases given in several wavelet treatises [6, 12, 29, 31]. No attempt to make new constructions of bases or to extend the existing constructions is made. Nevertheless, we have tried to include various categories of Riesz wavelets with a comprehensive coverage of analytical properties. And we will come to realize that there is really no need to extend the existing constructions if the associated two-scale scaling function or father wavelet is not changed, that any other individual wavelet in literature falls within our characterizations, and that a few fractal-oriented sparse wavelets [28, 26] are just as impractical as they may be in our applications.

The wavelets tested are dyadic wavelets with "mathematical sampling rate" 1 (no unit). They possess the most practical interest and easiness in applications for discretely sampled signals. Furthermore, we restrict our scope to laboratory water waves. Various criteria are used for the entropy statistics of discrete transform coefficients, including Fourier coefficients.

3.2 The entropy criteria

Entropy is a terminology in the statistical field, thus it gives indication without absolute assurance. And the entropy can be viewed as a measure of the "distance" between the original signal and its reconstructed signal using partially truncated transform coefficients. To avoid the somewhat mystified notions as one might get from some of the available readings, it may be better to give straightforward descriptions by going through the actual numerical process first and returning to its statistical implication later.

Let suppose that we have a 1024-point sampled data, then there is a set of 1024 wavelet coefficients (C=$\{c_i\}$). Take the absolute or squared value of these coefficients, sort them, and then divide the sequence into M (say, 100 or 200 or 300) divisions which are equally

spaced from 0 to the maximum value of the coefficients. Then we have the statistics of occurrence for each division, and the distribution of these normalized occurrences is the probability density distribution or probability density function (denoted by pdf), say $\{p_1, p_2, \cdots, p_{M-1}, p_M\}$. The entropy is

$$H(p) = -\sum_i p_i \log p_i. \tag{3.1}$$

Where, when $p_i = 0$, it is assumed that $0 \log 0 = 0$, since in reality one can assumed that there exists an almost zero probability in that interval without affecting the total sum of probability, after all it is only a statistics and the modification virtually has no influence on the norm value. If absolute values of c_i are taken, $H(p)$ is the L^1-norm entropy; if squared values are taken, it is squared L^2-norm entropy. Of course another power can be used, but the squared L^2-norm, being the energy, is physically the most significant. The practical aspect of this definition of entropy is: let suppose two probability distribution functions sorted in a decreasing order are p and q, if p decreases faster than q, then $H(p) \leq H(q)$ [34]. The above inequality of entropy is only one-way correct and the reverse is not always true, but smaller entropy implies that more energy is concentrated within a smaller number of wavelet coefficients. Therefore, if only a fixed percentage of coefficients is kept, the truncated error, i.e., the distance from the total sum, is likely to be smaller for set of coefficients with smaller entropy

There is another notion, sometimes referred as the geometric notion [34], for calculating the entropy. Again, the procedures is given first and the simple physical interpretation next. By setting the number of divisions to be the same as the number of coefficients and by defining probability density to be the normalized (with respect to the total power) value of the squared wavelet coefficient, that is to say, the total energy is $\|C\|^2 = \sum_i |c_i|^2$ and the probability density is $p_i = |c_i|^2/\|C\|^2$, we get the alternative form of entropy by

substituting P_i into Equation 3.1:

$$H(p) = \log \|C\|^2 - \frac{\sum_i |c_i|^2 \log |c_i|^2}{\|C\|^2}. \tag{3.2}$$

The notion here is simple: if one just put more weight on coefficients of small energy and less weight on coefficients of large energy (all coefficients being normalized), then the weighted energy is an indication of entropy. And since taking the log of a value is sort of a weighting operation and since the total energy is finite, small entropy therefore means that the number of significant coefficients is small, or stated otherwise, more energy is concentrated in fewer coefficients.

One equivalent indicator of entropy of a pdf is the theoretical dimension $D(p)$ and is defined as [34]

$$D(p) = e^{H(p)} = \prod_i \left(p_i^{-p_i}\right). \tag{3.3}$$

As was stated, entropy does not tell how conclusive the result is. But our numerical results yield little ambiguity regarding the judgement that we can make.

3.3 The ultimate best discrete basis

To increase the definiteness of the comparisons, we calculate entropy based on several setups: direct coefficient entropy related to L^2-norm based on Equation 3.3 (column 1 in Tables 3.1 (H–F+ON+SO) and 3.2 (H–BO0+D)), pdf entropy related to L^2-norm with 300 (column 2) and 200 (column 4) divisions, and pdf entropy related to L^1-norm based on Equation 3.1 (column 3). Theoretical dimension for one of the setups is also given (column 5). The tables show the results using a wind-wave signal from a wave tank experiment. It is noted that if the peak frequency (or the primary scale) of other signal is significantly different, then, to be consistent in comparison, the analyzed signal lengths and the sampling rates should be properly adjusted according to its peak frequency. This is because in the discrete wavelet transform we need to keep track of the actual physical size of translation

so as to have physical perception of the wave forms. Table 3.1 (*H*–F+ON+SO) give results from all orthonormal wavelets (including B&L, Meyer, ONxxA, ONxxS, and ONxxC), semi-orthogonal wavelets (Cubic B-spline, SO3O and SO3D), as well as from Fourier spectrum. Table 3.2 (*H*–BO0+D) give results from bi-orthogonal wavelets. Many distinctive features can be derived from the tables.

- The dual wavelet always gives much smaller entropy than as given by their counterpart wavelet. This certainly verifies that, for our water-wave signals, using

$$f(t) = \sum_{j,k} \langle f, \widetilde{\psi}_{j,k} \rangle \psi_{j,k} \tag{3.4}$$

  provides a much better efficiency in decomposition and reconstruction than using

$$f(t) = \sum_{j,k} \langle f, \psi_{j,k} \rangle \widetilde{\psi}_{j,k}. \tag{3.5}$$

  This also points out that dual wavelets rather than their counterpart wavelets should always be used as the decomposing basis for either better physical implications or improved computational efficiency. It may also worth noting that the practical shapes of all the listed bi-orthogonal wavelets, especially those with small x and y values, are visually quite unrealistical (such as those shown in figures 2.29 (BU–BO31O) and 2.30 (BU–BO35O)). Furthermore, for these bi-orthogonal wavelets, it can be concluded that there is going to be very little improvement by further extending the support width related to y without extending the support width related to x; since increasing the width (y) from some point on gives no effect on the shape of dual wavelets (such as $y = 7$ or 9 for $x = 3$) and since it is the dual, rather than the counterpart, wavelet that matters for better approximation.

- Entropy values of all orthonormal subgroups do not fall to the level of non-orthogonal ones. Besides, difference in entropy values of long and short supports can barely be differentiated, even though there seems to be a very slight indication that entropy

values related to longer support are somewhat smaller. Here the property reflects the role of linear phase filtering as mentioned earlier.

- Among all the orthonormal wavelets none distinguishes itself from the others. And we see no clear tendency within any subgroup. However, from the analytical point of view, the Meyer wavelet is infinitely differentiable or smooth, the B&L is second order differentiable, and the others have various degrees of differentiability or regularity [12]. It is therefore understandable that at the present stage many analytical properties of orthonormal wavelets are of little practical interests for our signals.

- The most striking result is that the dual Cubic B-spline wavelet yields a far smaller entropy value, even lower than that of the spectral coefficients. Figure 3.1 (p–W+WP+F) shows the comparisons of the cumulative probability distribution curves for several wavelet bases as well as for Fourier basis. This striking feature is reflected by the extreme flatness of the SO3D curve, nearly horizontal up until 90 percent of energy ratio. At about 96 percent of the energy ratio there is a crossing between spectral curve and the SO3D curve. These features practically imply that semi-orthogonal wavelet coefficients are better than Fourier coefficients in describing the details of the signals. Figure 3.3 (ReC–Signal) shows the reconstructions of a section of a signal from its spectral and SO3D wavelet coefficients of which 35 percent are kept. It is seen that the wavelet basis yields truer details than does Fourier basis. Again, the reasons for the SO3D's strong performance can be attributed to the following characters: total positivity of the scaling function and complete oscillation of the wavelet. That is to say, the scaling function has no oscillation or zero-crossing; the corresponding wavelet has no unnecessary oscillation, or no oscillation that is without zero-crossing. Physically, the two characteristics hint that our laboratory water waves are far less transient when compared with orthonormal or bi-orthogonal wavelets, and also imply that the description of waves based on suitable support length or life span is more likely to adhere to the physics.

- For the wavelet packet category we have the best basis and best level criteria. It may not be difficult to gain a prior idea that the chance is slim for getting better results using either of the bases. The obvious reason is due to the inherent limitation of wavelet packet transform — wavelet packet transforms are associated only with orthonormal bases. Since the primitive analyzing functions are orthonormal and since orthonormal wavelets perform poorly as just given above, it is therefore hard to anticipate the same strong performance as that of semi-orthogonal wavelets. Nevertheless, both wavelet packet criteria do show improvements when compared with the original orthonormal basis, and the performance of the best basis is certainly better than that of the best level. Figure 3.1 (p–W+WP+F)–(b) gives the wavelet packet best bases and best level curves for B&L and Meyer's wavelets; they do show improvements when compared with the corresponding curves in Figure 3.1 (p–W+WP+F)–(a) using regular wavelet transforms. It is quite certain that the improvement is not to the degree of semi-orthogonal wavelet or that of the Fourier spectrum.

- Figure 3.2 (p–WP BB+BL) shows cumulative distribution curves of the best level, best basis, and a few different levels bases wavelet packet coefficients, as well as the curve for the corresponding regular wavelet transform coefficients; here, all the curves are associated with ON77S. The curve for the best level comes close to that for the best basis. Again, wavelet packet best basis and best level yield lower entropy values than other relevant wavelet bases, but still their curves are far away from that of SO3D.

- Among orthonormal wavelets, we do not see clear differences arising from different degrees of symmetry (least asymmetric ONxxS or most asymmetric ONxxA); however, semi-orthogonal and bi-orthogonal wavelets are symmetric or antisymmetric, and their entropy values (concerning dual wavelets) are comparatively lower. It therefore indicates that the linear phase filtering is desired since symmetry or an-

tisymmetry implies linear phase of the two-scale sequence [6, 12]. Without the linear phase filtering visual impairment may occur. The non-symmetric distribution of time-frequency windows shown in figures 1.1 (TFW–WP BB) illustrates such a significant impact. Though symmetry is desired, it is hard to describe its influence since there are other factors that need to be considered (such as the support length and regularity, e.g., Meyer and B&L wavelets are also symmetric but their entropy values are not comparable to that of the ideal one).

3.4 Summary

Using various criteria of entropy statistics of transform coefficients we have identified among a vast array of Riesz wavelet bases the best basis for our water wave signals. It is found that the most prominent player is the semi-orthogonal cardinal spline wavelet with clear superiority over the Fourier basis in all criteria. And no other wavelets can ever reach the level of approximation given by Fourier spectra. Still, the results entail that many of the properties of the wavelets studied here are more of analytical interests and hard to be physically significant.

The solid performance of the semi-orthogonal wavelet indicates the usefulness of the modulated Gaussian wavelet or the Morlet wavelet in the continuous transform domain for our applications. Coupling with a few additional features that are specific to continuous wavelet transforms – such as its nature of redundancy, the flexibility in time-frequency resolutions, and the conciliatory choices of data segment of interest; there is something to be anticipated. ❖

Tab 3.1 (*H*–F+ON+SO) Entropy statistics of transform coefficients under various criteria for the orthonormal and the semi-orthogonal wavelet groups, as well as the orthonormal Fourier basis. The orthonormal groups cover the most symmetric and the most asymmetric group, as well as the most narrowly-banded (referring to frequency) Meyer wavelet and the most narrowly-distributed (referring to time) Battle and Lemarié wavelet. And the semi-orthogonal wavelet is devised by Chui [6, 7]. Note that the results in all categories for the dual semi-orthogonal wavelet are not only clearly better than the spectral ones but also far superior to any other wavelet groups.

Wavelet	L**2 coefficient entropy (0 division)	L**2 probability entropy (300 divisions)	L**1 probability entropy (300 divisions)	L**2 probability entropy (200 divisions)	Theotetical dimension (L**2 300 divisions)
B&L	4.691	1.330	3.417	1.179	3.782
Meyer	4.647	1.294	3.365	1.132	3.646
SO3O	4.833	1.669	3.756	1.488	5.307
SO3D	1.823	0.219	1.306	0.172	1.245
Spectrum	2.809	0.270	3.044	0.244	1.310
ON22A	4.993	1.761	3.891	1.516	5.815
ON33A	4.773	1.384	3.499	1.225	3.975
ON44A	4.790	1.517	3.596	1.363	4.559
ON55A	4.819	1.553	3.631	1.367	4.727
ON66A	4.790	1.373	3.456	1.203	3.946
ON77A	4.675	1.355	3.461	1.203	3.877
ON88A	4.645	1.229	3.283	1.082	3.418
ON99A	4.719	1.412	3.501	1.252	4.106
ON00A	4.787	1.423	3.511	1.244	4.149
ON44S	4.835	1.461	3.557	1.281	4.311
ON55S	4.758	1.492	3.576	1.298	4.426
ON66S	4.754	1.402	3.501	1.225	4.065
ON77S	4.751	1.336	3.331	1.188	3.804
ON88S	4.714	1.366	3.481	1.224	3.918
ON99S	4.755	1.469	3.570	1.288	4.345
ON00S	4.635	1.278	3.378	1.134	3.591
ON11C	4.938	1.696	3.832	1.457	5.452
ON22C	4.827	1.468	3.520	1.284	4.342
ON33C	4.756	1.488	3.573	1.333	4.427
ON44C	4.690	1.297	3.337	1.157	3.658
ON55C	4.644	1.309	3.405	1.154	3.703

Tab 3.2 (*H*–BO0+D) Entropy statistics of transform coefficients under various criteria for the bi-orthogonal wavelet groups. Again, none of the results here is comparable to those of the dual semi-orthogonal wavelet. And it is noted that a shorter distribution of convolution weights yields extreme and inferior value. Thus, the efficiency of computation is not pertaining to the intimacy of physics.

Wavelet	L**2 coefficient entropy (0 division)	L**2 probability entropy (300 divisions)	L**1 probability entropy (300 divisions)	L**2 probability entropy (200 divisions)	Theoretical dimension (L**2 300 divisions)
BO11O	5.395	2.623	4.502	2.299	13.777
BO11D	5.395	2.623	4.502	2.299	13.777
BO13O	4.943	1.806	3.883	1.627	6.084
BO13D	5.266	2.371	4.373	2.053	10.708
BO15O	4.866	1.678	3.755	1.495	5.357
BO15D	5.227	2.291	4.327	1.987	9.882
BO22O	5.282	2.362	4.363	2.083	10.609
BO22D	4.434	1.181	3.284	1.034	3.257
BO24O	4.963	1.862	3.985	1.634	6.438
BO24D	4.359	1.090	3.220	0.962	2.975
BO26O	4.881	1.703	3.835	1.492	5.490
BO26D	4.332	1.064	3.174	0.940	2.899
BO28O	4.857	1.624	3.782	1.452	5.073
BO28D	4.318	1.069	3.157	0.941	2.914
BO31O	5.824	3.174	4.741	2.835	23.894
BO31D	4.377	1.058	2.655	0.936	2.880
BO33O	5.084	2.001	4.062	1.756	7.393
BO33D	4.205	1.102	2.827	0.965	3.011
BO35O	4.850	1.697	3.847	1.506	5.457
BO35D	4.125	1.026	2.776	0.908	2.789
BO37O	4.790	1.658	3.821	1.442	5.247
BO37D	4.106	0.986	2.737	0.873	2.679
BO39O	4.776	1.660	3.835	1.432	5.258
BO39D	4.098	0.967	2.713	0.866	2.629

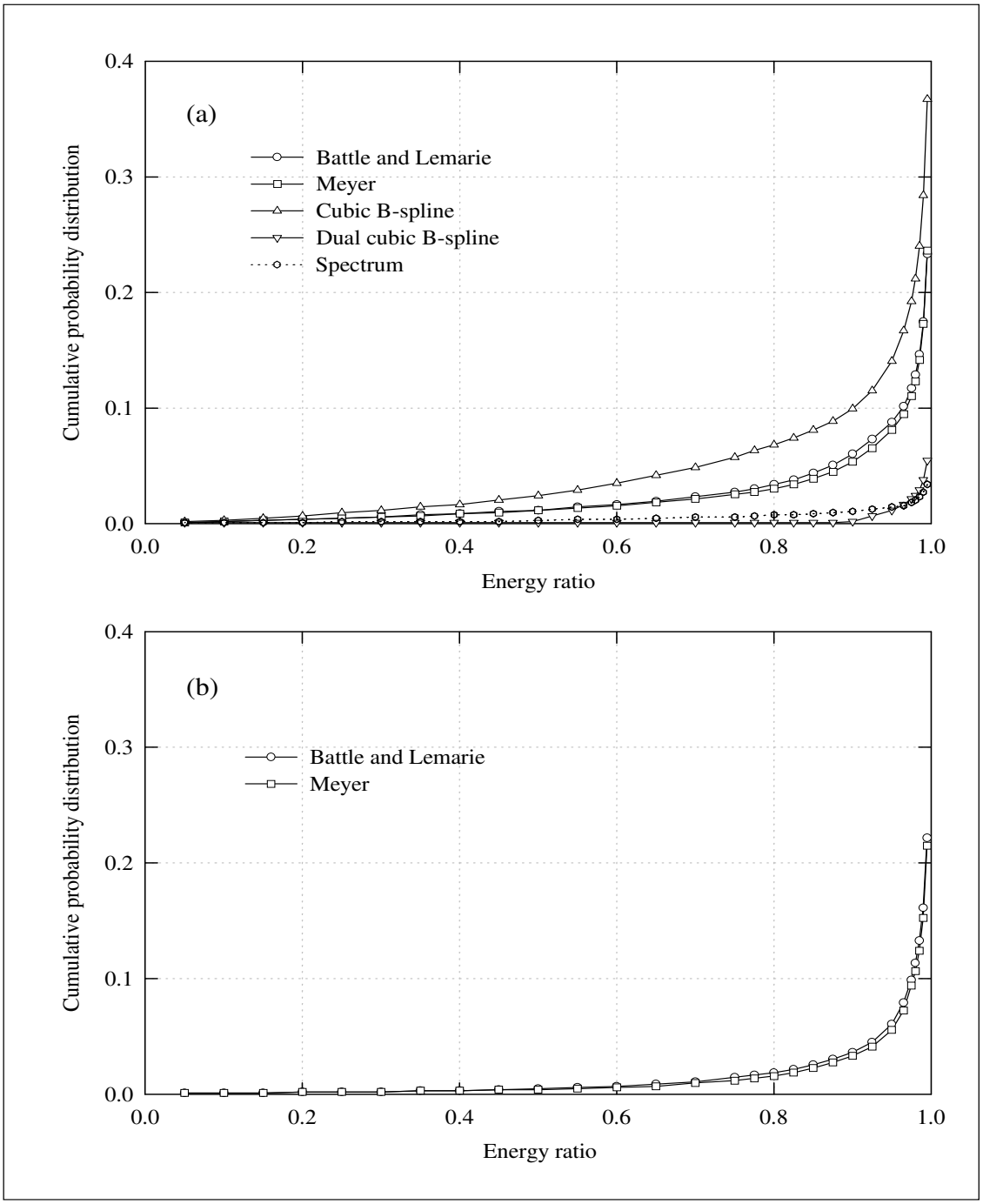

Fig 3.1 (p–W+WP+F) The cumulative probability distribution curves of the transform coefficients associated with three different transform categories. The coefficient PDFs intimately reflect L^2-norm energy relevance. Here the various bases include:
(1) Wavelets: Meyer, Battle and Lemarié, semi-orthogonal cubic B-spline, dual semi-orthogonal cubic B-spline `(top)`;
(2) Wavelet packets: those of the best packet bases based on Meyer wavelet and Battle and Lemarié wavelet `(bottom)`;
(3) Spectrum: Fourier spectral basis `(top)`.
Note the outstanding performance of the dual semi-orthogonal cubic B-spline wavelet (SOD). And its distribution clearly outperforms that of the Fourier spectrum for nearly all the energy ratio.

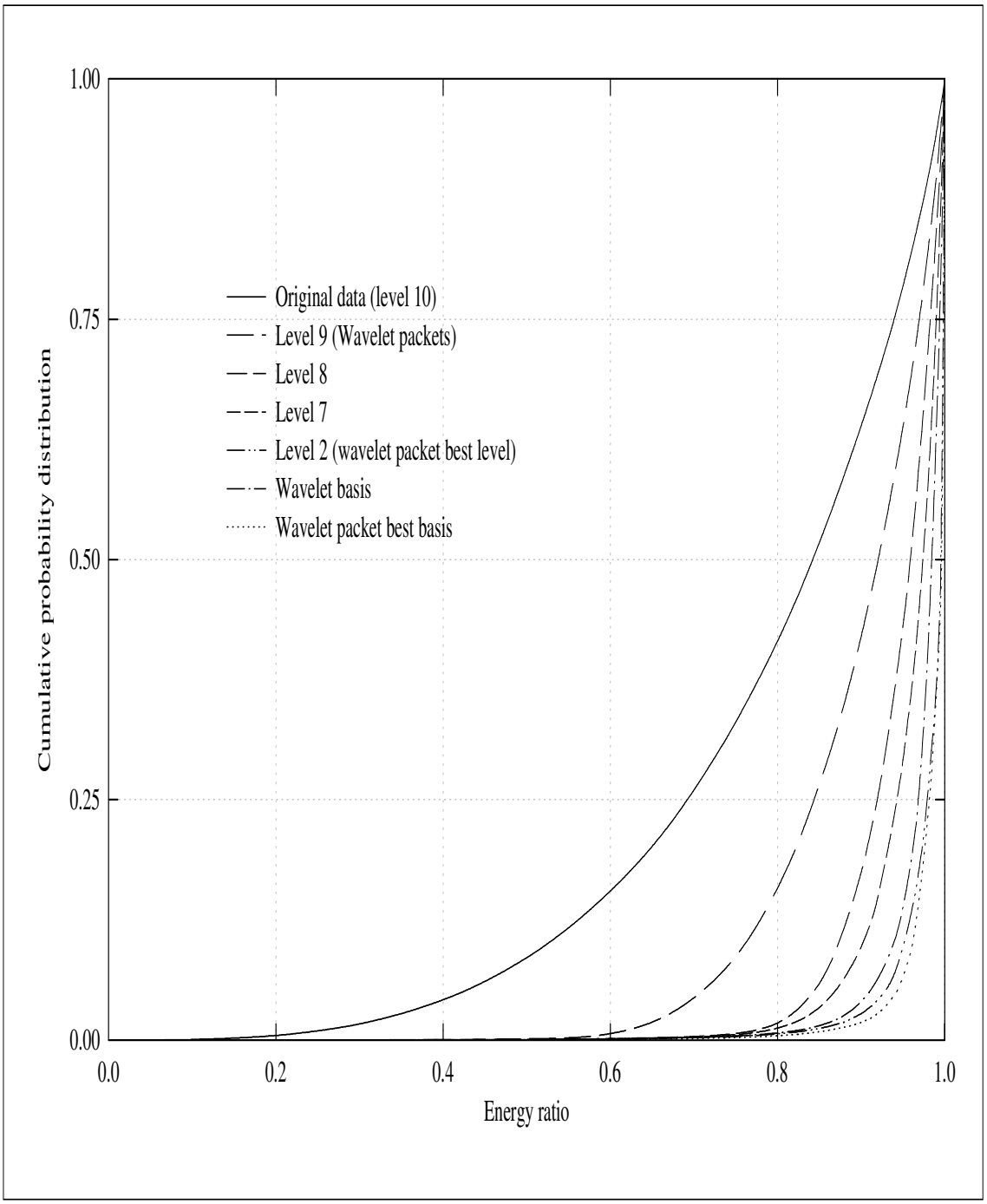

Fig 3.2 (p–WP BB+BL) The cumulative probability distribution curves of the Wavelet packet transform coefficients for the various bases derived from the seeding orthonormal mother wavelet ON77S. The PDFs are of L^2-norm energy content. The function bases include:
(1) Wavelet packet of the lowest levels (normal instance: wavelet basis);
(2) Wavelet packet of a specific level (9, 8, 7);
(3) Wavelet packet of the best level (2);
(4) Wavelet packet of the best basis (combined levels: dotted line).
Note that the best situation is the one for the best basis; but none of these curves is comparable to that of the dual semi-orthogonal wavelet (SOD) shown in the preceding figure.

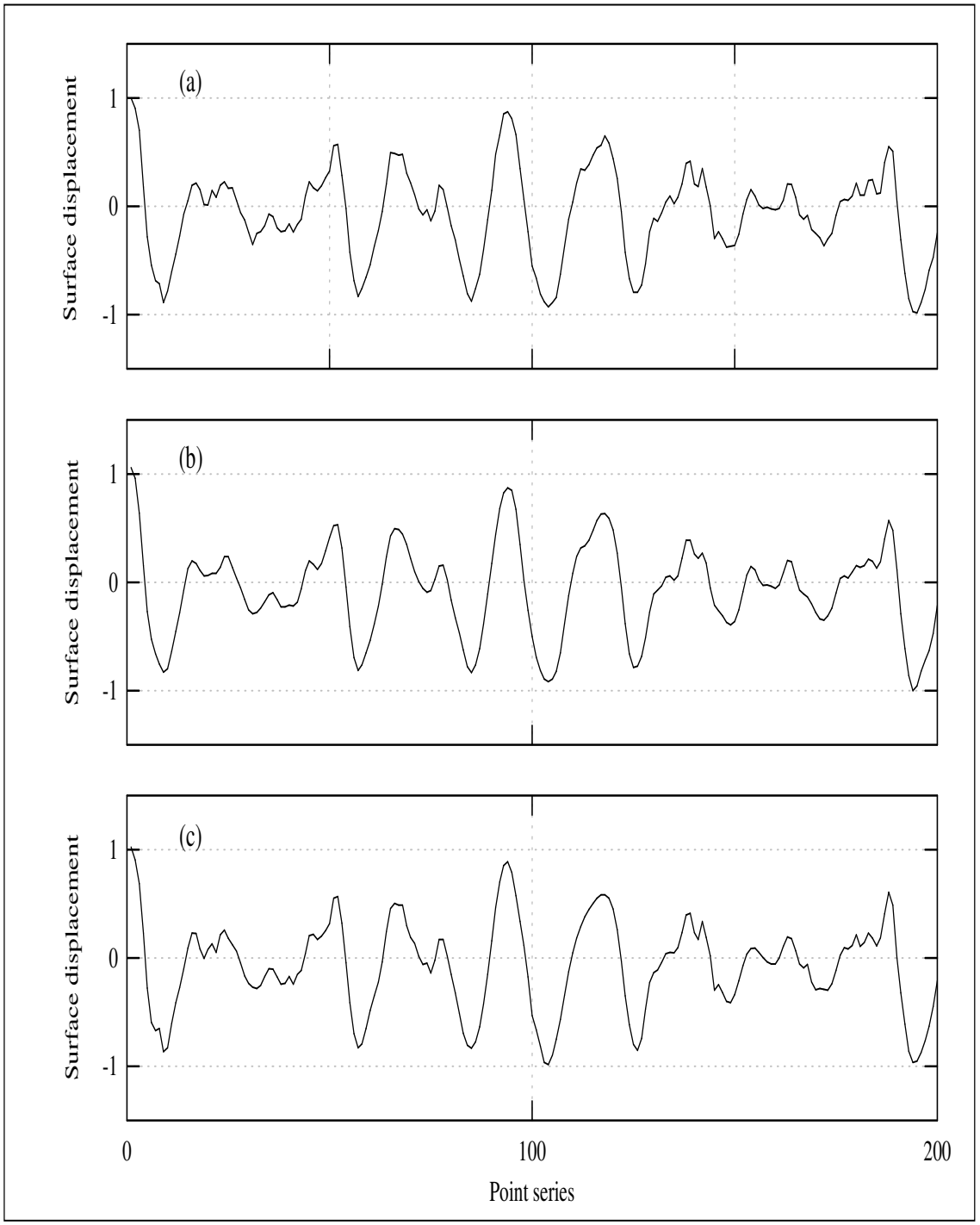

Fig 3.3 (ReC–Signal) Comparison of reconstructed signals associated with the best wavelet basis (i.e., the dual semi-orthogonal wavelet) and the Fourier basis. The semi-orthogonal wavelet is seen to better portrait the original signal, in particular, small scale transient features.
Here 35% of the transform coefficients are kept. The sub-figures show:
(1) a section of the original signal `(top)`
(2) reconstructed signal using the spectral coefficients `(middle)`;
(3) reconstructed signal using the best wavelet basis `(bottom)`.
The figure reflects the L^1-norm entropy relevance.

Chapter 4

The Characteristic Phase Distributions

4.1 The wavelet characteristic function m_0

In the last chapter, the entropy of transform coefficients is used as a performance measure for wave simulation. The entropy approach is completely statistical and provides no mathematical insight of the basis property that leads to the usefulness of a basis in its modeling of water waves. Herein, we furnish the analytical essence that is connected to the modeling utility of a wavelet function basis. Moreover, practical implications of mathematical analyticity are stated. Herein the essence is concerning the phase distribution of a wavelet characteristic function for any individual basis. More specifically, the characteristic function is related to the filtering effect or convolution result associated with liner or non-linear phase filtering.

Following the convention used by Daubechies [12], the wavelet characterizing function is termed as the $m_0(\xi)$ function, which is the kernel of individual wavelet and has the following mathematical content:

A multiresolution analysis consists of a sequence of the closed subspaces V_j of the nested ladder,

$$\cdots V_2 \subset V_1 \subset V_0 \subset V_{-1} \subset V_{-2} \subset \cdots, \tag{4.1}$$

and satisfies the requirement

$$f \in V_j \Longleftrightarrow f(2^j \cdot) \in V_0. \tag{4.2}$$

The invariance of V_0 under integer translations states that

$$f \in V_0 \Longrightarrow f(\cdot - n) \in V_0 \text{ for all } n \in \mathbb{Z}. \tag{4.3}$$

Now comes the main statement that there exists $\phi \in V_0$ so that

$$\{\phi_{0,n};\, n \in \mathbb{Z}\} \text{ is an orthonormal basis or a relaxed Riesz basis in } V_0, \tag{4.4}$$

where, for all $j, n \in \mathbb{Z}$, $\phi_{j,n}(x) = \sqrt{2^{-j}}\phi(2^{-j}x - n)$, and the relaxation refers to the orthonormality. Quite often the ϕ here is formally called the scaling function of the multiresolution analysis. Furthermore, for the $\{\phi_{j,n};\, j, n \in \mathbb{Z}\}$ there exists its counterpart wavelet basis $\{\psi_{j,k};\, j, k \in \mathbb{Z}\}$, $\psi_{j,k}(x) = \sqrt{2^{-j}}\psi(2^{-j}x - k)$, such that

$$P_{j-1}f = P_j f + \sum_{k\in\mathbb{Z}} \langle f, \psi_{j,k}\rangle \psi_{j,k}, \tag{4.5}$$

where $P_j f$ is the projection onto V_j.

Since $\phi \in V_0 \subset V_{-1}$ and $\phi_{-1,n}$ are basis in V_{-1}, we have

$$\phi = \sum_n h_n \phi_{-1,n}, \tag{4.6}$$

with

$$h_n = \langle \phi, \phi_{-1,n}\rangle. \tag{4.7}$$

We therefore have

$$\phi(x) = \sqrt{2}\sum_n h_n \phi(2x - n) \tag{4.8}$$

or

$$\widehat{\phi}(\xi) = \frac{1}{\sqrt{2}} \sum_n h_n e^{-in\xi/2} \widehat{\phi}(\xi/2). \tag{4.9}$$

In an alternative form

$$\widehat{\phi}(\xi) = m_0(\xi/2)\widehat{\phi}(\xi/2), \tag{4.10}$$

where

$$m_0(\xi) = \frac{1}{\sqrt{2}} \sum_n h_n e^{-in\xi}. \tag{4.11}$$

Suffice it to say that the $m_0(\xi)$ function is intrinsic to the transcendental formulations of the mother wavelet and the two-scale equation. And it is comprised of the summation of convolution coefficients of wavelet construction (or filter coefficients corresponding to the support length of the wavelet) multiplied by the complex exponential functions of their individual scales.

4.2 Phase distributions and implications

Figures 4.1 ($m_0(\xi)$–MELE) to 4.7 ($m_0(\xi)$–BOD) show the phase distributions of $m_0(\xi)$ for all the wavelet categories listed in this study. Notable points are summarized below.

- Wavelets with similar visual appearance may possess extremal difference in the characterizing phase distributions, such as those shown in figures 4.1 ($m_0(\xi)$–MELE). Note that, regarding to the symmetrical wavelets, the Meyer wavelet is the most compactly supported wavelet in frequency domain while the Battle and Lemarié wavelet is the most compactly supported wavelet in time domain. For these two categories of wavelet, both their mother and father wavelets have quite similar distributions with respect to each other, as shown in 2.15 (MFW–SO0) and 2.14 (MFW–B&L). But the behavioral difference between their phase curves suggests that there exists theoretical complexity both in mathematics and numerics of the two wavelet constructions; moreover, it hints that physical applicabilities might not sensitive to theoretical differences.

- Combing the entropy results yielded in the preceding chapter with the phase distributions of all the wavelet categories shown here, we see that a linear phase distribution is unable to guarantee the best performance for modeling signals of water waves. What should be emphasized is that the most outstanding feature leading to the modeling usefulness of the semi-orthogonal wavelet lies in the characteristic of a peculiarly constant phase distribution for either the wavelet or its dual, as shown in figure 4.2 ($m_0(\xi)$–SO). Besides, the intuitive byproduct is that there is the strong implication that most wavelets are too exotic, as well as too alienating, to water waves.

- The more asymmetric the shape of a wavelet is the more complex of its phase distribution comes along. The distributions of the least asymmetric orthonormal group ONxxS are shown in figure 4.3 ($m_0(\xi)$–ONS) and those of the most asymmetric are shown in figure 4.4 ($m_0(\xi)$–ONA). These distributions, together with those of the previous figures, denote the relation between wavelet symmetry and water wave physics and also imply the poor performance in modeling for compactly supported wavelets (i.e., with limited number of filtering wights).

- The lengthening of the support length of a wavelet group may still yield even more irregular phase distributions as are shown in figure 4.4 ($m_0(\xi)$–ONA). And this disproves any possible benefit that may arise from further expansion of the construction concerning the support length of these orthonormal wavelets.

- The Coiflets are symmetry and have vanishing moments for both the mother and father wavelets but their phase distributions are not much different from those of the least asymmetric wavelets, as are shown in figure 4.5 ($m_0(\xi)$–ONC). It is therefore expected that their modeling capability can be of little refinement from the ONxxA group.

- The phase distribution curves for the bi-orthogonal wavelets and their duals are the same not only for all the support lengthes within their subgroups but also for the

respective crossovers, as are shown in figures 4.6 ($m_0(\xi)$–BO0) and 4.7 ($m_0(\xi)$–BOD). Again, this shows that lengthening the support length of these wavelets provides no benefit.

- Judging from all those mentioned above and that extremal mathematical properties of wavelet categories have been covered in this study, we therefore don't see any possibility that there exists other orthonormal or compactly supported wavelets that might provide suitable or better characterization for water wave physics.

4.3 Summary

Simply put, the most important and practical entailment of this chapter is to furnish the idea that water waves in their shapes or forms are intrinsically extremely "regular" when compared to those of almost all of the discrete wavelets (except the cardinal spline wavelet). And, in a simple and blunt way, those mathematical complexity of wavelet formulations do not reverberate our real world anticipations for physics and may be overkill.

❖

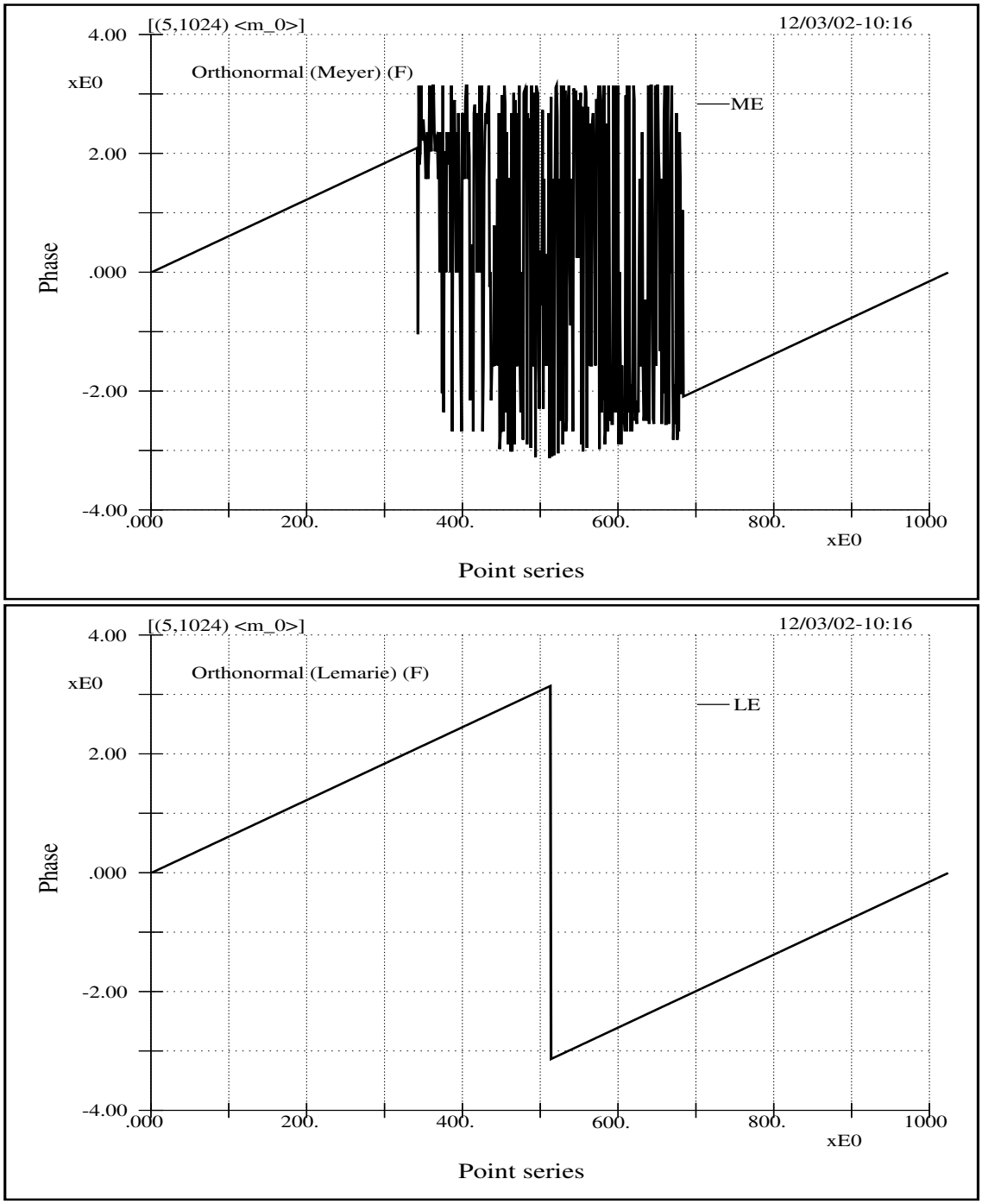

Fig 4.1 ($m_0(\xi)$–MELE) The phase distribution of the wavelet characteristic function $m_0(\xi)$ for two categories of wavelets: the Meyer wavelet (`Top`) and the Battle and Lemarié wavelet (`Bottom`). For the two categories of wavelets, both their mother and father wavelets, respectively, have quite similar distributions, as are shown in 2.15 (MFW–SO0) and 2.14 (MFW–B&L). Whereas, on the one hand, the Meyer wavelet is the most compactly supported wavelet in the frequency domain; on the other hand, the Battle and Lemarié wavelet is the most compactly supported in the time domain. Here the difference between the two distributions implies the possible ramification both in mathematics and numerics of the two wavelet constructions. Besides, it hints the intricate concerns among theoretical complexity and physical applicabilities.

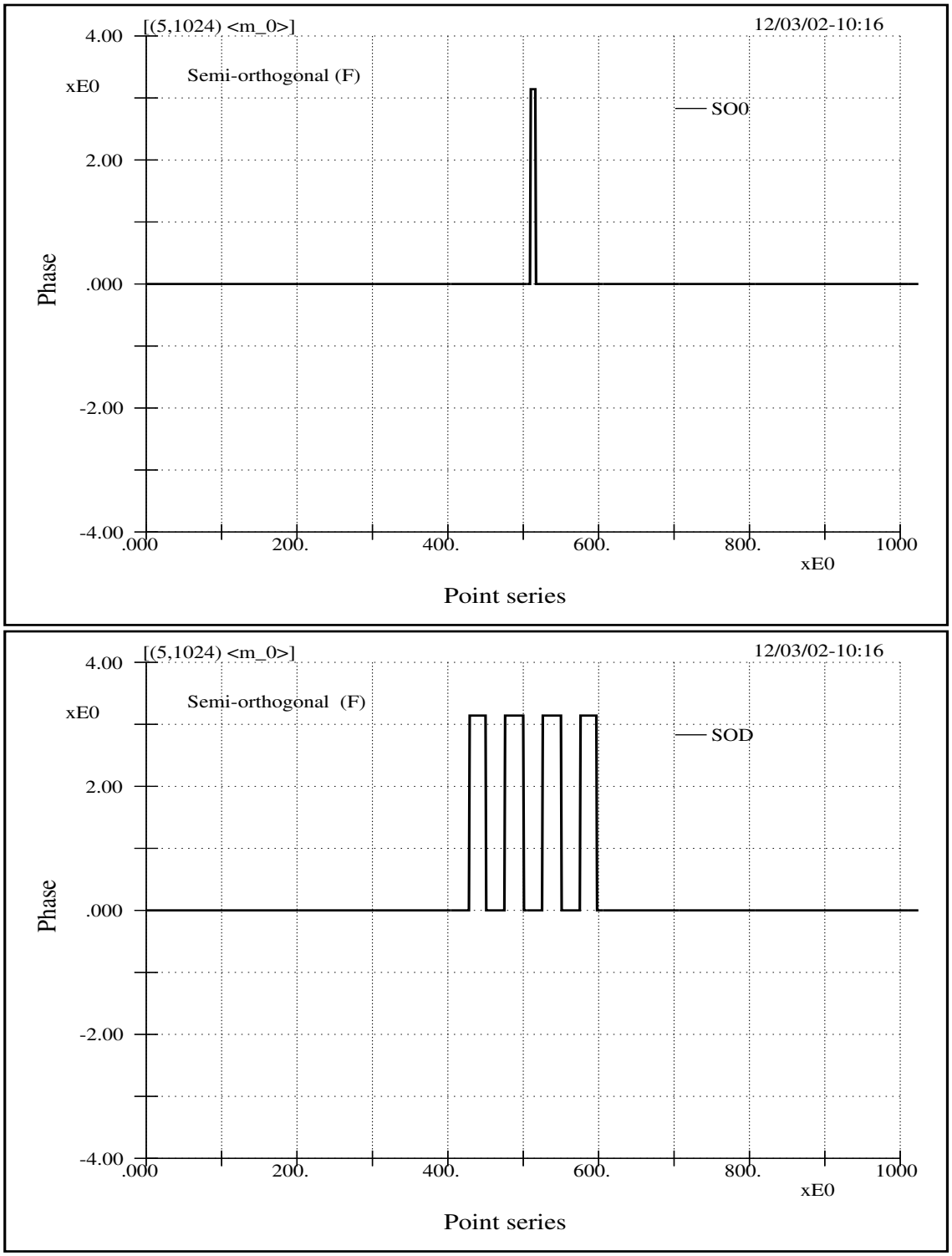

Fig 4.2 ($m_0(\xi)$–SO) The phase distributions of the wavelet characteristic function $m_0(\xi)$ of the semi-orthogonal cardinal spline wavelet (`Top`) and its dual (`Bottom`). Here the most outstanding feature, which leads to the usefulness in its modeling of water waves, lies in the peculiar distribution of a constant characteristic phase. Besides, there is an important implication that most of the wavelets are too exotic, as well as estranging, to water waves.

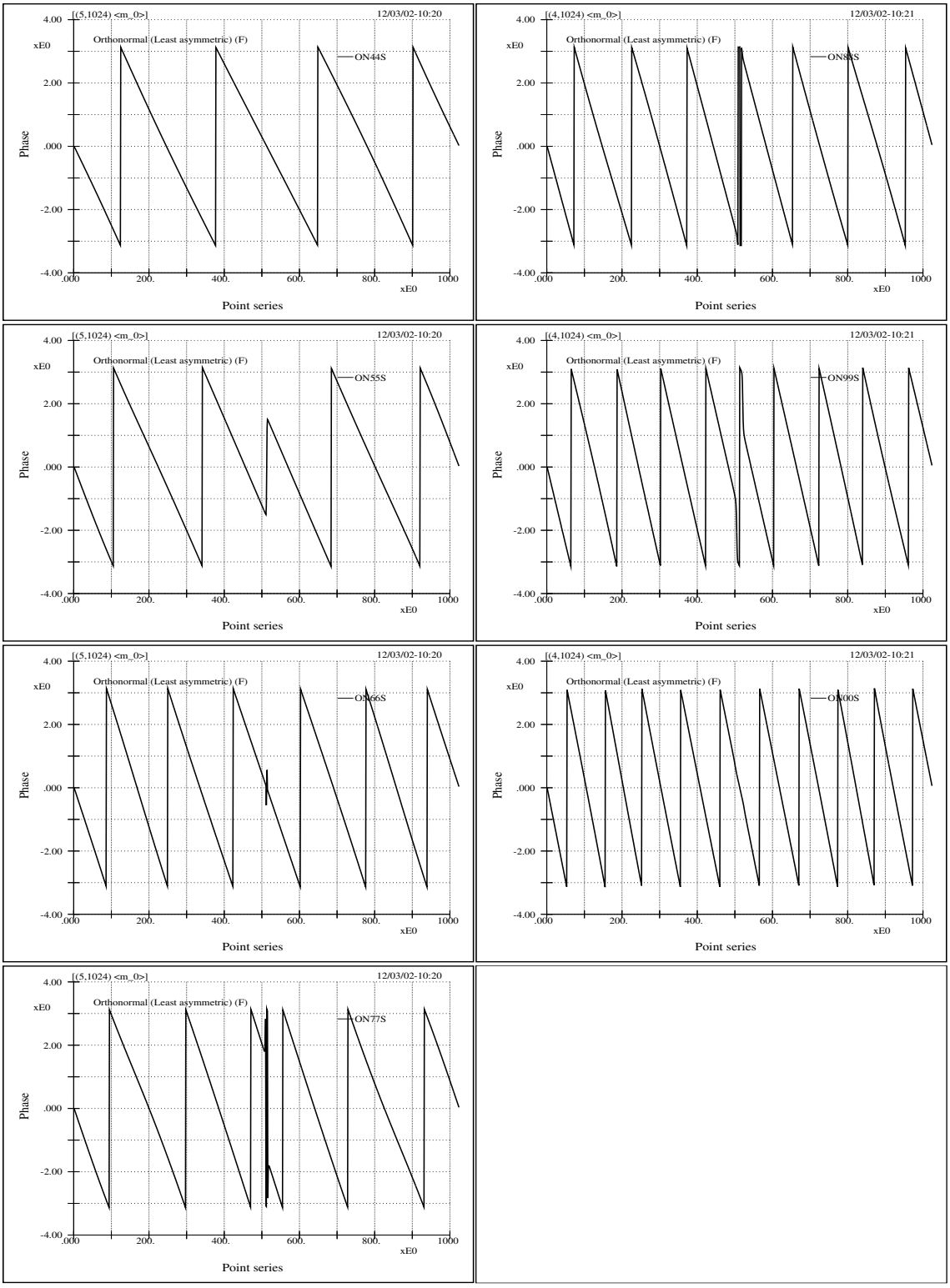

Fig 4.3 ($m_0(\xi)$–ONS) The phase distributions of the wavelet characteristic function $m_0(\xi)$ for the least asymmetric orthonormal group ONxxS. Comparing the curves here with those of the next figure we see that the more asymmetric the wavelet is the more the complication of its phase distribution comes along. This phenomenon implies the worsening modeling performance for the asymmetrical group and hints the relation between wavelet symmetry and water wave physics.

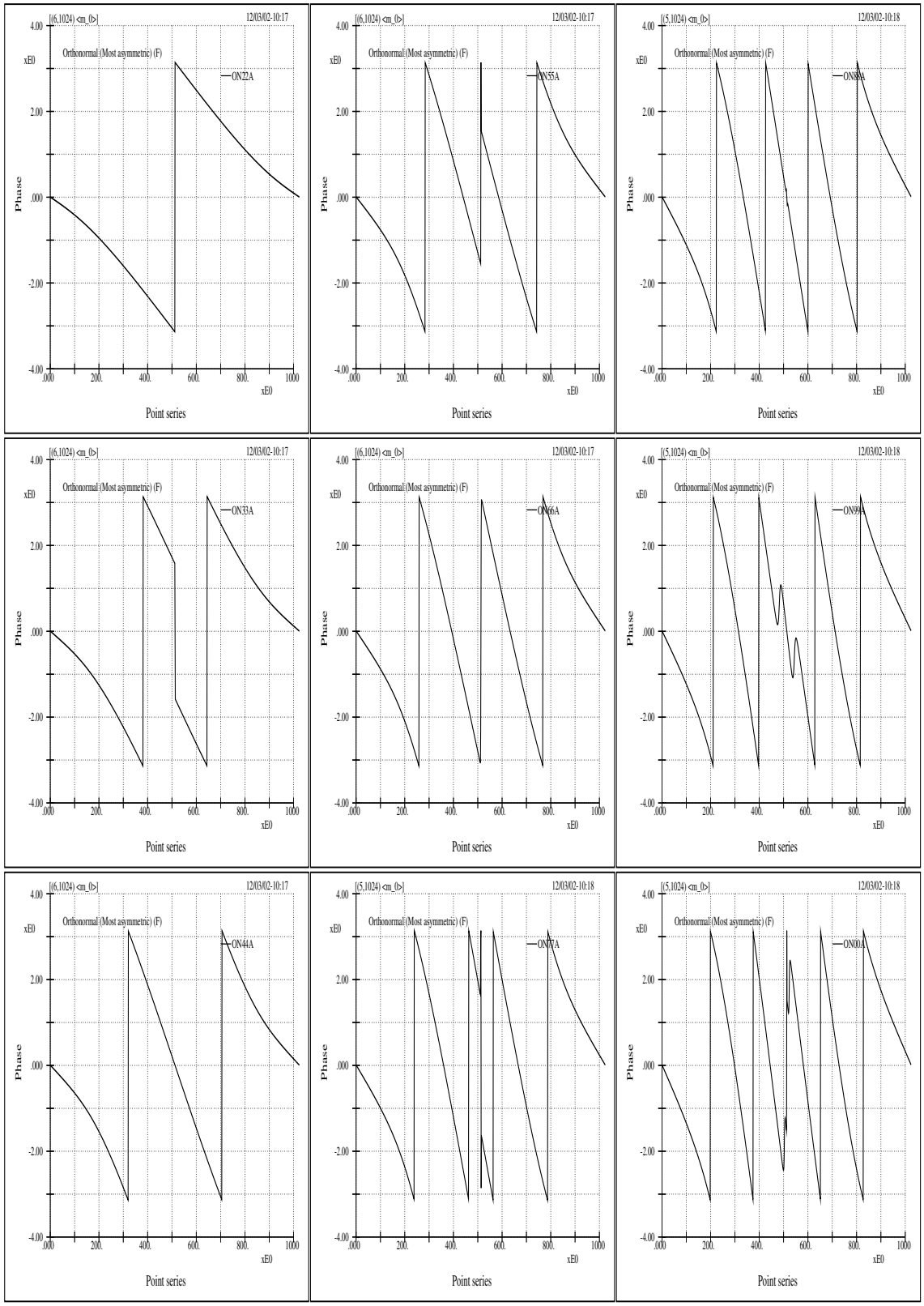

Fig 4.4 ($m_0(\xi)$–ONA) The phase distributions of the wavelet characteristic function $m_0(\xi)$ of the most asymmetric group ONxxA. Note that the lengthening of support length of the wavelet yields even more irregularity in distribution. Again, this disproves any possible benefit that may arise from any further expansion of the construction of these orthonormal wavelets.

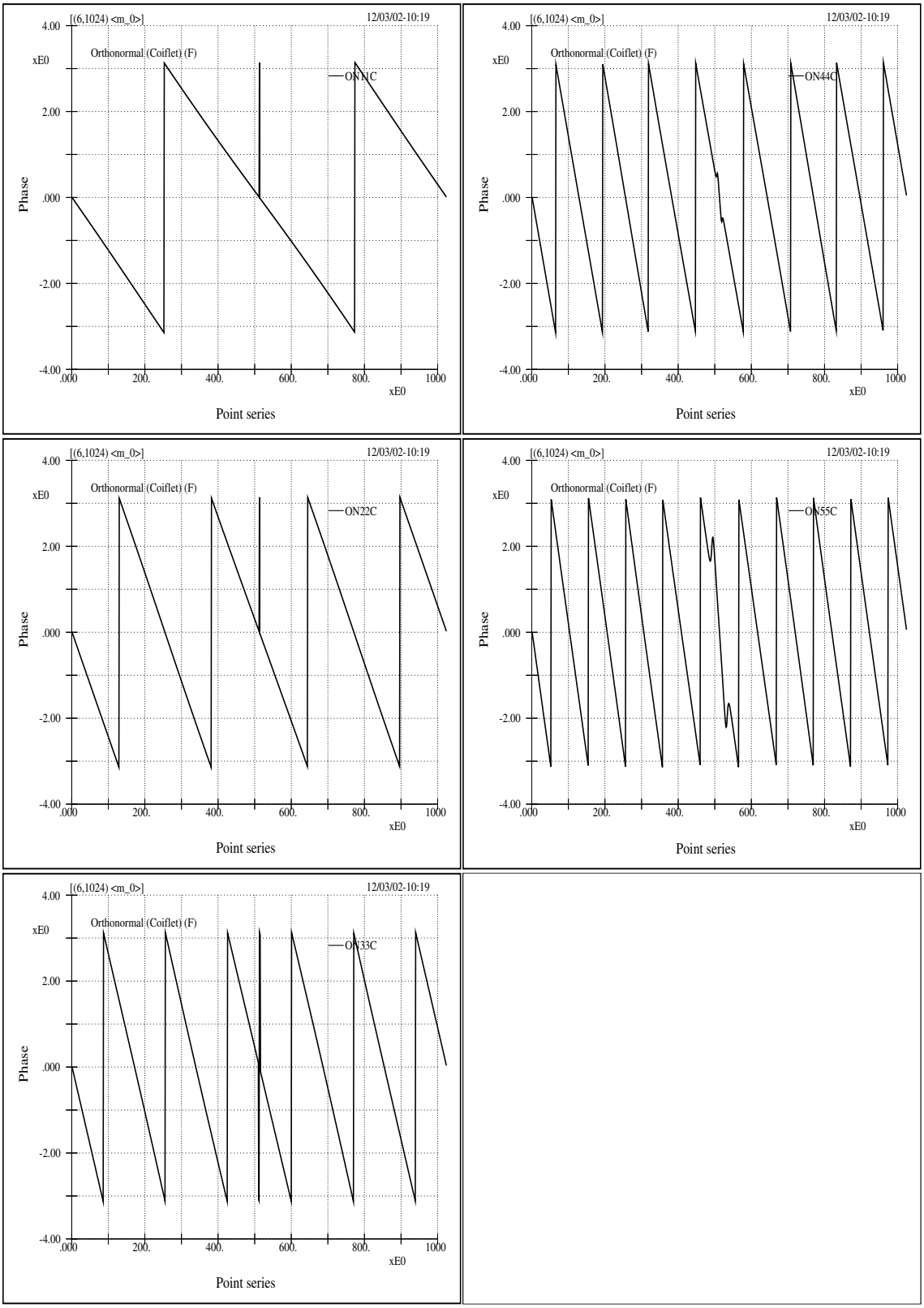

Fig 4.5 ($m_0(\xi)$–ONC) The phase distributions of the wavelet characteristic function $m_0(\xi)$ of the Coiflets. The Coiflets are symmetry and have vanishing moments for both their mother and father wavelets; but their phase distributions are not much different than the least asymmetric compactly supported group ONxxA. It is therefore expected that their modeling performance is of little betterment.

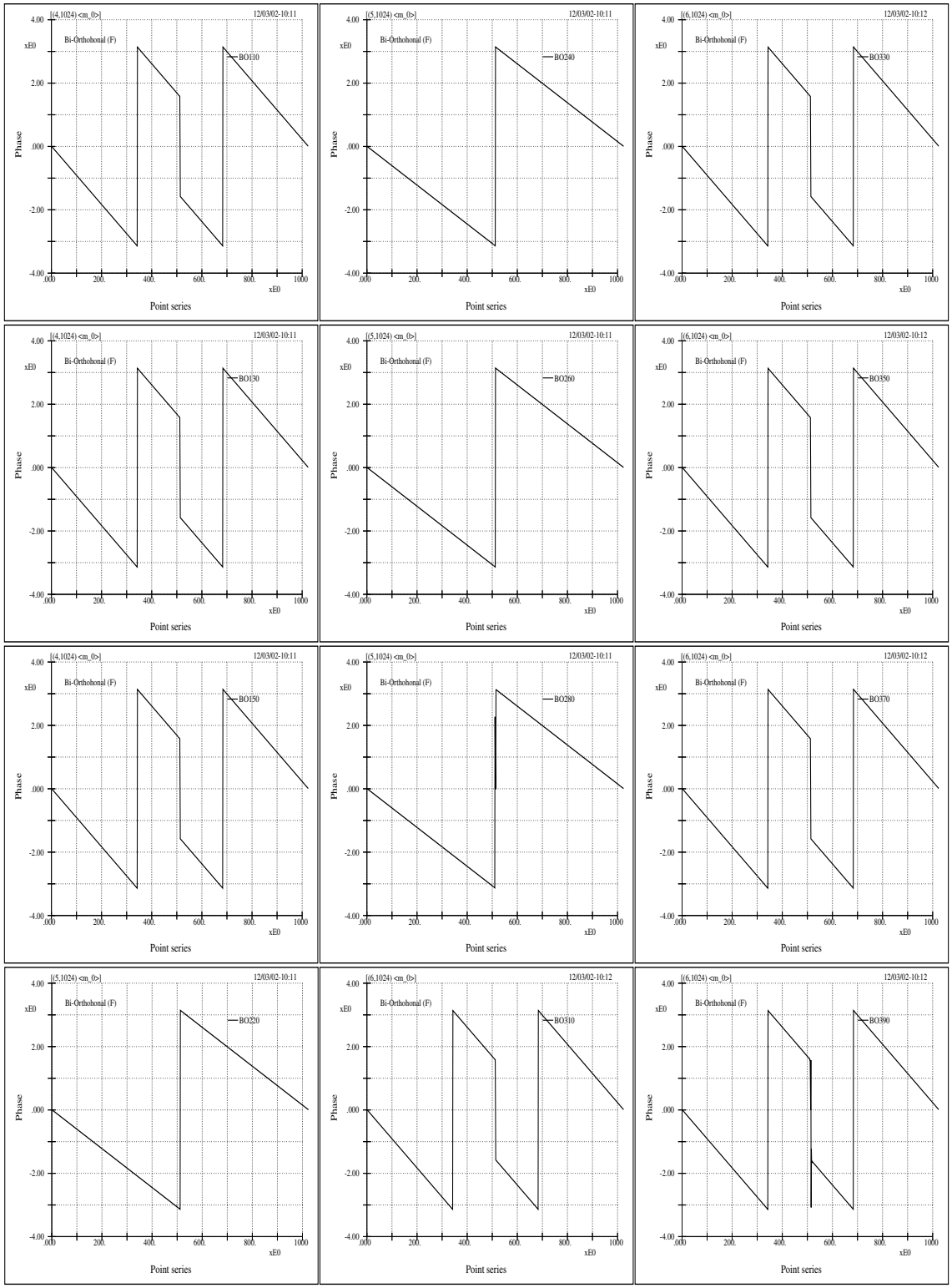

Fig 4.6 ($m_0(\xi)$–BO0) The phase distributions of the wavelet characteristic function $m_0(\xi)$ of the bi-orthogonal wavelets BOxy0. Their distributions are almost identical to those of their dual wavelets as to be shown in the next figure; nevertheless, the entropy values of these wavelets are clearly inferior to those of their dual wavelets. Again, the phenomenon implies the possible ramification both in mathematics and numerics of the wavelet constructions and hints the intricate concerns among theoretical complexity and physical applicabilities.

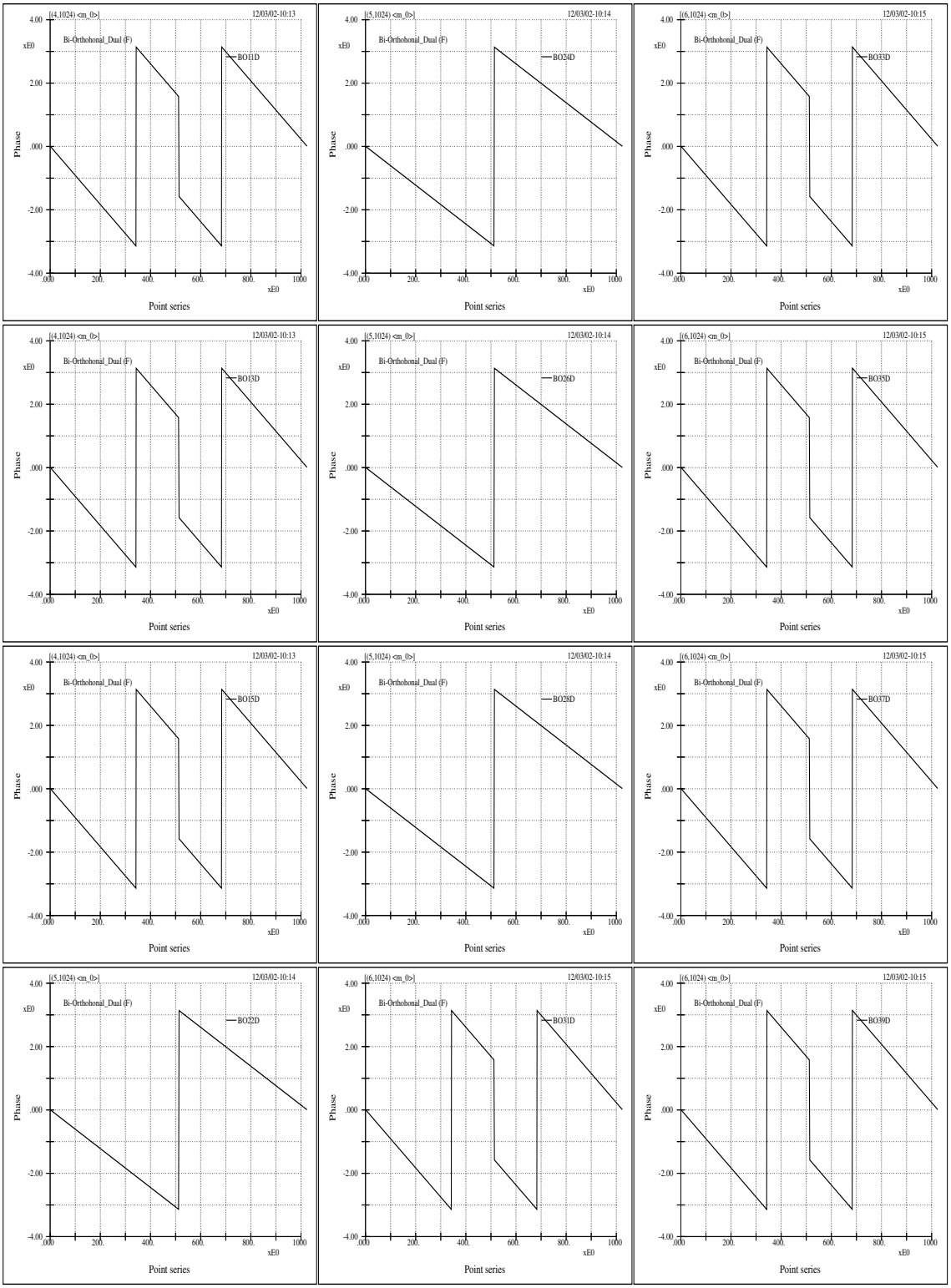

Fig 4.7 ($m_0(\xi)$–BOD) The phase distributions of the wavelet characteristic function $m_0(\xi)$ of the dual bi-orthogonal wavelets BOxyD. These phase distribution curves and those of their duals are the same not only for all the support lengthes within their subgroups but also for the respective crossovers, as shown in the last one (figures 4.6 ($m_0(\xi)$–BO0)). Moreover, here it also indicates that the mathematical complexity of wavelet formulation does not reverberate our real world anticipations and may be overkill.

Chapter 5

The Best Wavelet in the Continuous Domain

5.1 Introduction

In the previous chapter on entropy the semi-orthogonal cardinal spline wavelet was identified as the most suitable Riesz wavelet basis for our signals. However, this discrete wavelet and its associated analyzing scheme is not what will be directly adopted in the verification of the optimality through the comparisons of coherent behaviors, as to be given later. The most fundamental concerns are in three aspects. First, the previous chapter concerns the discrete wavelet transform where each translation step is an integer multiple of the dilation scale which is in the logarithmic measure with base 2; therefore, both the translation and the dilation vary in logarithmic measure. Whereas in the study of coherences the scheme used concerns the continuous wavelet transform where the translation step can be as small as the sampling interval for all scales which can basically be specified arbitrarily. Second, the wavelets in the previous chapter handle bases with frame bounds that are either tight or relatively tight. Whereas the wavelet employed here does not involve frame bounds and might not have frame bounds at all when it is analyzed in the sense of discrete wavelet transform, i.e., not even related to a Riesz wavelet. Third, all the discrete wavelets listed here are real wavelets; therefore, they are only related to the term of "scale" and how can the phase come by so as to render a more practical term of

real physics.

Herein we will make further clarifications for these two points and try to illustrate their respective advantages and disadvantages since they are keys to the usefulness of the analyzing basis and the associated scheme for our applications.

5.2 The counterpart best continuous wavelet

Let the Gaussian function be

$$g_\alpha(t) = \frac{1}{2\sqrt{\pi\,\alpha}} e^{-\frac{t^2}{4\alpha}}, \tag{5.1}$$

where α is a representative value of the second moment of the Gaussian function and the constants is for the purpose of normalization, the modulated Gaussian is

$$G^\alpha_{b,\omega}(t) = e^{i\omega t} g_\alpha(t-b). \tag{5.2}$$

And the Gabor transform of a function f is

$$\left(\mathcal{G}^\alpha_b f\right)(\omega) = \langle f, G^\alpha_{b,\omega}\rangle = \int_{-\infty}^{\infty} f(t) e^{-i\omega t} g_\alpha(t-b)\mathrm{d}t. \tag{5.3}$$

As is stated by Daubechies ([12]) that the Morlet wavelet is almost identical to a modulated Gaussian, and as is given by Chui ([6]) a modulated Gaussian matches almost exactly with cardinal B-spline wavelet of order greater than or equal to three, i.e., for $m \geq 3$, the even order ψ_m's (such as the cubic spline wavelet ψ_4) match almost exactly with

$$\mathrm{Re}G^\alpha_{b,\omega}(t) = (\cos\omega t) g_\alpha(t-b) \tag{5.4}$$

and the odd order ones with

$$\mathrm{Im}G^\alpha_{b,\omega}(t) = (\sin\omega t) g_\alpha(t-b) \tag{5.5}$$

for a certain set of values α, b, ω.

In accord with these observances we therefore have an extremely natural transition from the best discrete basis to the following continuous wavelet, i.e., the Morlet wavelet,

$$\psi(t) = \pi^{-1/4}(e^{-i\omega_0 t} - e^{-\omega_0^2/2})e^{-t^2/2}. \tag{5.6}$$

Most importantly, such a correspondence introduces two terms in physics, i.e., the phase and carrier frequency, and thus make possible the enhancements of physical modeling of water wave signals, as to be provided in the following chapter.

5.3 Discrete versus continuous transforms

In the introductory chapter we listed a few properties related to different time-frequency analysis methodologies, such as Fourier transform, short time Fourier transform (STFT), Hilbert transform and the analytical signal procedure, the discrete wavelet transform (DWT), as well as the continuous wavelet transform (CWT). In fact, one of the main themes for all those discussions centered on the aspiration regarding the minimization of uncertainty effects ([17]). And this is the most outstanding feature that the continuous transform comes into play. And why there is a need of the counterpart continuous wavelet with regard to the best discrete wavelet.

In this chapter, inheriting the identified discrete optimum basis, we mainly focus on the different usages of DWT and CWT concerning their practical applications to water waves related signals. That is to say, what is the counterpart wavelet in the continuous wavelet transform to the semi-orthogonal cardinal spline wavelet and why there is the need of a continuous one.

Herein we emphasize that DWT and CWT should be treated as two different entities — since, unlike the discrete and continuous Fourier transforms where they are dealing with the same basis as well as deploying basically the same formulations, DWT and CWT

generally refer to two quite different methodologies which focus on their individual function bases as well as different data treatment schemes. Most profoundly we press on the concerns of the following points:

- In general, the dilation lattice is in logarithmic measure for discrete wavelet transform (e.g., the ${a_0}^j$ in the stability condition to be mentioned) and in linear measure for discrete short time Fourier transform (e.g., the $e^{-i2\pi mt}$ in the above mentioned Gabor type frame). Continuous transforms do not involve lattice. The concept of lattice is associated with the concept of time-frequency density, which is defined as the inverse of the product of dilation and translation steps [12]. For short time Fourier transform frames, due to Shannon sampling theorem, the time-frequency density must not go beyond the value of generalized Nyquist density, $(2\pi)^{-1}$. For wavelet transform, however, there is no such a clear-cut limit of time-frequency density. Moreover, Balian-Low theorem depicts that there is no good time-frequency localization for a short time Fourier transform frame if constructed under a strict time-frequency lattice; on the contrary, numerous wavelet bases with good time-frequency localization have been given [6, 12, 29]. These physically imply that wavelet transform may provide better zoom-in.

- The existence of a lattice structure can be either practical or impractical. For water waves, if we don't anticipate any significant gaps in the scale contents, that is to say, the physical process involves time and spatial scales that are "changing" or "evolving" in a relatively continuous sense, we generally do not appreciate the use of frames. Here a continuous transform may provide better chance of success.

- Both continuous and discrete wavelet transforms implement a process of integral wavelet transform over the real line $\mathbf{R}$ in a continuous sense but they analytically emphasize the use of different integration symbols: $\sum$ and $\int$. Digitally sampled signals are certainly discrete, but this is irrelevant to the methodology of continuous wavelet transform or discrete wavelet transform. The main difference, from

the application point of view, is that there is no practical interest of reconstruction (or inverse transform) for continuous wavelet transform due to the redundant or non-orthogonal nature of its wavelet coefficients. Both methods are capable of decomposing either functions defined over the real line or signals sampled discretely. In reality, applying continuous wavelet transform to sampled data is implemented in a discrete manner; vis-à-vis, doing discrete wavelet transform for an unlimited ladder, such as that of the standard multiresolution analysis of [25], can describe any function in infinite detail, i.e., over the whole real line. The concept of unlimited ladder of discrete wavelet transform is illustrated by two examples shown in figures 2.23 (BU–BO2yO) through 2.30 (BU–BO35O) where the blow-ups of individual segments of wavelet curves are shown. The figure also illustrates possible bizarre behaviors of certain wavelets and indicates that mother wavelets with short support lengths might not be of ideal choices. In addition, a few discrete wavelet transform formulas when generalized in the limit sense are quite helpful in explaining a few continuous wavelet transform characters.

- All of the Riesz wavelets studied in the previous chapter handle bases with frame bounds that are either tight or relatively tight; whereas the continuous wavelet does not involve frame bounds and might not have frame bounds at all when it is analyzed in the sense of discrete wavelet transform, i.e., not even qualified as a Riesz wavelet. However, we will see that there is a very natural transition from the discrete wavelet to its continuous counterpart.

- Apart form the specific features listed in the above items, there is a practical interest in what can be done to improve the physical relevance between the basis functions and the wave constituents of our signals. For example: does the decaying features of basis functions akin to the physics of component waves? And this is the topic to be discussed in the next chapter.

5.4 The physical perspective of Morlet wavelet

The combination of "Wave" and "let" hints the core concept of wavelet analysis. And the concept implies that the distribution properties of the basis functions both in time or frequency domains are at the heart of all sorts of function bases. More specifically, different intricate analytical properties of wavelets are just manifestations to these distribution features. However, since two decay properties that are analytically or mathematically quite differentiable may only have very minor visual differences in their wave forms (such as those shown in figures 2.13 (MFW–Meyer) and 2.14 (MFW–B&L)), one generally bears the feeling that wavelets' physical implications is not proportional to their analytic interests. Nevertheless, we still can benefit from the wavelet approach due to its flexibility in devising the analyzing wavelets as well as its adaptability in forging the algorithms. But versatility does not come without the price of ambiguity. For example, the power spectra of a function are shift-invariant; whereas, wavelet spectra are highly shift-variant [27]. Figure 5.1 (Pha–Eff-1) and 5.2 (Pha–Eff-2) shows such a property and it gives us the idea of how significant the phase effects may be. And this figure should be regarded as the counterpart figure in the wavelet analysis to those in the Fourier analysis given in a previous study on the analytic signal approach by the author [23]. Note that all these figures indicate the possible usefulness associated with the uses of non-orthonormal or redundant function bases, as well as the drawbacks of bases with tight frame bounds.

5.5 Wavelet frame bounds and redundancy

If a function $\psi(t)$ is to be qualified as a wavelet of CWT, then the only requirement is that $\psi(t)$ meets the "admissability condition,"

$$2\pi \int_{-\infty}^{\infty} \frac{|\widehat{\psi}(\omega)|^2}{|\omega|} d\omega = C_\psi, \tag{5.7}$$

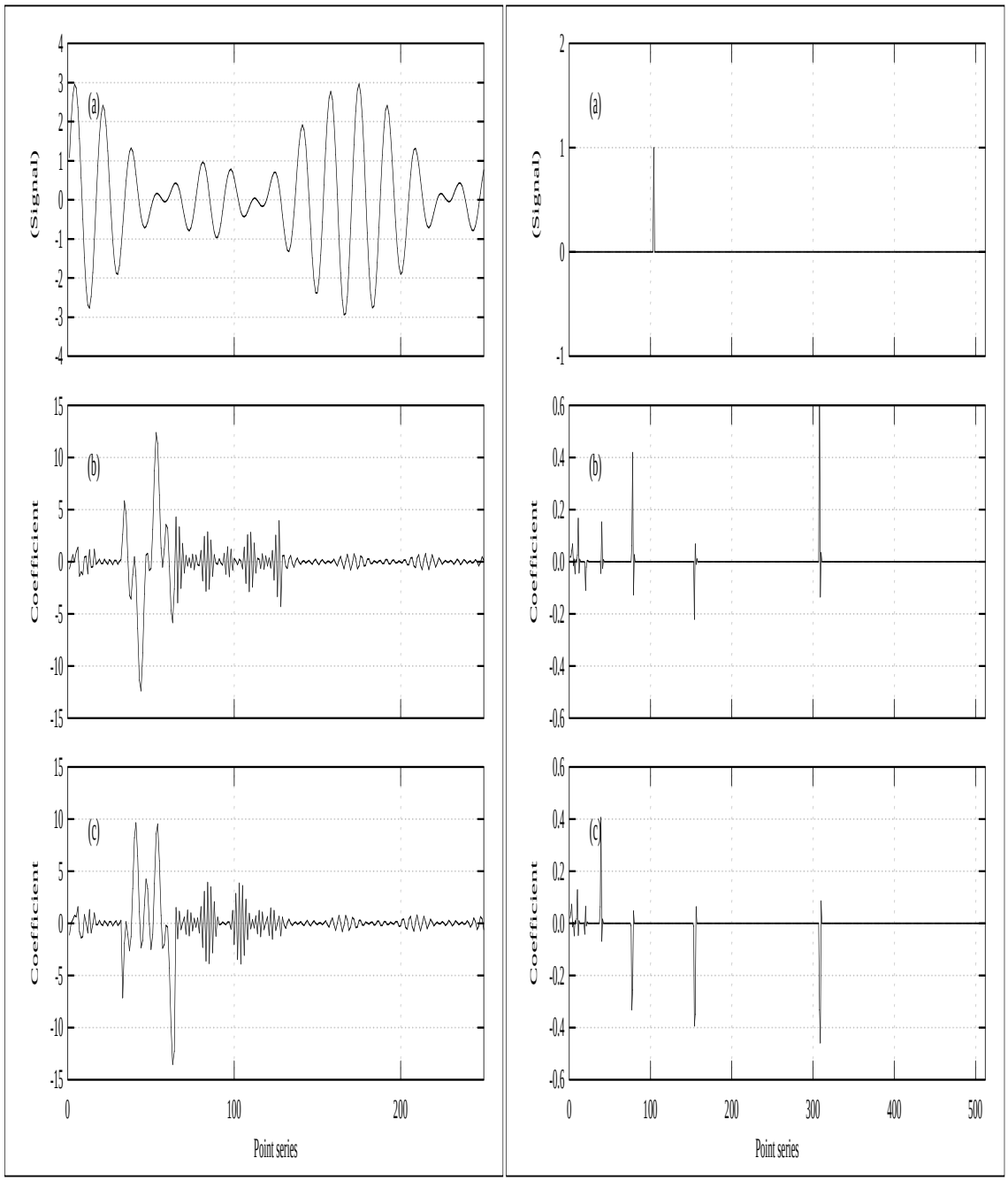

Fig 5.1 (Pha–Eff-1) The concerns related to the shift non-invariant property of wavelet transforms are shown in this figure. This property has important implications in the practical usefulness in physical applications of wavelets between discrete and continuous bases.
The top sub-figure in each column shows original signal individually.
The middle one shows its wavelet transform distribution.
The bottom one shows the transform result for its individually shifted signal.
For the signal in the left column it is shifted 3 points to the left and the wavelet used is ON33A. For the signal in the right column it is shifted 20 points to the left and the wavelet used is BO22D.
The property shown in this figure is linked to the vast difficulty arising from phase noise and its poor performance in coherent studies.

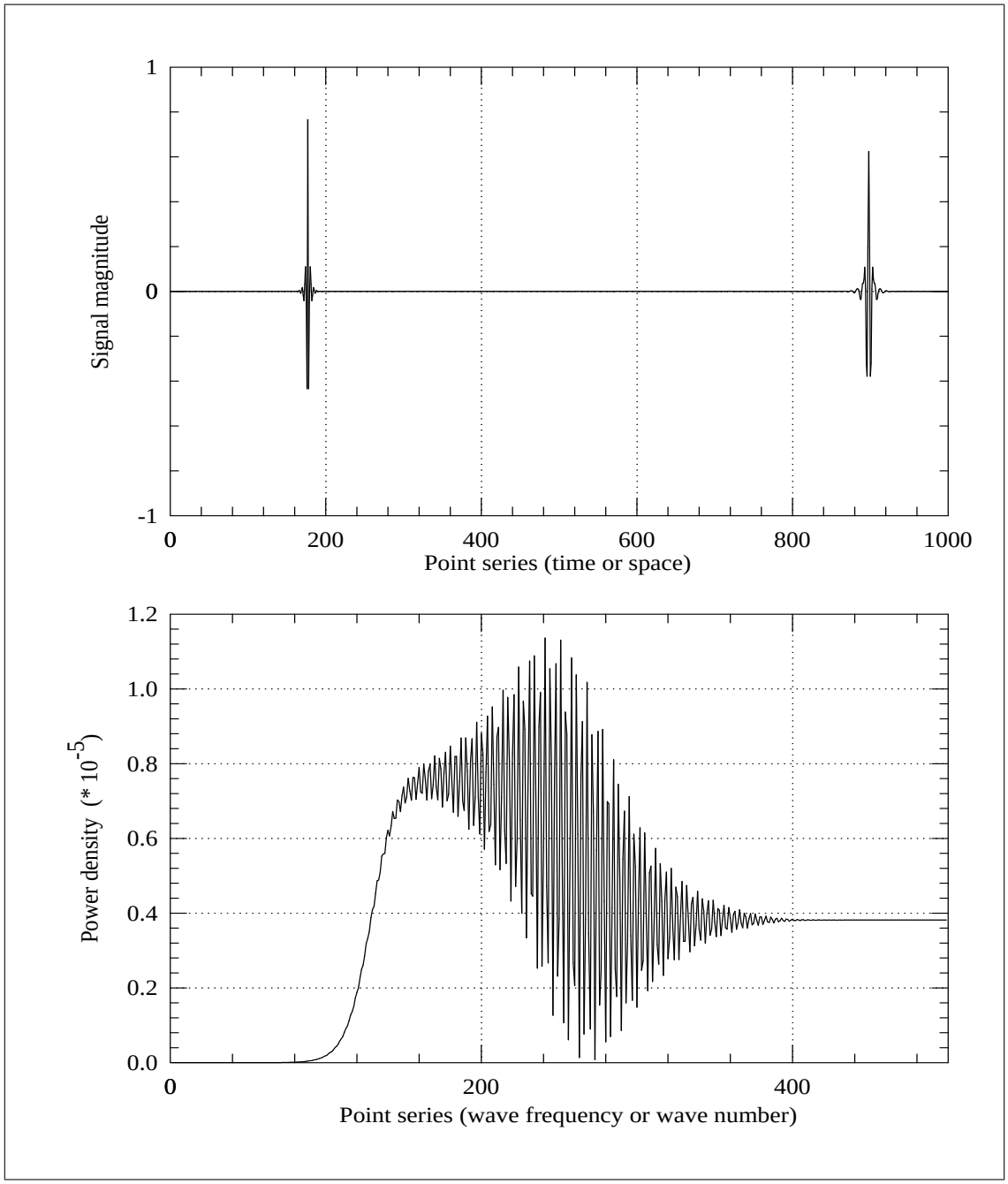

Fig 5.2 (Pha–Eff-2) This figure shows the same concern as that of the preceding figure, but with different method of rendition. More precisely, the effects of ambiguity and phase noise arising from local transient features of a signal are illustrated using a signal comprised of two separated wavelets.

The top sub-figure shows the signal comprised of two Lemarié wavelets located at two neighboring scales (the least two scales within a 1024-point series). And the pulse at left corresponds to the inverse wavelet transform for unit wavelet coefficient at point 600, i.e., e600; the right corresponds to e470.

The Fourier power spectrum is shown in the bottom sub-figure. The distracting consequence arising from extreme variation should be comprehendible.

where C_ψ is a constant specific to individual ψ, and $\widehat{\psi}(\omega)$ is the Fourier transform of $\psi(t)$. Here, among several definitions of the Fourier transform forward and inverse pair, the adopted one is:

$$\widehat{\psi}(\omega) = \frac{1}{\sqrt{2\pi}} \int_{-\infty}^{\infty} \psi(t) e^{-i\omega t} dt \tag{5.8}$$

and

$$\psi(t) = \frac{1}{\sqrt{2\pi}} \int_{-\infty}^{\infty} \widehat{\psi}(\omega) e^{i\omega t} d\omega. \tag{5.9}$$

The admissability condition is the integration of power spectrum weighted by the inverse of the absolute value of frequency; therefore, it implies that the wavelet should have little power at low frequency and is total nil at zero frequency, i.e., the area between the wavelet curve and the abscissa integrates to zero. This feature of reasonable decay and finite support length is the outright instinct of wavelet. The dilated and translated versions of this wavelet are $\psi_{a,b}(t) = \frac{1}{\sqrt{a}}\psi(\frac{t-b}{a})$, where $a > 0$ and $a \in \mathbf{R}$ and $b \in \mathbf{R}$ are the dilation and translation parameters, respectively; and $\frac{1}{\sqrt{a}}$ is the normalization factor for L^2-norm. The $\psi_{a,b}$ satisfies admissability condition too.

The admissability condition is a very loose constrain; it does not provide a clear concept of redundancy concerning applying CWT to discretely sampled signals. To illustrate this redundancy, let us use the discrete wavelet frame (since the frame wavelet certainly qualifies as a wavelet for CWT): $\psi_{a_0,b_0;j,k}(t) = {a_0}^{-j/2}\psi({a_0}^{-j}t - kb_0)$, where a belongs to the set of discrete dilations a_0^j and b to the set of discrete translations $a_0^j k b_0$; $j, k \in \mathbf{Z}$; and $a_0 \neq 1$ and $b_0 > 0$ are fixed positive constants. For such a discrete wavelet frame we need to impose a more restrictive condition on $\psi(t)$ for its admittance, i.e., the stability condition,

$$b_0 A \leq 2\pi \sum_{j \in \mathbf{Z}} |\widehat{\psi}({a_0}^j \omega)|^2 \leq b_0 B, \tag{5.10}$$

where A and B are positive constants and $0 < A \leq B < \infty$. The fixed constants b_0 and 2π are intentionally kept since they are related to normalized wavelet basis and since the magnitudes of A and B are related to the redundancy of the basis.

The stability condition may look abstract, but we give its physical implication as: to be able to let a function be reconstructed from its wavelet coefficients, i.e., the operation is reversible, we need a process which is convergent when summing all its scales or frequency components. It is therefore necessary that the sum of the power of all the constituent elements can neither be nil or infinity. If the sum is zero, then the elements are all of zero measure — nothing exists. If the sum is infinity, then the elements are significantly overlapping in time and frequency — there is either too much dependence or too much ambiguity and tangling (just like two vectors paralleling to each other do not constitute a good vector basis for two dimensional vector space).

Speaking of the reconstruction of a function from its wavelet coefficients one always involves a dual wavelet except for orthonormal basis where the wavelet itself is its own dual — self-dual. And since the roles of a wavelet and its dual can always be interchanged in both decomposition and reconstruction, the above statements apply equally well for dual wavelet; but their frame bounds will generally be different since the sets of convolution coefficients are different as hinted by the different entropy values given in the previous chapter.

If the basis functions are normalized and the inequality of the stability condition are optimized for both the greatest lower bound and the lowest upper bound, i.e., when A and B are defined as

$$A = \inf\left[\frac{2\pi}{b_0}\sum_{j\in\mathbf{Z}}\left|\widehat{\psi}(a_0{}^j\omega)\right|^2\right], \tag{5.11}$$

$$B = \sup\left[\frac{2\pi}{b_0}\sum_{j\in\mathbf{Z}}\left|\widehat{\psi}(a_0{}^j\omega)\right|^2\right], \tag{5.12}$$

then an indication of the redundancy is the average value of A and B, $\frac{A+B}{2}$, supposed that A and B are close to each other (almost tight). We elucidate the possible extreme redundancy of CWT as follows. If the dilated and translated versions of a function originating

from a certain set of discrete steps (a_0, b_0) constitute a frame with frame bounds A and B, then the frame bounds of a basis using the same function but with finer discrete steps, say $a_0/2$ and $b_0/2$, will contain the bounds of coarser discrete steps; therefore, the new lower and upper bounds both grow together. This nested relation can be extended infinitely and in the limit sense it is included in the algorithm of CWT. This is the reason why there is no practical value of numerical reconstruction in CWT, although CWT is reversible analytically. Another intuitive explanation is even easier to comprehend: when apply CWT to discretely sampled signal, since for each scale the number of wavelet coefficients is the same as the number of data points and since we can specify scales in whatever resolution we like, we virtually have an unlimited number of wavelet coefficients. The sum of the powers of these coefficients can be unimaginatively huge, or even unbounded; On the other hand, the sum of signal energy is fixed. If we generalize the redundancy concept of DWT, i.e., the ratio between the two sums indicates the degree of redundancy, then for discretely sampled signal a continuous wavelet transform can possibly yield immense redundancy.

Even though extreme redundancy may exist for the continuous wavelet transforms, the content of information or its usefulness may behave like a cumulative pdf curve of a Gauss function which will saturate at a later stage. Our numerical results from studies of coherent behaviors among wind, wave and current related signals vindicated undoubtedly such a situation [20].

5.6 Beneficial scenarios due to redundancy

Redundancy may be a nuisance in certain applications such as those that focus on the perfect reconstruction of signal or on the efficiency of coding and decoding; however it has also shown its promising aspects in several applications. Three prominent points are the results of established cases: (1) Redundancy does not mean that a whole bunch of coefficients are needed to give a good replicate of the original signal, that is to say, significant

signal contents can still be retrieved from only a comparatively small amount of coefficients with respect to that of tight or almost tight wavelet frames. (2) Redundancy means that effects of noise either embedding in the sampled signal or arising from the nature of numerical processes (such as frequency leakage) can be reduced by taking advantage of the vast sample space of transform coefficients. (3) If additional features, such as "total positivity" and " complete oscillation" of wavelet are incorporated, the effects on noise reduction or ambiguity removal may be greatly enhanced; together with the redundancy effects they facilitate the design of a very beneficial analyzing scheme. An example of the first point is Mallat and Zhong's [27] (see also Froment and Mallat [13]) signal reconstruction from local maxima using a quadratic spline wavelet. In fact, the mother wavelet they used is basically a loose wavelet (i.e., a wavelet with analytical aspects not being well defined and therefore not really to be qualified as a wavelet), but they were able to recover images quite well using only local peak values of wavelet coefficients that are associated with only dyadic scales. For the second and third points, our studies on the coherent features in the wind, wave, and rain coupling system serve as an example [20].

One last point to note is to compare the admissability condition of CWT with the stability condition of DWT. Here one can easily perceive the great difference in flexibility between the two. In addition, the stability condition is a necessary condition, and not all choices for ψ, a_0, and b_0 lead to wavelet frames. Moreover, stability may not guarantee a good numerical behavior. Figures 6.1 (W Quirks-1) and 6.2 (W Quirks-2) show the results of a few numerical experiments in which the problems of numerical convergence are illustrated using the blow-ups of wavelet curves. In the figures two bi-orthogonal wavelets are blown up around their individual points using refinement cascade, and the blow-up curves show the possible intrinsic absurdity arising from peculiar analytical properties associated with these wavelets. Here, the two bi-orthogonal wavelets are, respectively, with four and twenty filter weights and both are constructed from quadratic spline scaling function [12]. The top sub-figure indicates a case where the DWT fails numerically to characterize the mother wavelet (not converging) even though the associated wavelet

frame qualifies theoretically as a Riesz basis. The bottom sub-figure shows strange alternating inclinations of wavelet curves with a poor convergence. The figure also illustrates the point that, for studying water-wave related signals and their physics, most of the fancy wavelets with bizarre wave forms are not of our choice, as are also indicated by their high entropy values given in the previous chapter.

5.7 Summary

In this chapter we point out the counterpart continuous wavelet to the best discrete wavelet. It will be observed that the three main additional ingredients, i.e, the phase, the carrier frequency and the redundancy, thus introduced make possible the physical optimization and lead to the outstanding results of wavelet coherences. ❖

Chapter 6

The Optimization for Physics

6.1 The demand for better physics

In addition to the various concerns about the peculiar properties specific to discrete and continuous wavelet transforms as are stated in the previous chapter, herein we focus on the practical interest in what can be done to improve the physical relevance between the basis functions and the wave constituents of our signals. For example: does the decaying features of basis functions akin to the physics of component waves? In fact, this simple question outlines another fundamental theme of this chapter: if time-frequency windows of fixed shape and size (the case of STFT) is less suitable than time-frequency windows of fixed size but with flexible shape (the cases of DWT and CWT) in characterizing multi-scale transient signals, then time-frequency windows which are flexible in both shape and size should provide even better adaptations. The theme is intuitive right, the background is not without commitments.

Based on this perception, further concerns evolving from the previous chapter can be put forward quite simply: (1) Can we utilize this redundancy to improve the relationship between wavelet's analytical form and its physical interpretability? (2) If redundancy leads to adaptation, does the adaptation still preserve the complete information content of the signal studied? (3) Is the scheme of adaptation efficient and easy to implement? Question one is related to the distribution or the degrees of freedom of time-frequency

windows in the phase plane and will be dealt with in the next chapter. Question two will be answered through the verification for the existence of a condition of "resolution of identity" using a special case of Morlet wavelet, as is also to be given in the next chapter; for now, a short explanation is that, if one just applies the adaptation to finite range(s) of scale, then what is lost or unaccounted for in the adaptation process can still be recovered from some dilated and translated versions of some finer scale wavelets originating from the same $\psi(t)$ in the CWT. The success of Mallat and Zhong's case also indicates such a possibility. Question three depends on the adaptation scheme. But, based on the somewhat intuitive adaptation used here, it is stated that nothing complicate is introduced.

One practical aspect for all the three points is: when analyzing signal we are almost always interested in only finite scale range(s), so what is really needed is to implement the adaptation locally. Hence it may be beneficial not to stick with stubborn time-frequency windows and to adopt a scheme that is numerically with the same easiness and physically more sound.

6.2 Degrees of freedom and the uncertainty relation

The flexibility of constructing wavelet function basis, i.e., the possibility of the adaptation, is associated with the number of degrees of freedom of the time-frequency windows within a phase plane. The number of degrees of freedom for an orthogonal basis is generally defined as the total area of the phase plane divided by the area of the time-frequency window corresponding to that determined by the mother wavelet. For any time-frequency kernel the maximum number of degrees of freedom is determined by the Heisenberg uncertainty relation or Heisenberg's inequality [5]. It is illustrated here that, even though it is impossible to increase the limiting degrees of freedom, there is no further limitation imposed upon the present adaptation. Besides, this section also serves two purposes: (1) illustrate the basic functionality of the modulation mechanism for STFT, which in turn is conceptually the same as the dilation mechanism for WT; (2) outline the relation between

redundancy and the Heisenberg uncertainty using possible distribution of time-frequency windows within a phase plane.

The uncertainty relation states that the product of bandwidth Δ_ω and duration Δ_t of a signal cannot be less than a minimum value of $\frac{1}{2}$ when the Δ_t and $\Delta\omega$ are defined as the standard deviations of packet energy $|f(t)|^2$ and power spectrum $|\widehat{f}(\omega)|^2$ with respect to their centroids, respectively:

$$\Delta_t{}^2 = \frac{\int_{-\infty}^{\infty}(t-\overline{t})^2|f(t)|^2dt}{\|f(t)\|^2}, \tag{6.1}$$

$$\Delta_\omega{}^2 = \frac{\int_{-\infty}^{\infty}(\omega-\overline{\omega})^2|\widehat{f}(\omega)|^2d\omega}{\|\widehat{f}(\omega)\|^2}, \tag{6.2}$$

where $\overline{t} = \int_{-\infty}^{\infty} t|f(t)|^2dt/\|f(t)\|$ and $\overline{\omega} = \int_{-\infty}^{\infty}\omega|\widehat{f}(\omega)|^2d\omega/\|\widehat{f}(\omega)\|$. As is also illustrated in Chui's treatise textbook [6], the time-frequency window, $\Delta_t\dot{\Delta}_\omega$, of the semi-orthogonal wavelet is nearly equal to the minimum value of the Heisenberg uncertainly principal, and this very optimistically provides the opportunity for applying the adaptations. That is to say, there is an easy to way get round of the uncertainty relation by going through a modulation process (i.e., multiplying a basis function with a complex exponential). Since in Fourier analysis a modulation in one domain corresponds to a shift in the other domain, such a process causes the new variance Δ_ω to increase dramatically. Figure 6.3 (Heisenberg) shows such a mechanism. It is seen that the new $\Delta_t\Delta_\omega$ is significantly larger than $\Delta_t D_\omega$, i.e., even larger than the limiting value for Heisenberg uncertainty relation; therefore, there is quite a lot of flexibility to devise the time-frequency windows. In view of the similarity between the modulation mechanism for STFT and the dilation mechanism for WT, especially for the case of Morlet wavelet, we anticipate that there is an ample space for adapting the time-frequency windows. Furthermore, as pointed out by Bracewell [5], there exists no theorem depicting the lower limit of $\Delta_t D_\omega$, i.e., no new restriction for D_ω; therefore no further limitation on the number of the degrees of freedom is induced. Overall, it is quite flexible to draw time-frequency windows which generally

do not violate the uncertainty relation when we express a signal in its two dimensional phase plane.

6.3 Time-frequency windows and the physics

The algorithm and the physics associated with the adaptation of time-frequency windows can be illustrated easily by going through practical examples. Though the adaptation does not need to be confined to any specific type of wavelet, the Morlet wavelet readily serves for such a purpose. As was stated in the previous chapter that the Morlet wavelet is almost identical to a modulated Gaussian, and a modulated Gaussian matches almost exactly with cardinal B-spline wavelet of order greater than or equal to three, which is exactly the identified best basis wavelet. Overall we therefore, on the one hand, benefit from an extremely natural transition from DWT to CWT, on the other hand, gain the practical merit of the adaptation.

Before we go into the adaptation, let us recount more explicitly two very important features that distinguish the identified optimum basis from the other bases and that definitely contribute to the causes of the optimum basis' successful applications: (1) The best basis' cardinal spline scaling function and its associated wavelets possess, respectively, the nice properties of "total positivity" and "complete oscillation". We note that these two properties physically imply that its wave form is relatively smooth and without ad hoc variations when compared with some fancy wavelets with finite support lengths. (2) The cardinal B-spline wavelet is either symmetric or anti-symmetric. Therefore, it benefits from the linear-phase filtering. The physical implication of this is: slight differences in wavelet coefficients will not cause significant differences in their reconstructed wave forms, or alternatively, the modulations of the wave forms are comparatively less abrupt. With more natural transitions for both forward and inverse transforms under various circumstances, the impacts to our perception or visualization of an interaction process due to varying input conditions are leaning toward relatively evolutionary tendencies rather

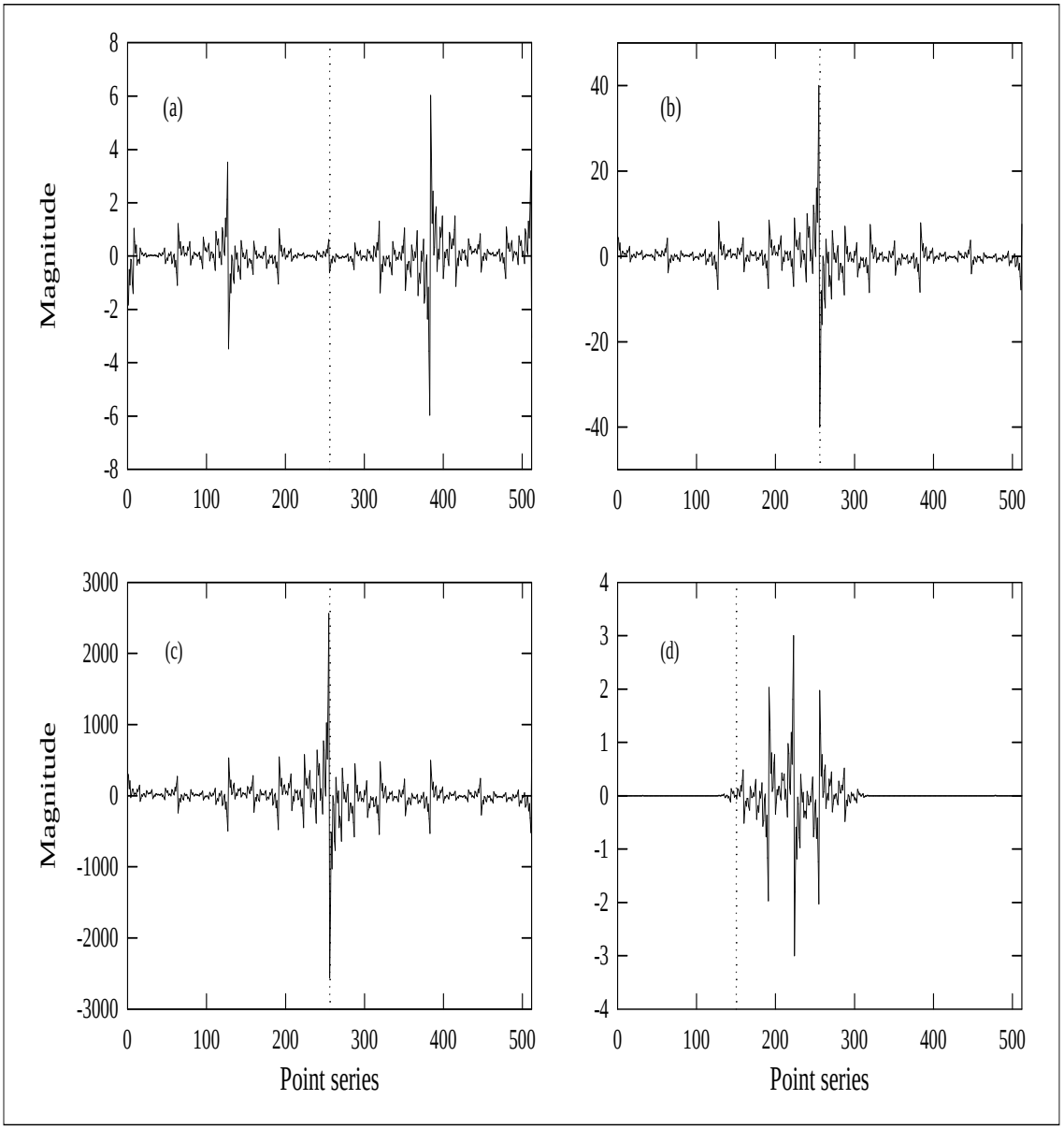

Fig 6.1 (W Quirks-1) Wavelets with fancy analytical properties are often of peculiar wave forms and are not of proper candidate for studying water-wave related physics — either judging from their entropy values given in the previous chapter or form their stability conditions shown in this figure.

The peculiarity and the sensitivity of these types of wavelet constructions are somewhat illustrated by the phenomena appear in the blow-ups of bi-orthogonal wavelets BO31O. In this case the blow-ups diverge rapidly and fail to identify itself numerically in the refinement cascade. The blowup details are as follows.

Scale interval between blow-ups: 2^6 between subsequent sub-figures (a), (b), and (c);

Unit value originating point (the point used to obtain the curve in sub-figure (d)): level 2, position 12, i.e., element U_2^{12} in the notation of figure 2.21 (WP Tree);

Blow-up point: point 150 indicated by a vertical dotted line in the sub-figure (d).

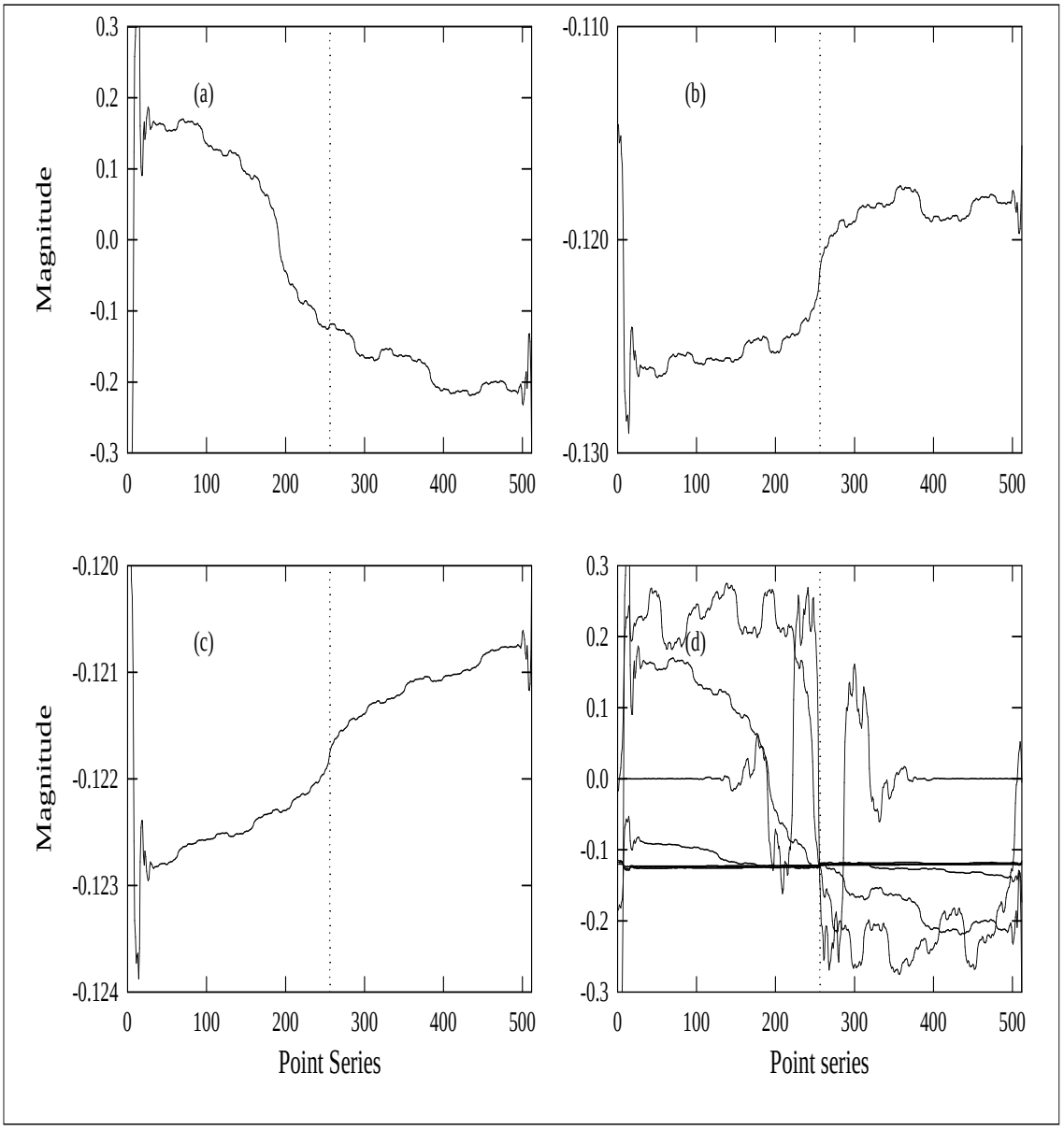

Fig 6.2 (W Quirks-2) Again, another instance of peculiarity and sensitivity arising from fancy wavelet construction is illustrated by the phenomena appear in the blow-ups of the bi-orthogonal wavelets BO35O.
The blow-ups here converge poorly and incline with opposite slopes.
The blowup details are as follows.
Scale interval between blow-ups: 2^6 between subsequent sub-figures (a), (b), and (c);
Unit value originating point (the point used to obtain the curve in sub-figure (d)): level 2, position 12, i.e., element U_2^{12} in the notation of figure 2.21 (WP Tree);
Blow-up point: point 256 indicated by the intersection point of various curves in the sub-figure (d).
It is noted that these peculiarities indicate the poor entropy values, as well as the consistently pathetic usages in water wave simulations. It is the author's belief that fancy constructions of wavelets do not adhere to the physics of water waves.

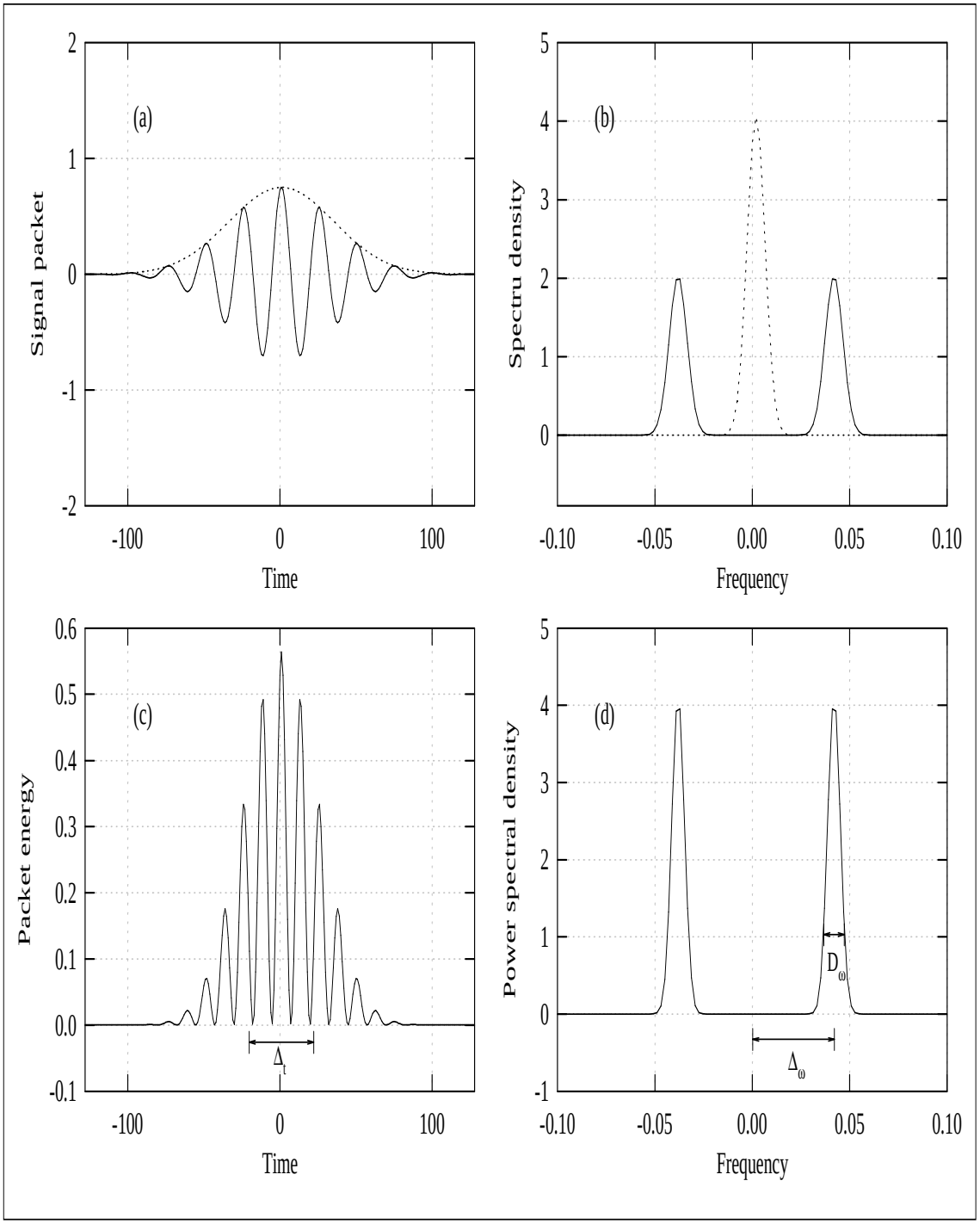

Fig 6.3 (Heisenberg) The Heisenberg uncertainty relation and the modulation versus shift property (adapted from Bracewell 1986). A modulation process renders $\Delta_t \Delta_\omega \gg \Delta_t D_\omega$. Where Δ_t, Δ_ω and D_ω are the root-mean-square departures from the centroids, respectively. The property helps significantly in possible adaptations of wavelets for the purpose of modeling water wave physics. That is to say, an adaptation generally will not violate the restriction of the minimum requirement of the product between the two moments of time and frequency distributions.

than drastic turnovers. Still, one additional implication of practical significance is: distortions are far less severe when noise and uncertainty are poignant. The phase plane in figure 6.4 (Adap–Simu) and the various blow-up curves in figures 6.1 (W Quirks-1) and 6.2 (W Quirks-2), 2.29 (BU–BO31O) and 2.30 (BU–BO35O), as well as figure 5.1 (Pha–Eff-1) manifest the problems and possible difficulties associated with wavelet bases that do not posses these properties.

Up to this point we have illustrated many specific properties, associated either with DWT or with CWT, that bestow upon our desires when analyzing our water wave related signals; even though their outstanding effects might only be appreciated when we get to the reality of analyzing experimental data. But here let us embark the further work on an improvement — enhancing wavelet's physical implication based on the affinity between the identified best basis and the Morlet wavelet.

The Morlet wavelet is the following complex function:

$$\psi(t) = \pi^{-1/4}(e^{-i\omega_0 t} - e^{-\omega_0^2/2})e^{-t^2/2}, \tag{6.3}$$

in which ω_0 is a constant related to the carrier frequency and the term $e^{-\omega_0^2/2}$ justifies the admissability condition. Its Fourier transform is almost a shifted Gaussian and is given by

$$\widehat{\psi}(\omega) = \pi^{-1/4}[e^{-(\omega-\omega_0)^2/2} - e^{-\omega^2/2}e^{-\omega_0^2/2}]. \tag{6.4}$$

In addition to the general meaning of the modulation frequency, the ω_0 has the physical implication of the amplitude ratio r — the ratio between the second highest peak and the first highest peak of $\psi(t)$ — i.e.,

$$r = \psi(t_2)/\psi(0), \tag{6.5}$$

in which t_2 is the abscissa of the second highest peak. The exact value of t_2 can be obtained by solving numerically the transcendental equation derived from the derivative of the ψ

function, but a fairly good estimate is obtained by simply dropping the second term of the above complex function since the second term is generally five order of magnitude less than the maximum value of the first term, i.e.,

$$\omega_0 \approx \frac{2\pi}{t_2} \approx \pi \left(-\frac{2}{\ln r}\right)^{1/2}. \tag{6.6}$$

The higher the ω_0 is, the smaller the ratio r becomes. If ω_0 is constant, then the ratio r for different wavelet dilations or scales keeps constant too. Here comes the core question: whether constituent wave components of different scales and time spans all possess this fixed decay feature? To show that this is not true, let us examine the composite water wave system that is with viscous damping.

For deep water waves with a clean surface the energy losses due to viscous dissipation arise almost entirely from the straining of the irrotational motion in the water column, and the part of contribution from viscous stresses in the surface layer is negligible. It was shown [15, 30] that the time rate of change of the energy density is

$$\dot{E} = -2\mu\sigma^2 {a_w}^2 k, \tag{6.7}$$

where μ, σ, a_w, and k are the dynamic viscosity of the water, the wave frequency, wave amplitude, and wave number, respectively. Since in deep water $E = (2k)^{-1}\rho\sigma^2 {a_w}^2$, where ρ is the water density, the attenuation coefficient

$$\gamma_\nu = -\frac{\dot{E}}{2E} = 2\nu k^2, \tag{6.8}$$

where ν is the kinematic viscosity of the water. Therefore the energy density of the wave evolves as

$$E = C_1 e^{-2\gamma_\nu t}, \tag{6.9}$$

where C_1 is a constant, and the amplitude decreases with time in accordance with

$$a_w = \sqrt{\frac{C_1 2k}{\rho\sigma^2}} e^{-\gamma_\nu t} = C_2 e^{-2\nu k^2 t}, \tag{6.10}$$

where C_2 is a constant if σ does not vary. Comparing the decay of wave amplitude of Morlet wavelet with the decay of the physical model, one sees both similarity and dissimilarity. The similarity is that the attenuation coefficients in both models have inverse square dependence on scales — the former in $(1/a)^2$ and the latter in k^2. The dissimilarity is in the time dependence of the exponent in the exponential — in Morlet wavelet it is in t^2 dependence, while in the physical model it is in linear dependence. It is therefore anticipated that Morlet wavelets based on a fixed modulation shape are not good representations of water waves of different scales. Or stated otherwise, basis functions originating form a single mother Morlet wavelet do not form a good basis.

Now the situation is clear: the constant ω_0 either overestimates the viscous decay of water waves at the low-frequency end or, otherwise, under-estimates those at the high-frequency end. Form a practical judgement of the modulation curves, it is quite reasonable to argue that the deviation is probably more significant for waves with a longer life span when a standard r value of Morlet wavelet, i.e., $r = 0.5$, is assumed. The perceptions here provide the footing for the present adaptation — with different values of amplitude ratio r for different wave scales we are really attemptimg to simulate the evolution process with a more realistic condition. The expansion or contraction of wavelet support length for a specific scale just reflects the devising of flexible constructions of time-frequency windows, and adjusting r is in turn using a variable ω_0. The general guideline is to use a comparatively larger ω_0 (associated with a narrower frequency band) for waves of a longer time support; and vice versa, a comparatively smaller ω_0 (a wider frequency band) for a shorter life span. Here it naturally comes to assume the ω_0 to be a function of scale, i.e., $\omega_0 = \omega_0(a)$. And the varying shapes and sizes of the time-frequency windows are

now determined by

$$\psi_a\left(\frac{t-b}{a}\right) = \pi^{-1/4}\left[e^{-i\frac{\omega_0(a)}{a}(t-b)} - e^{-\omega_0(a)^2/2}\right]e^{-\frac{(t-b)^2}{2a^2}}. \tag{6.11}$$

6.4 The carrier frequency and the adaptation

Earlier we have stated a few nice features of the identified best basis. There is one additional feature that is practically significant because of its relevance to the Morlet wavelet — the physical perception of the sizes and shapes of "scales". Without such a property everything will look obscure. In fact, we have seen a lot of ambiguities or abstractions in many studies where they only involve presentations using non-dimensional scales rather than using the more appropriate physical quantities of carrier frequency even though they are working on modulated Gaussian or Morlet wavelets. We note that the wavelet coefficient generally refers to "scale" not to "frequency". Scale has no dimension, but carrier frequency has a physical unit and is associated with a Gaussian bell modulator. Furthermore, scale generally corresponds to complicate combination of several frequency bands such as what implied by the compactly supported orthogonal wavelets shown in figure 6.4 (Adap–Simu). Therefore, in order to have a clear picture of a "scale" one needs to consider: What does the basic wavelet look like? What is the actual support length? And, what is the physical sampling interval? All these severely tangle our thought, and we get lost easily. Take as an example: the numerical processes for both discrete Fourier transform and DWT care nothing about the physical units and only the index is important; however, there is an easy conversion from index to frequency for Fourier coefficient, but not for wavelet transforms except the ones associated with the Morlet wavelet. It is totally impossible to visualize the corresponding object just from the index of a wavelet coefficient. For the best basis and the related adaptation the difficulty is avoided, since the precise and physical "carrier frequency" is easily seen to be $\omega = \omega_0(a)/a$, supposed that $\omega_0(a)$ is large enough, say above 5. Again, the point to caution is: illustrations using

scale parameter a can be confusing and misleading since the same a may correspond to different actual scales or frequencies when different adaptations or different wavelets are used.

As was stated in the previous section that the present adaptation can always be applied to finite scale range(s) and that the transform only needs to be implemented for scale range(s) that we are interested in. Still, we give an additional description of the flexibility concerning this. Since one can always regard that the set of sampled data points is derived from a certain specific function, but there are basically infinitely many functions which can pass all these sampling points. And since the functions passing through these points may be either band-limited or -unlimited but the sampled signal is always band-limited (since numerical analysis is always associated with finite scale range); therefore, the situation indicates that there exists freedom to make adaptation for ω_0 and also implies the possible redundancy when CWT is applied to the sampled signals. The remaining problem is how to define a suitable decay parameter ω_0. Nevertheless, based on the above mentioned practical concern of wave decay and the somewhat intuitive adjustment, we show the possible improvements in time-frequency resolutions when the adaptation is applied to experimental data. But let us first give a numerical simulation.

For the simulated data we use a parabolic chirp where the frequency range of interest covers the whole band width of the signal, i.e., from almost zero frequency to that corresponding to Nyquist sampling rate. And a linear variation of $\omega_0(a)$ from 10 (for large scale end) to 7 (for small scale end), as opposed to the commonly adopted fixed value of 5.3 (corresponding to $r \approx 0.5$), is assumed. As is seen from figure 6.4 (Adap–Simu), the adapted one gives better frequency localization for almost all frequencies except the lowest two carrier frequencies (in fact the adaptation can be further adjusted for this part, and to have better resolutions for these two carrier frequencies the values of their $\omega_0(a)$ should be less than 5.3, but the concern here is mainly on the serious edge effects). A phase map for the complex wavelet coefficients derived from a refined ridge extraction scheme is also shown as the top right sub-figure. Here it provides a much better identi-

fication of scales of main power contents than what can be provided by Morlet wavelet. F:TFM-WindWave

For the experimental data water waves measured in the wind blowing oval tank are used, in which reasonable frequencies should lie between 1.5 and 10 Hz. Earlier we mentioned that the Morlet wavelet is likely to overestimate the decay of longer waves in the long run; therefore, relative to higher frequency waves, we should reduce the decay parameter ω_0 for low frequency ones. Based on this understanding we heuristically assume

$$\text{Erfc}\left[\frac{4}{10}\left(\frac{\omega_0}{a}+2.5\right)-2\right]3+5=a\omega \tag{6.12}$$

where Erfc is the complimentary error function and ω is the carrier frequency. This equation may be modified according to the type of signal studied or according to the frequency range of one's interest. Figure 6.5 (Adap–Erfc) shows the curve of the function. The logic for the choice of its constants is self explained in the attached program piece. Figure 6.6 (Adap–Wave) shows results without and with the adaptation. Here, the varying $\omega_0(a)$ is from 9.16 (for the large scale end) to 5.26 (for the small scale end), as opposed to the fixed value of 5.3. Again there are less smearing effects at the lower portion of the time-frequency plane since we mainly adjust decay parameters for the low-frequency end.

A few additional points are: (1) The dominant carrier frequency is about 2.4 Hz in this case; (2) Waves of all frequencies keep constantly evolving, since light and dark regions constantly interlace; (3) There are grouping effects. Waves with significant energy contents are more enduring and the durations of darker bands are much longer than those of higher frequencies. This indicates that our adjustment for decay parameters is based on a reasonable ground; (4) There is an obvious bifurcation among scales, especially for the intermediate frequency range of about 3 to 4.5 Hz; it suggests that the phenomenon of energy cascade from where energy concentrates to neighboring areas. Judging from these characters it seems that the energy phenomenon in a multi-scale wave field is somewhat similar to that in a turbulent flow field (see Tennekes and Lumley [32]).

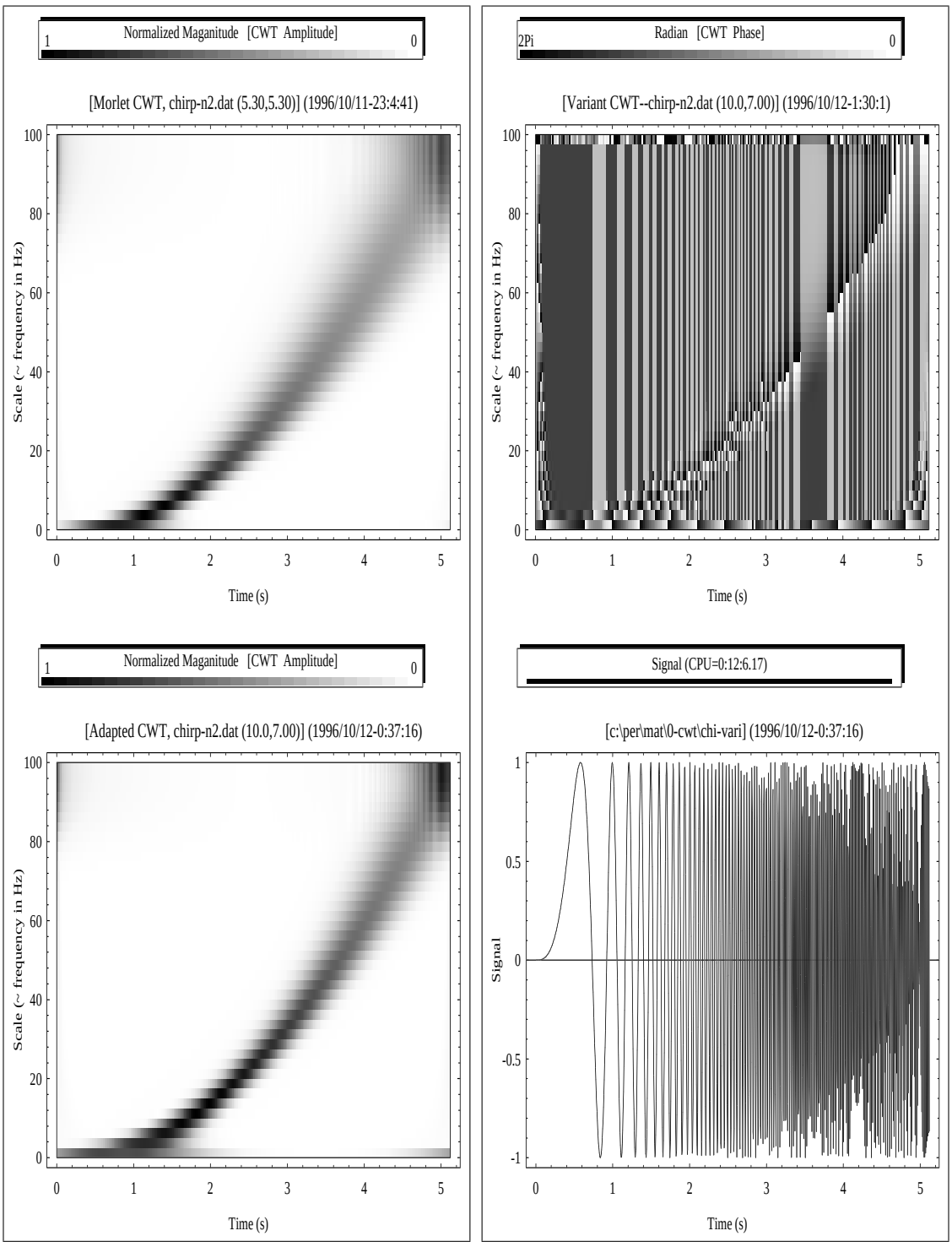

Fig 6.4 (Adap–Simu) The time-frequency distributions of a parabolic chirp `(bottom right)` with `(top left)` and without `(bottom left)` adaption of the carrier frequency parameter ω_0. In generally the adaptation yields a more concise distribution and a better coverage of frequency range.
An additional time-frequency map is shown in the top right. In which the transformation is associated with a wavelet variant devised by the author (Lee and Wu [21]). The wavelet variant has refined capability in ridge extraction and shows less ambiguity.

```
obeg=11.;  oend=5.;
fcenter=2.5;  fdilation=10/4;   fshift=2. ;

perfc=Plot[ Erfc[(1/fdilation)* (freq +fcenter)-fshift]*
                          (obeg-oend)/2+ oend, {freq, -2.5, 8.5} ]
```

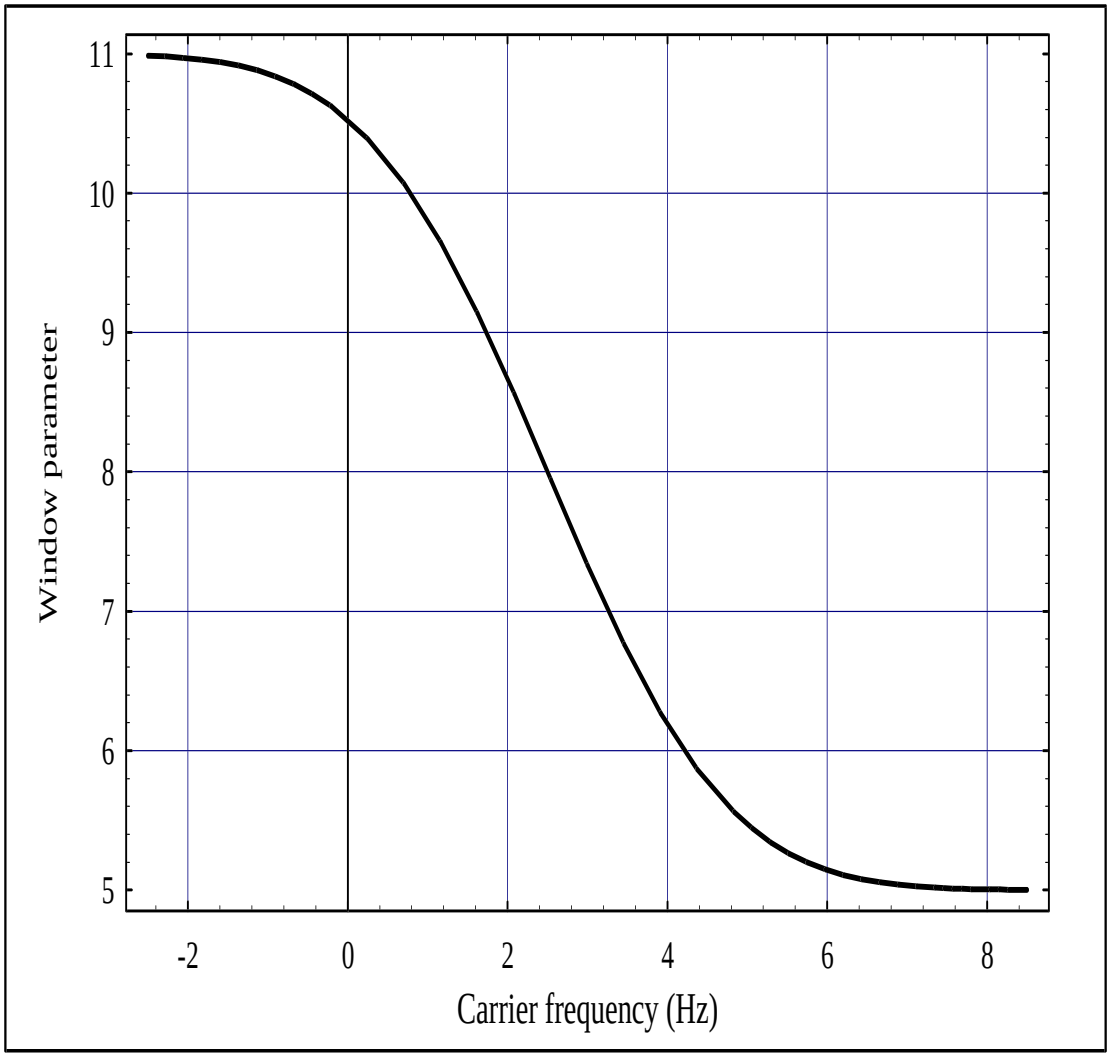

Fig 6.5 (Adap–Erfc) The ω_0 is a representative character of the wavelet time-frequency window kernel and intrinsically is the carrier frequency parameter. It has the physical indication of wave decay tendency. A constant ω_0 does not adhere to water waves of a board range of scale.

Here an adaptation of ω_0 in accordance with the carrier frequency is assumed and hinted by the program piece. The window kernel parameter as a function of carrier frequency is presumed to be the complementary Gauss error function Erfc.

And the curve can be adjusted according to several parameters of wave feature as indicated in the attached program piece: approximate peak frequency; significant range of frequency; range of decay parameter; as well as a shift adjustment parameter.

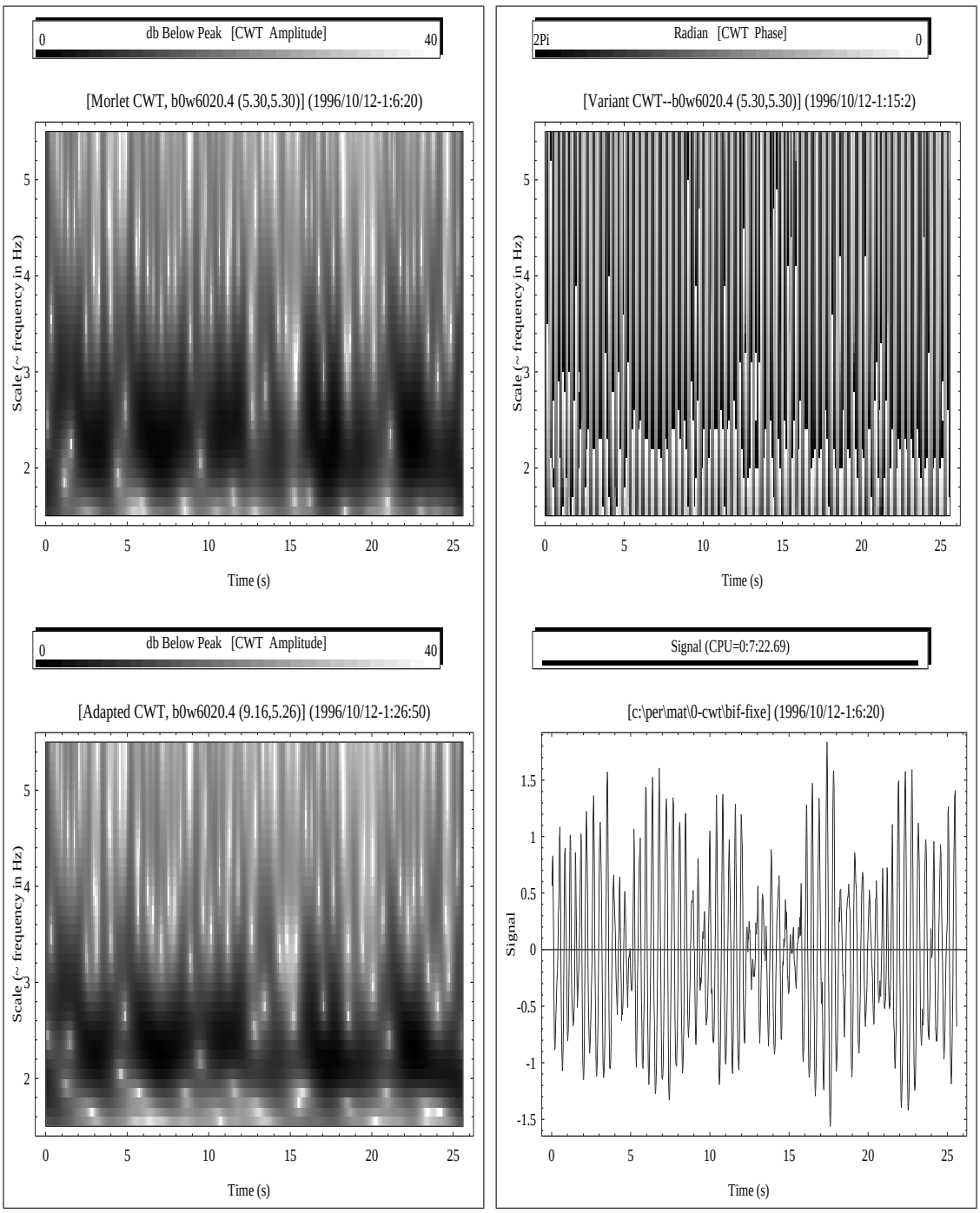

Fig 6.6 (Adap–Wave) The time-frequency distributions of a wind-generated water wave signal `(bottom right)` in a laboratory tank with `(top left)` and without `(bottom left)` adaption of the carrier frequency parameter. The assumed adaptation mainly adjusts the decay coefficients toward a mild decline for low-frequency part. Here we see less smearing for the main frequency band.
Note that due to the narrow-banded nature of the laboratory wind wave the adaptation may show more prominent effects for signals of a broad range of scales.
Besides, the time-frequency plot `(top right)` using the same wavelet variant as mentioned in figure 6.4 (Adap–Simu) provides an easy identification of the main power ridges as is generally infeasible using the Morlet wavelet.

6.5 Existence of the admissability condition

Earlier we gave a somewhat physical description on how the present adaptation manages to provide an almost "lossless" operation. Lossless means that the full information of a function is preserved during the transform and that we can recover the function from its wavelet coefficients, i.e., there exists a reverse operation. In the following we provide a more formal description through validating the existence of the identity resolution, which is basically just to show the existence of an admissability condition.

In an earlier illustration of the adaptation, a modified basis of wavelets was formed by adjusting the support length of dilated versions of $\psi(t)$ using different values of ω_0 which is further assumed to be a function of a. Furthermore, as explained in the previous section, a simple adaptation is the modification of carrier frequency according to $\omega = \omega_0/a$, i.e., $\omega_0 = a\omega$, we therefore further assume that ω_0 is a generalized function of $a\omega$ and the wavelet is

$$\psi_{\omega_0}(t) = \psi(t\,;\omega_0(a\omega)). \tag{6.13}$$

Its dilated and translated versions are given by

$$\psi_{a,b;\omega_0}(t) = \frac{1}{\sqrt{|a|}}\psi\left(\frac{t-b}{a};\omega_0(a\omega)\right). \tag{6.14}$$

And the wavelet coefficients of a function $f(t)$ are given by

$$\begin{aligned}
\mathrm{W}f_{\omega_0}(a,b) &= \langle f,\, \psi_{a,b;\omega_0}\rangle \\
&= \int_{-\infty}^{\infty} \frac{1}{\sqrt{|a|}} f(t)\overline{\psi_{\omega_0}\left(\frac{t-b}{a}\right)}dt \\
&= \int_{-\infty}^{\infty} \sqrt{|a|}\,\widehat{f}(\omega)\overline{\widehat{\psi}_{\omega_0}(a\omega)}e^{-ib\omega}d\omega,
\end{aligned} \tag{6.15}$$

in which $\widehat{\psi_{\omega_0}}(\omega) = \widehat{\psi}(\omega;\omega_0(a\omega))$. We follow the formalism to check that the inner

product of two functions f and g, $\langle f, g\rangle$, can be recovered from the integration of the projection of $\mathrm{W}f(a,b;\omega_0)$ into $\mathrm{W}g(a,b;\omega_0)$ along both real lines of dilation and translation variables. That is, whether the following equation exists:

$$\int_{-\infty}^{\infty}\int_{-\infty}^{\infty}\frac{1}{a^2}\mathrm{W}f(a,b;\omega_0(a\omega))\overline{\mathrm{W}g(a,b;\omega_0(a\omega))}dadb = C_{\psi_{\omega_0}}\langle f, g\rangle, \tag{6.16}$$

where $C_{\psi_{\omega_0}}$ is a constant. If it exists, then when g is taken as the Gaussian function with its variance approaching zero (i.e., g is practically the delta function $\delta(t)$), the inner product $\langle f(t'), g(t'-t)\rangle = \langle f(t'), \delta(t'-t)\rangle$ will recover $f(t)$ and the condition of the identity resolution is guaranteed.

The right hand side of the above equation equals to

$$\int_{-\infty}^{\infty}\int_{-\infty}^{\infty}\frac{1}{a^2}\left[\int_{-\infty}^{\infty}\sqrt{|a|}\,\widehat{f}(\omega)e^{-ib\omega}\overline{\widehat{\psi}(a\omega;\omega_0(a\omega))}d\omega\right]\times$$

$$\left[\int_{-\infty}^{\infty}\sqrt{|a|}\,\overline{\widehat{g}(\omega')}e^{ib\omega'}\widehat{\psi}(a\omega';\omega_0(a\omega'))d\omega'\right]dadb. \tag{6.17}$$

With the following two identity equations

$$\begin{aligned}&\widehat{F_a}(t,\omega_0(a\omega))\\ &\quad=\frac{1}{\sqrt{2\pi}}\int_{-\infty}^{\infty}e^{-it\omega}\sqrt{|a|}\,\widehat{f}(\omega)\overline{\widehat{\psi}(a\omega;\omega_0(a\omega))}d\omega\\ &\quad=\frac{1}{\sqrt{2\pi}}\int_{-\infty}^{\infty}e^{-it\omega}F_a(\omega;\omega_0(a\omega))d\omega,\end{aligned} \tag{6.18}$$

$$\begin{aligned}&\overline{\widehat{G_a}(t,\omega_0(a\omega))}\\ &\quad=\frac{1}{\sqrt{2\pi}}\int_{-\infty}^{\infty}e^{it\omega}\sqrt{|a|}\,\overline{\widehat{g}(\omega)}\widehat{\psi}(a\omega;\omega_0(a\omega))d\omega\end{aligned}$$

$$= \frac{1}{\sqrt{2\pi}} \int_{-\infty}^{\infty} e^{it\omega} \overline{G_a(\omega; \omega_0(a\omega))} d\omega, \tag{6.19}$$

one has

$$\int_{-\infty}^{\infty} \int_{-\infty}^{\infty} \frac{2\pi}{a^2} \widehat{F_a}(t; \omega_0(a\omega)) \overline{\widehat{G_a}(t; \omega_0(a\omega))} da dt$$

$$= \int_{-\infty}^{\infty} \int_{-\infty}^{\infty} \frac{2\pi}{a^2} F_a(\omega; \omega_0(a\omega)) \overline{G_a(\omega; \omega_0(a\omega))} da d\omega$$

$$= \int_{-\infty}^{\infty} \int_{-\infty}^{\infty} \frac{2\pi}{|a|} \widehat{f}(\omega) \overline{\widehat{g}(\omega)} |\widehat{\psi}(a\omega; \omega_0(a\omega))|^2 da d\omega$$

$$= 2\pi \int_{-\infty}^{\infty} f(t) \overline{g(t)} dt \int_{\infty}^{\infty} \frac{|\widehat{\psi}(a\omega; \omega_0(a\omega))|^2}{|a|} da$$

$$= 2\pi \langle f, g \rangle C_{\psi_{\omega_0}}. \tag{6.20}$$

Now the resolution of identity is fulfilled if the following admissability condition is satisfied,

$$\int_{-\infty}^{\infty} \frac{|\widehat{\psi}(a\omega; \omega_0(a\omega))|^2}{|a|} da = C_{\psi_{\omega_0}}. \tag{6.21}$$

This condition is more restrictive than Equation 5.7 in that $\widehat{\psi}(0, \omega_0(u)) = 0$ for all $u \in \mathbf{R}$. Otherwise, there is no other restriction since what is changed in the integration is limited to finite range and is anticipated to be finite. The case using Morlet wavelet complies with such a validation and therefore satisfies this condition.

6.6 Summary

The unrealistic aspect of the best wavelet in the simulation of water waves is pointed out and the importance of the existence of a physical quantity of carrier frequency is stressed. And a somewhat intuitive adaptation based on the adjustment of the time-frequency win-

dow parameter is proposed. The adaptation mainly focuses on better modeling of wave energy phenomena or energy dissipation for different wave lengthes. Such an optimization shall be more significant for board band signals. ❖

Chapter 7

Wavelet Coherences against Fourier Coherences

7.1 Introduction

Coherence connotes mutual relationship or inter-dependency; it manifests from an intimacy of complete cloning to an alienage of total irrelevance. In a multi-scale, multi-factor coupling system the levels of coherence between different target quantities symbolize the phenomena of reciprocal interactions among various playing elements. By studying variations of coherences under different experimental setups or different input parameters it is possible to show evolutions of different scales and to isolate key influential factors, as well as to identify issues thus consorted.

In this chapter solid evidences will be provided regarding the the proof of "the ultimate last word" on best wavelet concerning water wave applications and physics. What will be furnished is the absolute superiority of the wavelet coherences associated with the ultimate best wavelet over the spectral coherences associated with Fourier basis. By the way, be that as it may, the author likes to emphasize that by no means it is equivalent to saying that Fourier basis is inferior to such wavelet basis in every aspect of water wave studies. In facts, it is still vastly important in many prospects, in particular, for those that are generally stationary or without significant local transient variations and for those related to water wave instability (such as side-band instability).

In two individual studies related to the methodologies of time-frequency analysis by the author ([19] [22]), the viewpoints based upon Hilbert transform and the analytic signal procedure ([14], [9]) were used to elaborate the influences of non-stationary effects and local transient variations, as well as some of the intrinsic mathematics and their connection with the uncertainties related to Fourier spectra. Herein, we will come to realize the same drawbacks imposing upon the Fourier basis due to these effects when comparing performances of spectral coherences with those of wavelet coherences. Moreover, let state a few basic differences between the two approaches.

Apart from the most instinctive and fundamental deviation between Fourier and wavelet's viewpoints concerning the appropriateness of depicting waves as finitely supported modulating signals, i.e., waves with a life span, there are two other major differences.

First, from the viewpoint of their origins from mathematics, the formulation of wavelet coherence is a more intimate replica of its analytical form than is the Fourier spectral coherence. Specifically, the wavelet coherence is a direct and natural extension of the wavelet "resolution of identity", and therefore involves less artificial intervention.

Second, the wavelet coherence presented here is derived from a set of coefficients with an extreme redundancy associated with no orthonormality whatsoever; while spectral coherence is derived from a set of coefficients associated with orthonormal basis functions. Such a redundancy is capable of providing not only a fine scale resolution but also a huge population space needed for outstanding coherent statistics; since it reduces impacts related to histogram processing, noises, and a few additional uncertainty factors, etc ([31], [35]). Most importantly, being based upon the basis with minimum entropy that clearly outperforms the Fourier basis, the wavelet transform coefficients possess utmost information contents and lead to clear and superior tendencies in coherent features.

Overall, what presented in this chapter will come to the conclusion: for water waves, the ultimate best wavelet in the discrete domain is the semi-orthogonal cardinal spline wavelet; and in the continuous domain it is the Morlet wavelet.

7.2 The Fourier spectral coherence

The cross correlation function of two functions $g(t)$ and $h(t)$ is the following inner product $c(t)$

$$c(t) = \langle g(t+\tau), h(\tau) \rangle, \tag{7.1}$$

where τ is a dummy variable with respect to t. The correlation coefficient function of $c(t)$ is $r_s(t)$,

$$r_s(t) = \frac{c(t)}{\|g(t)\| \|h(t)\|}. \tag{7.2}$$

For real $g(t)$ and $h(t)$, its Fourier transform is

$$\frac{\widehat{c(t)}}{\|g(t)\| \|h(t)\|} = \frac{G(\omega)\overline{H(\omega)}}{\|G(\omega)\| \|\overline{H(\omega)}\|}. \tag{7.3}$$

The Fourier spectral coherence is the following induced form,

$$R_s^2(\omega) = \frac{|\mathbf{E}[G(\omega)\overline{H(\omega)}]|^2}{\left(\mathbf{E}[|G(\omega)|^2]\mathbf{E}[|H(\omega)|^2]\right)^{1/2}}, \tag{7.4}$$

where the symbol **E** stands for taking expected value. Comparing the two equations above, the artifacts introduced into the spectral coherence are associated with the form of expected values and the introduction of normalization.

This equation is in fact identically unity for all component frequencies if no additional man made manipulation is adopted. Since expected values take no action without introducing one more dimension. As such, the introduction of an additional dimension is the manipulation of data segmentation, that is to say, the whole data sequence is segmented, and each segment is individually transformed and arranged in a matrix thus creating the one additional dimension. The process of this segmentation is completely identical to that commonly implemented in calculating Fourier power spectra, and it aims to reduce the uncertainty or standard deviation of the spectral estimation. There is no doubt that various inherent properties of the discrete Fourier analysis inflict their symptoms and impose

similar limitations to the conclusiveness of spectral coherences.

7.3 The wavelet coherence

It was a stumbling when the subject of both wavelet and spectral coherences caught the author's attention. Reading a paper by Liu [24], the author was dissatisfied with the paper's definition of wavelet coherence and the ambiguity and lack of information thus yielded. And it turns out that the derivation of wavelet coherence is even much simpler mathematically and more intuitive theoretically, along with fewer artifacts.

The wavelet's "resolution of identity" of two functions (g and h) is

$$\langle g, h\rangle = \frac{1}{c_\psi}\int_0^\infty \frac{1}{a^2}\int_{-\infty}^{\infty}\langle g,\, \psi_{a,b}\rangle\overline{\langle h,\, \psi_{a,b}\rangle}dbda, \tag{7.5}$$

in which c_ψ is a constant and $\psi_{a,b}$ is a wavelet with scale a and translation step b. For a component scale a

$$\langle g_a, h_a\rangle = \frac{1}{c_\psi}\frac{1}{a^2}\int_{-\infty}^{\infty}\langle g,\, \psi_{a,b}\rangle\overline{\langle h,\, \psi_{a,b}\rangle}db. \tag{7.6}$$

Here the integration with respect to the translation parameter b is physically, as well as intuitively, similar to the operation of taking an expected value by summing up the elements in the population space. It is therefore quite straightforward to define the wavelet coherence as the natural extension of the normalized equation of resolution of identity:

$$R_w^2(a) = \frac{|\mathbf{E}_b[\langle g,\, \psi_{a,b}\rangle\overline{\langle h,\, \psi_{a,b}\rangle}]|^2}{\left(\mathbf{E}_b[|\langle g,\, \psi_{a,b}\rangle|^2]\mathbf{E}_b[|\langle h,\, \psi_{a,b}\rangle|^2]\right)^{1/2}}, \tag{7.7}$$

where $\mathbf{E}_b$ stands for sampling average with respect to the translation parameter, the subscript b.

It is clear that the wavelet coherence has a more direct linkage to its analytical counterpart than does the spectral coherence.

Unlike the spectral coherence, there is no need to segment the data. The expected values can be obtained in a sense of summing up all the results of wavelet transforms at all locations. And each elemental transforms can be obtained through simple convolution, i.e., an operation of time reversal and time shift if the data is a time sequence. Therefore, the population size of the sample space of wavelet coefficients for any given scale (or carrier frequency as adopted here) is generally two or three orders of magnitude larger than that for spectral coherence. That is to say, the amount of available sampling coefficients is generally not a concern for the wavelet scheme.

In fact the fundamental difference between the present definition based on equation 7.7 and the one adopted by Liu [24]) is the state of subsistence of the expected values. Without the statistics of an expectation the results seemed scanty and the depictions sounded skimpy.

Although the equation of the wavelet coherence (eq. 7.7) applies equally well to a discrete or a continuous basis, there is one significant and practical advantage that facilitates the use of the continuous one. Since we can focus only on the portion of scale range that is meaningful and substantial to us. Nevertheless, for the spectral coherence, in the handling we have no control at all over the frequency range of interest. As such, a great portion of the spectral result might be entirely irrelevant to our concerns.

Judging from the fact that we generally only want to, and are just able to, focus on a finite scale range or some frequency bands in practically any real world situation. Even though computation efficiency is not our concern, We know that the spectral approach wastes its effort and resource in the unwanted while the wavelet coherence does just the most appropriate.

7.4 The experiments

The data involved here is related to a subset of experiments aimed at the study of the energy cascade and the interaction scales in the wind, wave and rain coupling system.

7.4.1 The oval tank

The experiments were carried out in an circulating oval tank equipped with wind blowing facilities and a mountable mechanical wave generator. Figure 7.1 (Oval Tank) shows the layout. The tank is 31 cm wide and 45 cm high and has a 5-meter observational straight section. The water depth was kept at 24 cm in all experiments. A fan of continuously variable rotation speed was located at the opposite side of the observational section. Horizontal guiding vanes were installed in front of the fan to regulate the airflows. And vertical guiding vanes were installed at the two semi-circle sections to reduce secondary flows in both air and water. The mechanical waves were generated by the plunger type motion of a wedge shape piston controlled by a variable-speed rotor. And the mechanical setup could be placed along the observational section.

7.4.2 The laser Doppler velocimeter

Aqueous flows at several depths in two sections along the tank were measured with a laser Doppler velocimeter (LDV) [1]. The LDV system is a TSI four-beam, two-component system with two-color, dual-beam backscattering, and counter type signal processor configuration. A few auxiliary instruments and accessories were also used in fine-tuning the whole system and in achieving optimum control of data quality. The main system components and the auxiliary instruments are: (1) Fiberoptic transmitting and receiving probes (TSI Model 9115, 9182, and 9140); (2) Photodetector and photomultiplier system (Model 9160); (3) Frequency shifter with acousto-optic modulator and electronic down-mix module (Model 9180A); (4) Signal input conditioner (Model 1994C); (5) Fringe timer (Model 1995B); (6) Frequency to analog conversion module (Model 1988). (7) Digital readout module; (Model 1992); (8) Intermittent burst data recording interface; (Model 1998); (9) Light-power meter; (10) TI Dual channel oscilloscope for high-end fast and sensitive real time monitoring.

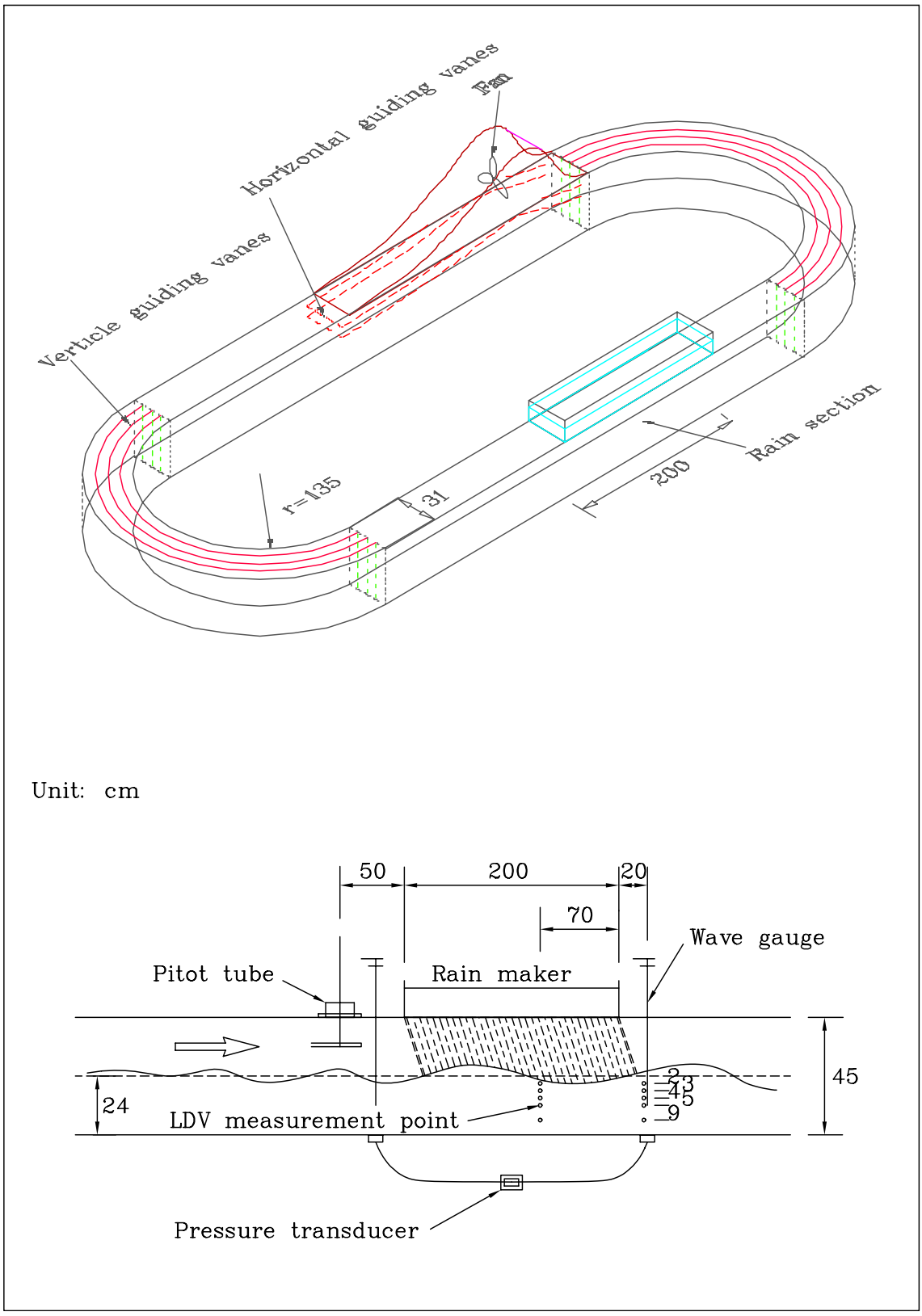

Fig 7.1 (Oval Tank) Schematic layout of experiment

7.4.3 The waves

Both wind and Stokes waves were generated. Major wind speed was 6.0 sec^{-1}. And the wind speed was measured with a Pitot tube located 50 cm upwind of the rain section and 11 cm above the still water surface. Stokes waves with different wave steepness were mechanically generated. Water surface displacements were measured with the capacitance type tantalum wire probes self-designed by the lab.

7.4.4 The real time system

A highly automated and specially optimized PC-based real time system for both data acquisition and data analysis was developed by the author using the **Asyst** programming language. Details can be found in the previous section on "*Program and workbench developments*". Its functions included: calibrations, noise detections either environmentally and instrumentally related, real time signal monitoring, on-site data processing and analyses, on-site generation of various curves and tables and figures either in terminal or in paper. Such a system ensures maximum controls and peak data quality, most importantly, the trouble-free and satisfactory results.

7.5 Comparisons and implications

The performance comparisons of the two approaches provided here concern the coherences between the surface wave and aqueous flow fields for both wind wave cases and Stokes wave cases.

These comparisons fully warrant the entropy results and vindicate the ultimate best wavelet for water waves. There must be reasons and implications.

- The absolute superiority of the wavelet coherences — The wavelet coherences using three different analyzing data lengthes of 1024, 2048, and 4096 points are shown in figure 7.2 (WC–$2^{10,11,12}$). The individual curve in each sub-figure indicate individual

measurement depth for aqueous flow at 2, 3, 4, 5, and 9 cm, respectively, below the still water surface. It is seen that all the corresponding curves for the three different analyzing data lengthes are extremely consistent. In contrast, figure 7.3 (FC–$2^{10,11,12}$) shows the Fourier spectrum coherences for the same data sets. The difference in performance of the two methods is quite obvious and can be grasped without explanation. Additionally, figure 7.4 (FC–2^{13plus}) shows the spectral coherences using a lengthy 9126-point with individual FFT segmentation length of 256- and 1024-point. It is noted that, when extremely lengthy data is used, the Fourier coherent curves may possibly come close to those of wavelet coherence but the trend is surely slow and costly, yet with certain defections still.

- The fitness of the nature of a life span — For short wind waves (such as the tank data here) the description of a life span fits the physics better. Component waves are inherently evolving and mutual interaction among them is a norm. And this is the basics that the wavelet depiction comes into play. Moreover, life spans of component waves are shorter than any analyzing data length used. That is to say, even the shortest data length of 1024-point sufficiently cover the support lengthes of all wave components in the experiments.

- Wind waves in the tank soon lose their identities — Figure 7.7 (Auto-corr) shows the auto-correlation coefficient distributions of two wind-wave signals in the oval tank measured at upstream and downstream location, respectively, and it provides the evidence of the life span argument. Here the correlation level is low and diminishes rapidly. A sensible feeling is that these waves lose their identities extremely fast when viewed from Fourier spectral perspective. Put differently, the behavior indicates the trouble related to the level of uncertainty of the Fourier decomposition.

- Spectral repeatability — Even with the acquaintance of the above explanations one might not grasp to what extent the problem of Fourier spectral repeatability may affect the conclusiveness in data interpretations, as well as the coherent performances

shown here. Measurements of the signals in the wind blowing oval tank provide further explanations. But let first present the data in a fundamental perspective based on zero-upcrossing statistics; compared with the spectral point of view, it helps illuminate different specific features that are associated with individual perspectives. Table 7.1 (Zeroup–Sta) shows the statistics from such a conventional method for three sets of measurements. These three measurement sets were made under the same wind velocity and the signals were sampled at a rate of 40 samples per second for a duration of 240 seconds. Channel 1 is for aqueous flows measured with LDV at a depth of 3, 4, and 5 cm, respectively, from the still water surface. Channel 2 is for water-surface displacements measured at nearly the same transverse cross section of the tank as that of the LDV measurement point (with a separation of 0.6 cm). Therefore, statistics for channel 2 can therefore be regarded as the results from repeated measurements. As are seen from the table, of all individual runs various statistical values for channel 2 are extremely consistent; hence, from the point of view of zero-upcrossing statistics, the wave field under the experimental setup is quite stationary. In contrast, figures 7.8 (FS–RP–L-1) and 7.9 (FS–RP–L-2) show that the idea of stationarity is hardly substantiated when viewed from the spectral perspective. In the two figures, the spectra are for the same data sets but with different values of one of the FFT parameters, i.e., two different segmentation lengthes. The top sub-figures are the power spectra for the repeated measurements of water-surface displacements. The bottom sub-figures are the LDV aqueous flows at each depth. Choices of parameters for these standard spectral numerics are labeled in the figure. For all cases the total length of data is multi-segmented with 50% overlapping, and the Blackman window is applied to each segment. A segment length of 512 points (with an approximate degrees of freedom of 36) is used for the left figures and 1024 points for right figures (with an approximate degrees of freedom of 17). As are shown in the top sub-figures, the repeatability of spectra is rather poor, not to mention the discrepancy arising from different length of segmentation.

The spectral resolution for those on the left is insubstantial, while the variations of spectra on the right is much more defective. In fact, the illustrated problem is the manifestation of the symptom associated with the deconvolution mechanism of a spectral blackbox operation [17].

- Phase effects — If we compare corresponding curves (surface wave and aqueous flow signals) in the top and the bottom sub-figures it is seen that the shapes of the two are generally in agreement. This provides a lucid illustration of the phase effects. Since the two signals are acquired at the same time and at almost the same cross section, there is little phase effect between the two spectra. On the contrary, we just do not have any control over the phases of component waves for different runs under the same experimental setups. An extreme illustration and further explanation for those effects can be found in figure 5.2 (Pha–Eff-2).

- Stationarity prerequisite — The truly remarkable point for the wavelet coherences is that the 1024-point data length has almost fulfilled the statistics of stationarity. There is little difference among the three analyzing lengthes. Such a behavior is even more proficient than that of the zero-upcrossing statistics (Table 7.1 (Zeroup–Sta)).

- The role of the redundancy — The Fourier basis is orthonormal and the discrete wavelet bases are either orthonormal (self-dual) or orthogonal to their duals (dual mother wavelet and dual farther wavelet). There is no redundancy for orthonormal transforms and little redundancy for those discrete transforms based on nonorthogonal bases. However the continuous wavelet transform is an extremely redundant operation. Without the redundancy a small change in signal causes enormous variation in scale information or transform distribution. The redundancy is able to yield purified coherences by minimizing effects from unrelated scales while provide a fine scale resolution. Redundancy is therefore a much desirable property for studies of coherent behaviors.

- Length requirements — There is no need to acquire lengthy data when wavelet approach is adopted, whereas for the spectral approach the need for more data sees no ending. In this regard, for the wavelet coherences, the lengthening of data provides not much additional information and the information content of redundancy saturates quickly.

- Water waves are inherently "regular" from wavelets' perspective — And again, it is emphasized that this statement is based upon the wavelets' point of view. Since, we have the facts:

  - that most of the wavelet basis functions other than one identified here look quite odd when compared to the Fourier sine and cosine functions;
  - that the various properties outlined in the previous chapter on phase distributions indicate the simplicity requirement of the wave forms and bespeak no ambiguity;
  - that the optimal continuous wavelet here is quite like a modulated Gaussian;
  - that, in the end, the fourier spectral coherences and the wavelet coherences somewhat approach similar distributions.

7.6 Summary

The absolute superiority of the wavelet coherence fully vindicates the present study. In short, the outstanding performances lie upon the two main factors: they have the truly best both from the optimal discrete basis and from the most upright continuous basis. That is to say, first, it is based on a clear-cut minimum entropy associated with the best discrete wavelet (the semi-orthogonal cardinal spline wavelet) for water waves; second, it further employs the beneficial property of the redundance and engages the existence of a meaningful physical quantity of the carrier frequency associated with the counterpart continuous wavelet (the Morlet wavelet). ❖

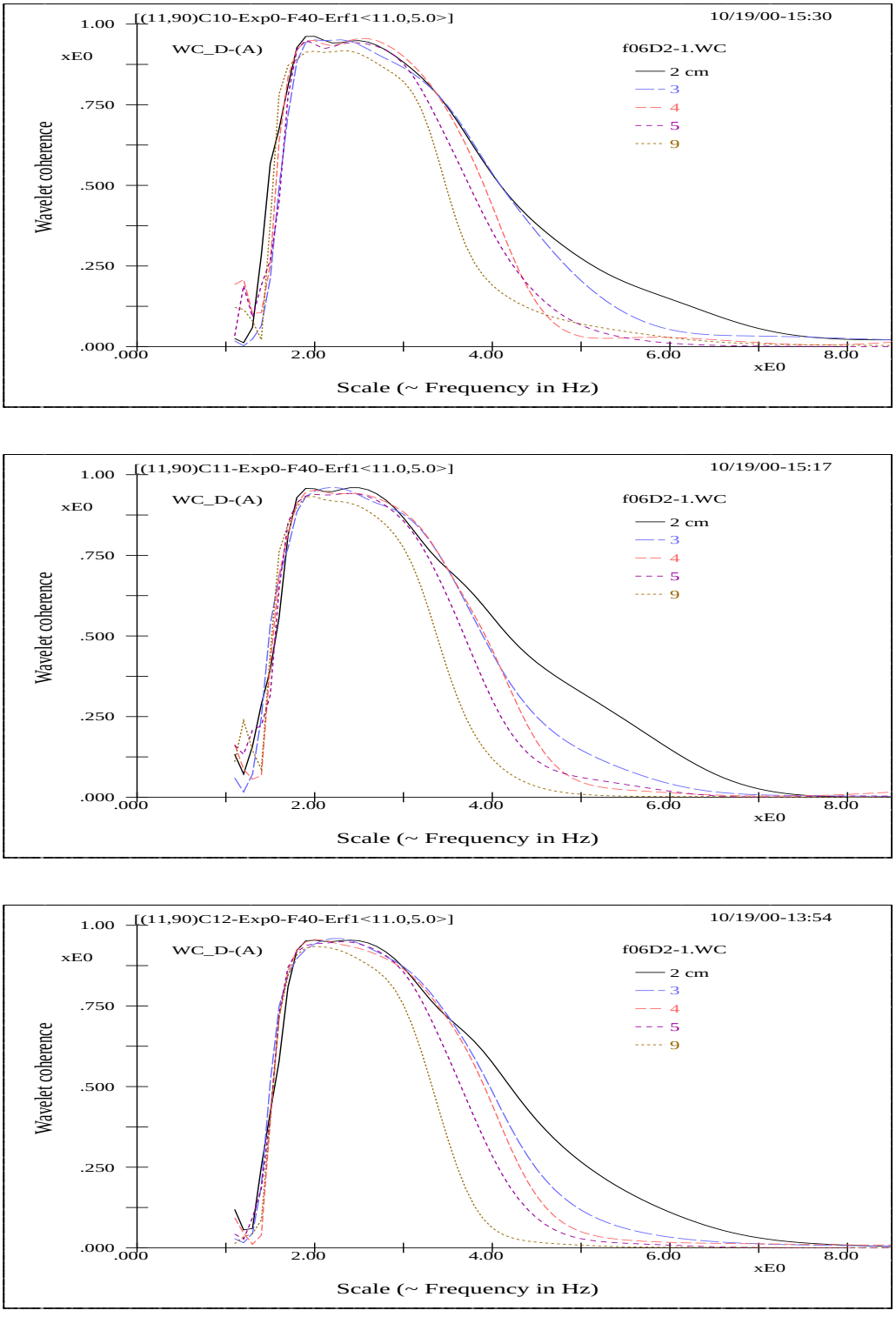

Fig 7.2 (WC–$2^{10,11,12}$) The wavelet coherences between the wave and aqueous flow using three different data lengthes: 1024 (`top`), 2048 (`middle`), and 4096-point (`bottom`). Each individual curve represents a different measuring depth of aqueous flow at 2, 3, 4, 5, or 9 cm, respectively, below still water surface as labeled in the sub-figures. Note the well consistency and behavior among curves.

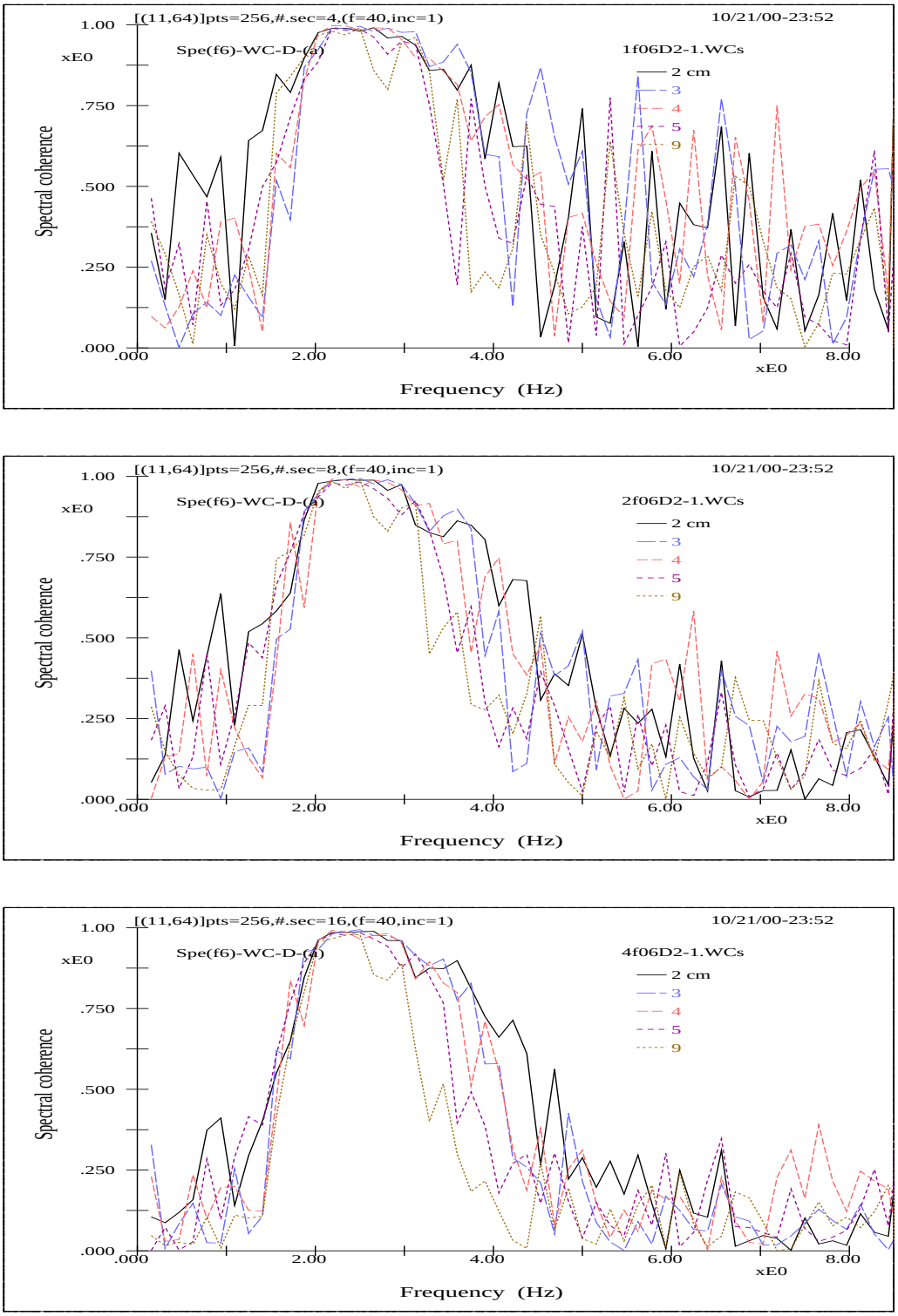

Fig 7.3 (FC–$2^{10,11,12}$) The Fourier spectral coherences between the wave and aqueous flow for the same set of data as that of the wavelet coherences (figure 7.2 (WC–$2^{10,11,12}$)). Note the extreme variation for all the curves.

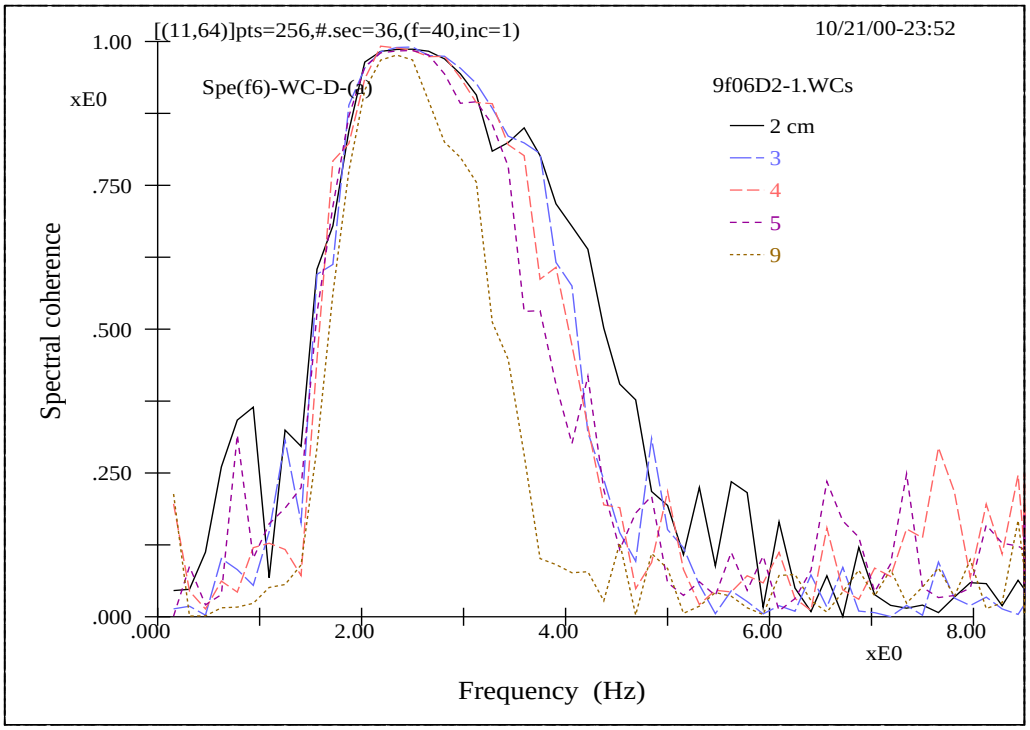

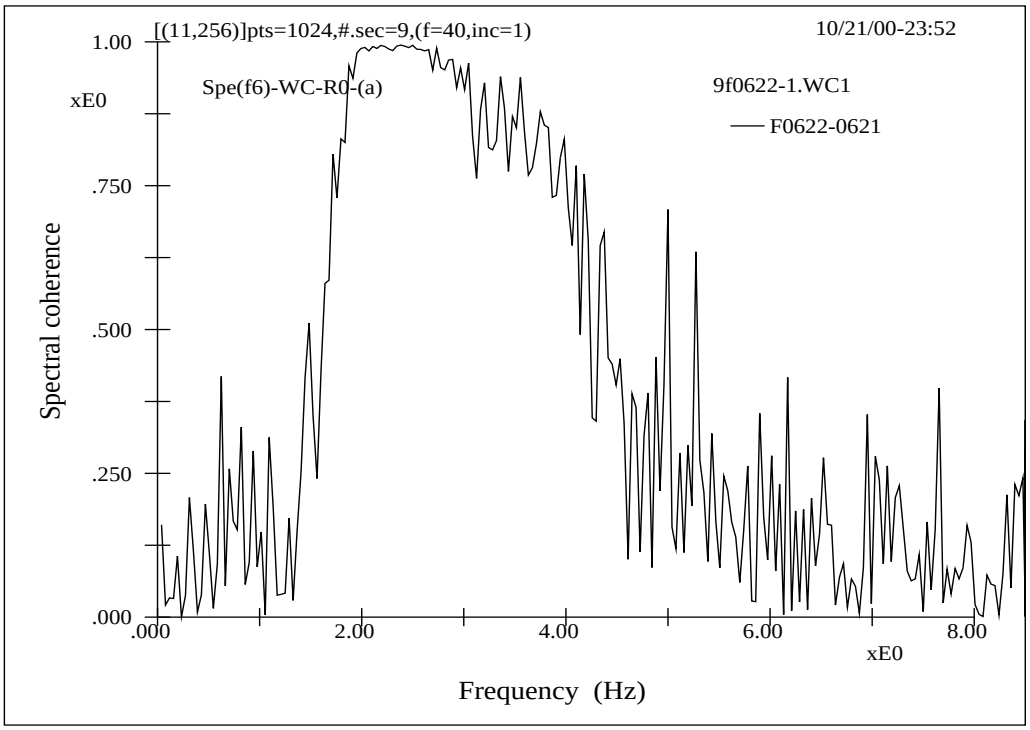

Fig 7.4 (FC–$2^{13 plus}$) The Fourier coherences using a data length of 9126-point for two different lengthes of spectral segmentation, 256 `(top)` and 1024 `(bottom)` points. It is seen that extremely lengthy data may possibly yield a somewhat similar distribution curve as that of the wavelet coherence `(top)`, but note the effects of degrees of freedom of the spectrum `(bottom)`.

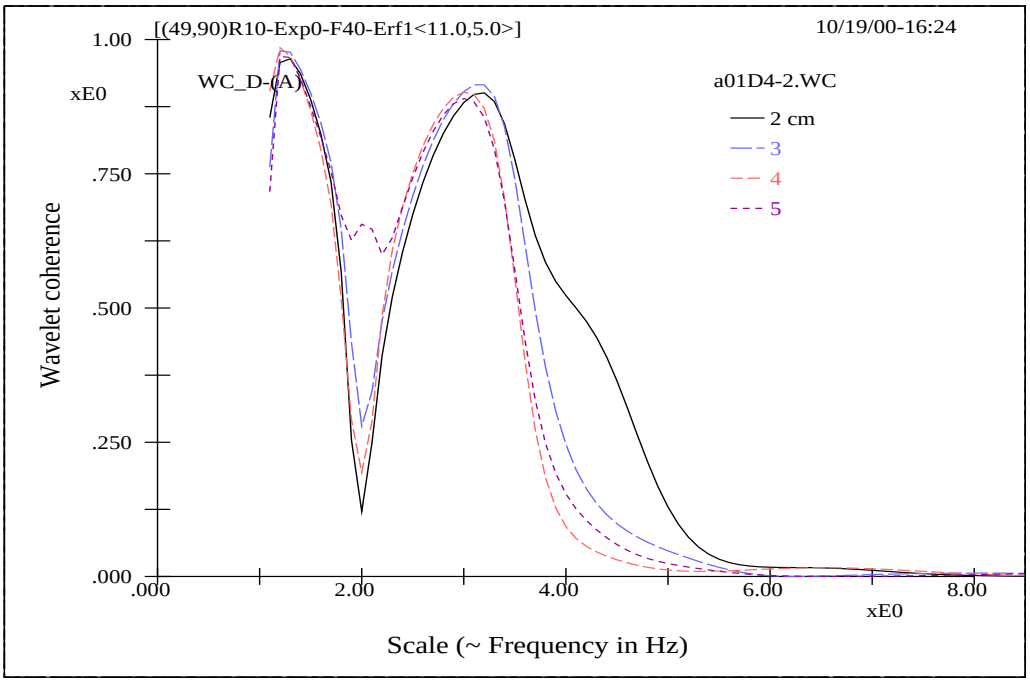

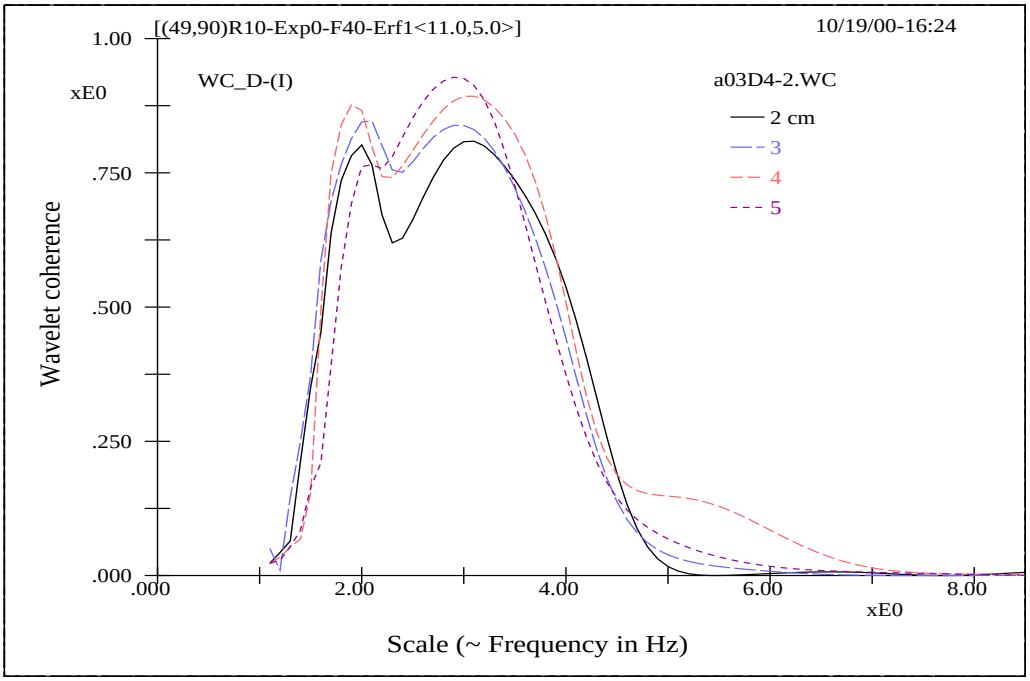

Fig 7.5 (WC–Stokes) The wavelet wave-current coherences at several depthes for two Stokes waves with wave steepness of 0.06 (top) and 0.30 (bottom) for a data length of 1024 points — Some prominent physics here may involve:
(1) the band distribution and degree of separation;
(2) the coherent level for individual band at individual depth;
(3) the tendency or the phenomena attributed to the side-band instability or nonlinear effect of water waves.

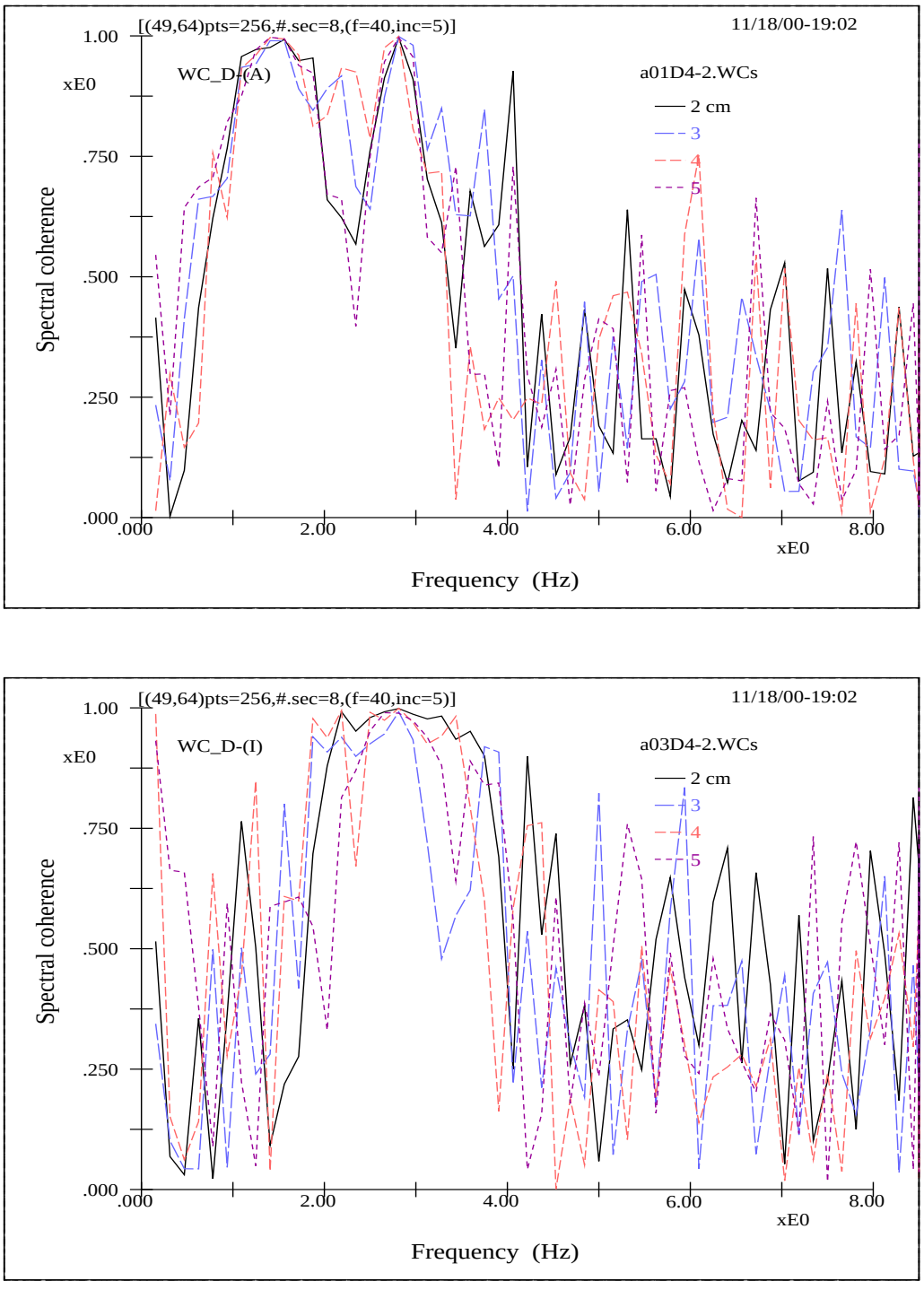

Fig 7.6 (FC–Stokes) The Fourier spectral coherences for the same data as in the last figure (7.5 (WC–Stokes)) (FFT parameters are labeled in the figure) — Can we infer anything?!

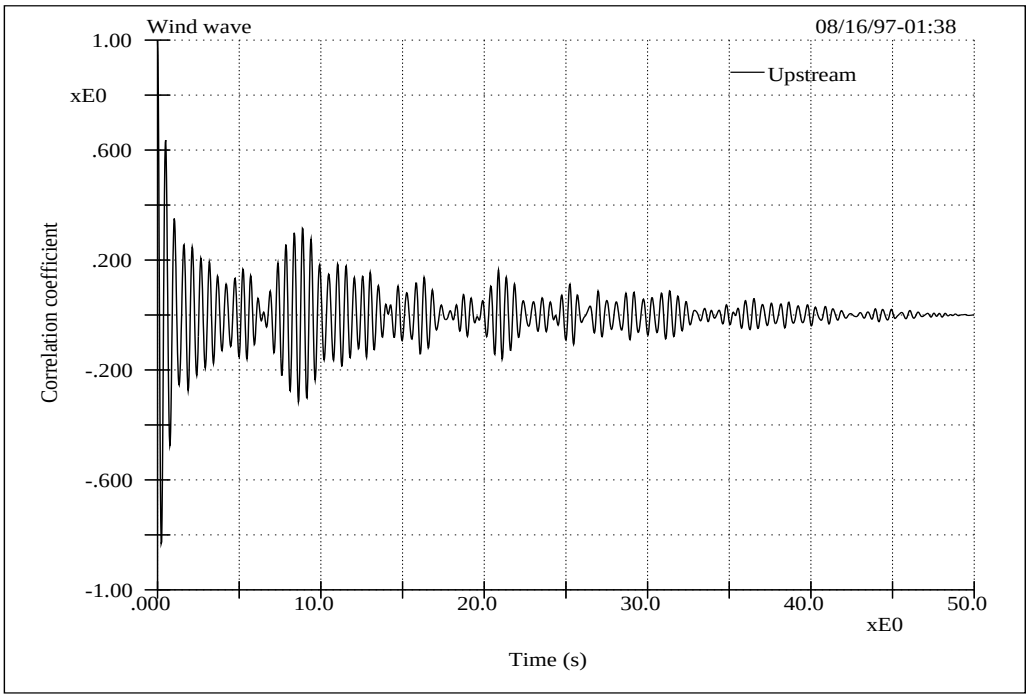

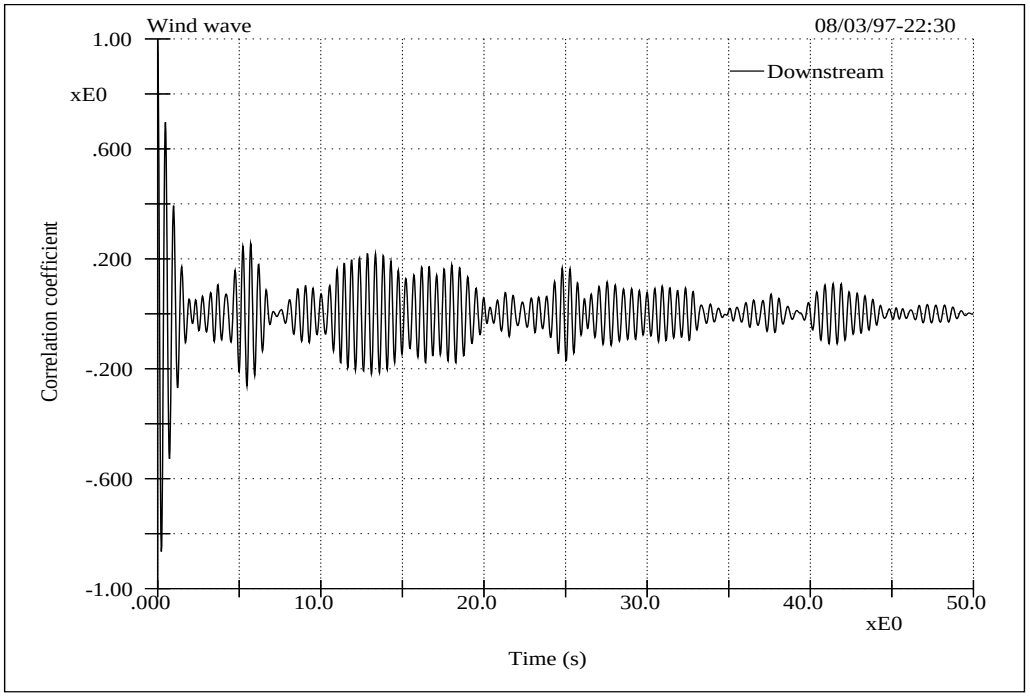

Fig 7.7 (Auto-corr) Wind waves in the tank soon lose their identities — the auto-correlation coefficients of two wind-wave signals measured at upstream and downstream locations in the oval tank. Here the correlation level is low and diminishes rapidly and a sensible feeling is that these waves lose their identities extremely fast when viewed from the Fourier spectral perspective. Alternatively speaking, the phenomenon manifests the trouble related to the level of uncertainty or (degrees of freedom) of the Fourier decomposition.

Tab 7.1 (Zeroup–Sta) The zero up-crossing statistics for three different sets of measurement under the same wind condition. Channel 1 is for LDV aqueous flows measured at different depths from the still water surface. Channel 2 is for surface displacements measured at the same location. Statistics for channel 2 can basically be regarded as results from repeated measurements. Comparisons of data related to channel 2 indicate that the wave statistics is in good stationary condition. Whereas, this is certainly not true when viewed from the Fourier spectral perspective, as shown in subsequent figures.

```
Case        :   f0w6030.dat  ( f1 p3 c1 s9 )
Date        :   01/05/96
Time        :   02:19:05.48                                  Sampling   frequency  :   40  Hz
Specifics   :                                                Sampling time length  :  240 Sec

 Ch   #_W    H.1    H.2    H.3    H1/10   H1/3   H1/2  H.ave  H.rms    T1/10  T1/3  T1/2 T.ave T.rms

  1.  554  26.74  23.67  23.04    20.20  17.38  15.92  12.03  12.93      .44   .44   .44   .43   .44
  2.  572   2.90   2.69   2.61     2.33   2.04   1.89   1.44   1.54      .44   .44   .43   .42   .42


Case        :   f0w6040.dat  ( f1 p3 c1 s9 )
Date        :   01/05/96
Time        :   02:14:05.76                                  Sampling   frequency  :   40  Hz
Specifics   :                                                Sampling time length  :  240 Sec

 Ch   #_W    H.1    H.2    H.3    H1/10   H1/3   H1/2  H.ave  H.rms    T1/10  T1/3  T1/2 T.ave T.rms

  1.  546  22.81  20.65  20.52    17.04  14.48  13.32  10.35  11.01      .45   .44   .44   .44   .45
  2.  563   2.98   2.88   2.72     2.35   2.04   1.89   1.46   1.55      .44   .43   .43   .43   .43


Case        :   f0w6050.dat  ( f1 p3 c1 s9 )
Date        :   01/05/96
Time        :   02:00:30.72                                  Sampling   frequency  :   40  Hz
Specifics   :                                                Sampling time length  :  240 Sec

 Ch   #_W    H.1    H.2    H.3    H1/10   H1/3   H1/2  H.ave  H.rms    T1/10  T1/3  T1/2 T.ave T.rms

  1.  546  17.62  16.49  16.30    14.02  11.94  10.97   8.22   8.88      .45   .44   .44   .44   .45
  2.  562   2.83   2.74   2.72     2.36   2.06   1.91   1.45   1.55      .44   .44   .44   .43   .43


-----------------------------------------------------------------------------------------------
Units::          Aqueous flow (Ch1:H): cm/s
                 Surface wave (Ch2:H): cm
                          Period (T): s
```

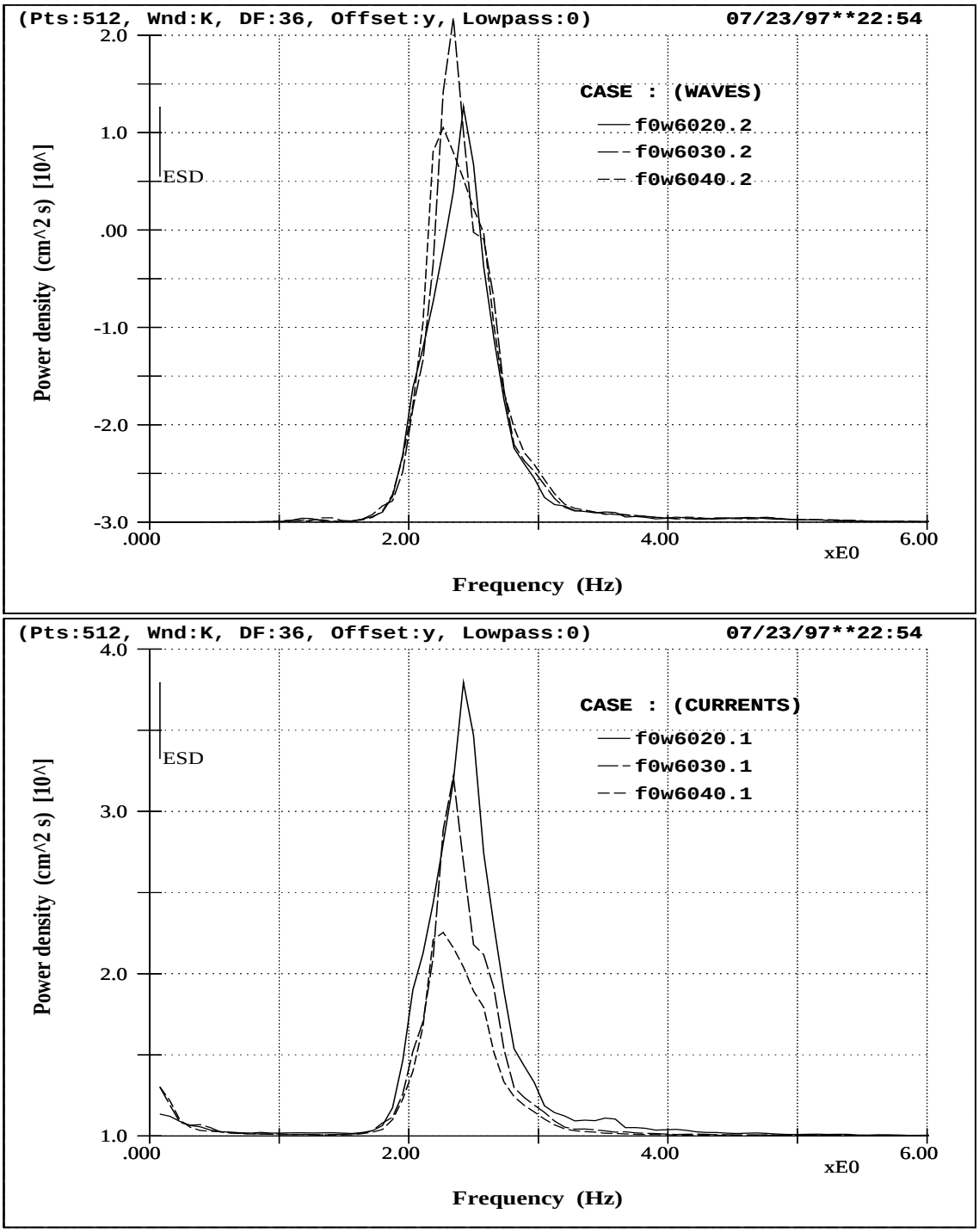

Fig 7.8 (FS–RP–L-1) Spectra of the surface displacement and aqueous flow for the same three sets of measurements as shown in table 7.1 (Zeroup–Sta). The top sub-figure shows power spectra of the repeated measurements of surface displacement. The bottom sub-figure shows power spectra of the LDV aqueous flow measurements at different depths. It is seen that the repeatability of power spectra is rather poor even though the zero up-crossing statistics has indicated the existence of a good stationary condition. This has profound entailment of the poor performances of spectral coherence, as well as the sure unfruitfulness of the blackbox deconvolution mechanism for two signals under any circumstance [16].

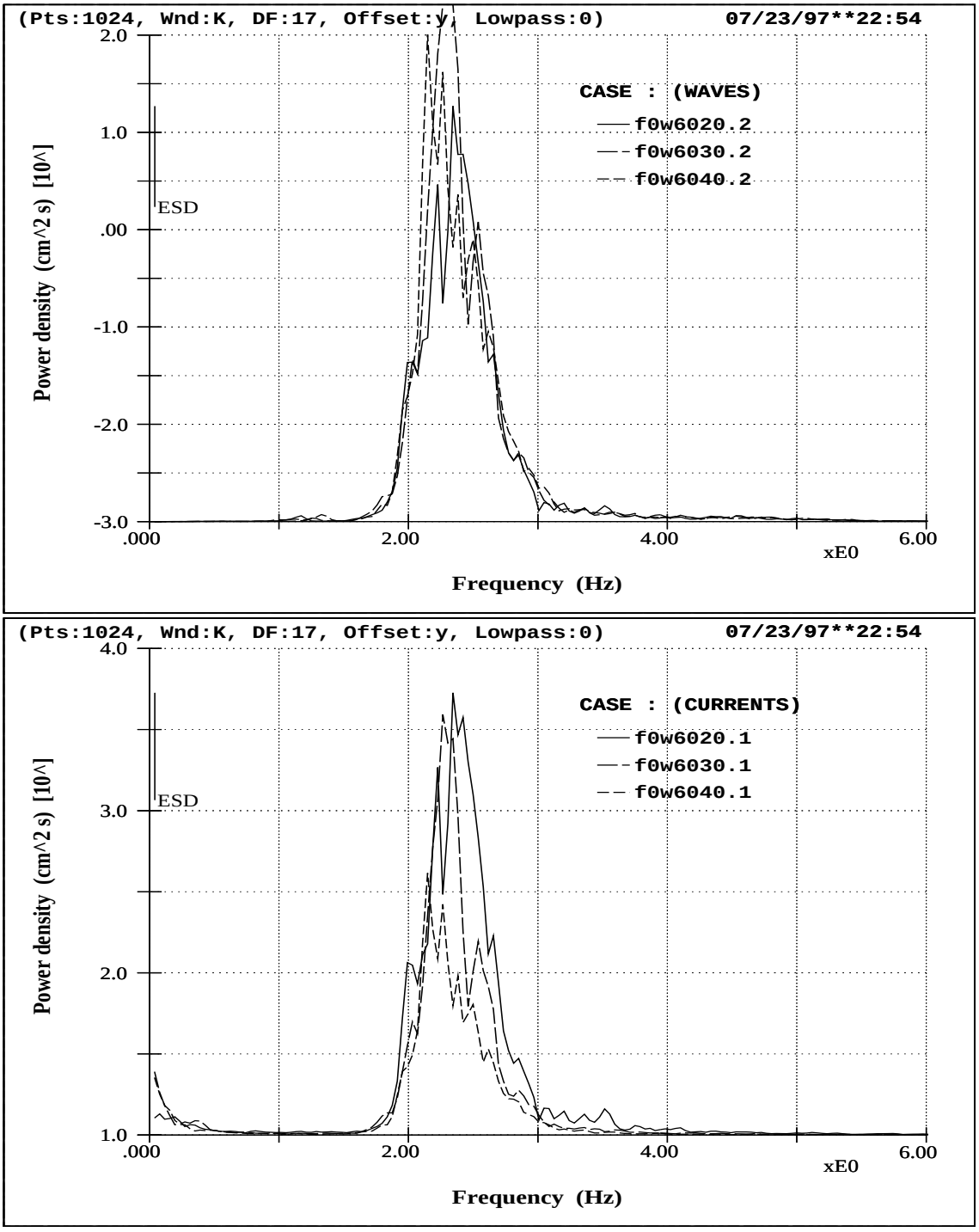

Fig 7.9 (FS–RP–L-2) Spectra for the same data sets as in the previous figure but with different FFT parameters. Here a longer 1024-point segmentation is used and the degrees of freedom is approximately halved. Whilst the resolution is increased the standard deviation intensifies. Again the figure shows the profound implication of the problems of Fourier spectral repeatability and the poor performances of spectral coherence.

Chapter 8

Conclusions

8.1 Introduction

The subject matter here can be divided into three main parts. The first part is the identification of a best wavelet basis for water waves. The second part is the practical optimization of the best basis for better modeling of physics. The third part is the validation of the aforenamed two parts through the performance comparisons on coherences between the wavelet approach and the Fourier spectral approach.

When the author embarked these wavelet studies for utilization on water waves each individual study was initiated completely independently and the downright interconnectedness was not foreseen. But, in the end, they sufficed to uphold the present conclusion on the ultimate best wavelet for water waves.

8.2 Summary

For the interest of water wave related applications, comprehensive categories of discrete wavelet bases, as well as the continuous wavelet, were studied. Extensive sets of **Asyst** programs were developed from the ground up and a comprehensive workbench was devised. The programs are able to illustrate various intrinsic properties of wavelets and their relevant characterizations, as well as their possible implications in water wave physics.

Employing the jurisdiction of entropy statistics and the probability distributions of transform coefficients the best wavelet basis in the discrete domain is identified. Furthermore, through the incorporation of the physics of the carrier frequency the corresponding best wavelet in the continuous domain is discerned. The best wavelet in the discrete domain is the dual semi-orthogonal cardinal spline wavelet devised by Chui [6, 7, 8] and the corresponding counterpart in the continuous domain is the Morlet wavelet.

In addition to the identification of the best wavelet we further discuss the best wavelet's deficiency in physical modeling and provide an intuitive and practical optimization catering wave decay phenomenon.

As a final vindication of the aforementioned realizations, the wavelet coherences associated with the best basis are compared to the Fourier spectral coherences for data of wave and current fields measured in a wind-wave tank. It is the author belief that the best, as well as the ultimate, wavelet for water wave modeling has thusly been named.

Below is a list of some of the main contents:

- The comprehensive discrete wavelet categories included:
  - orthonormal;
  - bi-orthogonal;
  - semi-orthogonal;
  - wavelet packet, both the best level bases and best branching bases;
  - from the most symmetrical till the least symmetrical orthonormal;
  - from the most compactly supported in the time domain till the most compactly supported in the frequency domain.
- The depictions of wavelet natures and their possible pragmatic implications:
  - mother and farther wavelets;
  - the concepts of wavelet translation and dilation;

  - time-frequency window and the difference between scale and frequency, as well as the Heisenberg uncertainty;
  - the zoom-in or blowup of any individual wavelet and the fractal nature of wavelets;
  - the phase distributions of wavelet characteristic functions — the concept of linear phase filtering versus the practical behaviors of wavelets, as well as relevant advantages or disadvantages in water wave applications.

- The identification and the inclusion of Fourier bases — the entropy statistics, the cumulative probability distributions:
  - based on broad and inclusive criteria of entropy statistics — from energy point of view, or from displacement point of view, etc;
  - wind wave signals from a small laboratory water tank are used for the jurisdictions — thusly, for water wave signals in the nature there cannot be any wavelet that is more suitable than the optimal wavelet identified here, since the present jurisdiction is made upon the highly transient short water waves generated by wind;
  - the relevance between the phase distribution of the wavelet characteristic function and the entropy;
  - the solely and distinctly identifiable value in every entropy category points to the same best discrete wavelet basis — the dual semi-orthogonal cardinal spline wavelet;
  - entropy values for orthonormal wavelets are inferior to those of nonorthogonal ones;
  - in all criteria the best wavelet's result is undoubtedly superior to the Fourier's.

- The role of the phase distribution of wavelet characteristic function for basis construction:

  - the phase distributions of the characteristic functions for all wavelet categories are provided;
  - the distribution feature of phase hints a wavelet's practical usefulness in water wave physics;
  - the entropy results are of statistics and they provide no analytical clues concerning the usefulness of a basis — the property of the constant phase filtering gives rise to the best performance concerning water wave simulations;
  - an indication of the level of regularity of the shapes of water waves.

- The counterpart in the continuous domain to the best discrete wavelet:
  - the Morlet wavelet and the carrier frequency;
  - the manipulation of wavelet redundancy or non-orthogonality for the purpose of minimizing uncertainty or ambiguity of wave analysis;
  - the additional and specific advantages associated with the continuous domain that lead to the usefulness in practical applications;
  - the relevances among the redundancy, orthogonality, and phase distribution;
  - the implications of the wavelet properties of "complete oscillation" and "total positivity";
  - the limited practicality of instituting multi-voice or multi-wavelet algorithms [12];
  - the savvying of flexible constructions of wavelets time-frequency windows.

- The further optimization for water wave physics:
  - the decaying properties of water waves of different scales and the adaptation of wavelet time-frequency window;

  - the constant decay parameter of the continuous wavelet — unrealistic description, as well as an over-estimation of decay for longer waves and an under-estimation for shorter waves;
  - scales verse frequencies — mathematics versus physics — the importance of the association of a wavelet and a carrier frequency parameter;
  - the adaptation of wavelet time-frequency window and the carrier frequency;
  - an intuitively proposed complementary error function and the modeling of wave decay phenomenon;
  - better ridge extractions for all scale range — numerical simulation using chirp signals and real data from laboratory wave tank;
  - a more suitable approach for discerning micro phenomena, such as possibly feeble features evolving under multi-agent interactions.

- The comparisons of the wavelet coherences and the Fourier spectral coherences
  - when compared to the Fourier coherence formulation, from mathematics to statistics, the wavelet coherence formulation is a natural extension with less artificial intervention;
  - the poor performance of spectral coherences is reflected by the rapid variation of the coherent curves as well as the extremely slow improvement when the data lengths are increased;
  - the wavelet coherent curves are consistently far superior to the Fourier coherent ones.

- The symptoms related to the Fourier coherence can be attributed to:
  - the unsatisfactory deconvolution mechanism of a blackbox operation;
  - the serious phase noise and ambiguity effects;
  - the uncertainties associated with Fourier numerics;

  - the rapid diminishing of autocorrelation functions;
  - critical variations due to slight changes of signal – a symptom that is associated with an orthonormal bases.

- The superior performance of wavelet coherences can be attributed to:
  - the basis functions being associated with the minimum entropy basis;
  - the set of continuous transform coefficients being extremely redundant;
  - with intimate analytical origin;
  - less interventions and fewer side effects in numerics;
  - with respect to their shapes of wave form, almost all the discrete basis functions, except those of the best basis here, are too odd to serve the practical simulation of water waves;
  - the physical significance of the present adaptation of time-frequency windows to the mimicking of wave decay or evolution;
  - probably, the most fundamental, as well as the most primal, factor is that component waves are intrinsically modulating in nature .

Lastly, a point to note again: Here we put up an optimal, as well as the ultimate, wavelet basis that is both mathematically and physically right for water waves. And the author firmly believes that the best basis identified is the last word in wavelets concerning their applications to water waves. ❖

BIBLIOGRAPHY

[1] Adrian, R.J. *Laser velocimetry*, chapter 5, pages 155–244. Hemisphere Publishing Corporation, New York, NY, USA, 1983.

[2] Akansu, A.N., W.A. Serdijn and I.W. Selesnick. Emerging applications of wavelets: A review. *Physical Communication*, 3:1–18, 2010.

[3] Auscher, P. Wavelet bases for L^2(R) with rational dilation factor. In M. B. Ruskai, G. Beylkin, R. Coifman, I. Daubechies, S. Mallat, Y. Meyer, and L. Raphael, editor, *Wavelets and Their Applications*, pages 439–452. Jones and Bartlett Publishers, Boston, New York, USA, 1992.

[4] Battle, G. Cardinal spline interpolation and the block spin construction of wavelets. In C.K. Chui, editor, *Wavelets: A tutorial in Theory and Applications*, pages 73–90. Academic Press, Inc., San Diego, California, USA, 1992.

[5] Bracewell, B. *The Fourier Transform And Its Applications*. McGraw-Hill Book Company, Singapore, second edition, 1986.

[6] Chui, C.K. *An Introduction to Wavelets*. Academic Press, Inc., San Diego, California, USA, 1992.

[7] Chui, C.K. On cardinal spline-wavelets. In M. B. Ruskai, G. Beylkin, R. Coifman, I. Daubechies, S. Mallat, Y. Meyer, and L. Raphael, editor, *Wavelets and Their Applications*, pages 439–452. Jones and Bartlett Publishers, Boston, New York, USA, 1992.

[8] Chui, C.K. *Wavelets: A Tutorial in Theory and Applications*. Academic Press, Inc., San Diego, California, USA, 1992.

[9] Cohen, L. *Time-Frequency Analysis*. Prentice Hall PTR, Englewood Cliffs, New Jersey, USA, 1995.

[10] Coifman, R., Y. Meyer, and M.V. Wickerhauser. Size properties of wavelet packets. In M. B. Ruskai, G. Beylkin, R. Coifman, I. Daubechies, S. Mallat, Y. Meyer, and L. Raphael, editor, *Wavelets and Their Applications*, pages 453–470. Jones and Bartlett Publishers, Boston, New York, USA, 1992.

[11] Coifman, R., Y. Meyer, and M.V. Wickerhauser. Wavelet analysis and signal processing. In M. B. Ruskai, G. Beylkin, R. Coifman, I. Daubechies, S. Mallat, Y. Meyer, and L. Raphael, editor, *Wavelets and Their Applications*, pages 153–178. Jones and Bartlett Publishers, Boston, New York, USA, 1992.

[12] Daubechies, I. *Ten Lectures on Wavelets*. SIAM, Philadelphia, USA, 1992.

[13] Froment, J., and S. Mallat. Second generation compact image coding with wavelets. In C.K. Chui, editor, *Wavelets: A tutorial in Theory and Applications*, pages 655–678. Academic Press, Inc., San Diego, California, USA, 1992.

[14] Greenberg, M.D. *Advanced Engineering Mathematics*. Prentice Hall PTR, Englewood Cliffs, New Jersey, USA, 1988.

[15] Lamb, H. *Hydrodynamics*. Cambridge University Press, Cambridge, England, sixth edition, 1932.

[16] Lee, Y.R. *Interaction Scales in a Wind, Wave, and Rain Coupling System*. Ph.D. Dissertation, University of Delaware, Newark, Delaware, Nov. 1999.

[17] Lee, Y.R. Signal Analysis from Wave Modulation Perspective. Technical report, No.2001–09, Institute of Harbor and Marine Technology, Taichung, Taiwan, 2001.

[18] Lee, Y.R. Time-Frequency Analyses and Their Applications — Wavelet Programming in **Asyst**. Technical report, No.95-H2DA003, Institute of Harbor and Marine Technology, Taichung, Taiwan, 2006.

[19] Lee, Y.R., and J. Wu. Time-frequency features and side band instability. In *Proc. 19th Conf. On Ocean Engineering in Taiwan*, pages 32–39, 1997.

[20] Lee, Y.R., and J. Wu. Wavelet coherences based on an optimum analyzing function basis. In *Proc. 20th Conf. On Ocean Engineering in Taiwan*, pages 109–116, 1998.

[21] Lee, Y.R., and J. Wu. A quasi-wavelet function bases for improved time-frequency characterizations. *Proc. 21th Conf. on Ocean Engineering in Taiwan*, pages 101–108, 1999.

[22] Lee, Y.R., and J. Wu. Fourier perspectives of rain's effects on surface waves. *Proc. 22th Conf. on Ocean Engineering in Taiwan*, pages 59–66, 2000.

[23] Lee, Y.R., and J. Wu. Wave characterizations based on Gabor's analytic signal procedure. *Proc. 23th Conf. on Ocean Engineering in Taiwan*, pages 208–215, 2001.

[24] Liu, P. Wavelet spectrum analysis and ocean wind waves. In E.F. Georgiou, editor, *Wavelets in Geophysics*, pages 151–166. Academic Press, Inc., San Diego, California, USA, 1994.

[25] Mallat, S. Multiresolution approximation and wavelets. *Trans. Amer. Math. Soc.*, 315:69–88, 1989.

[26] Mallat, S. *A Wavelet Tour of Signal Processing*. Academic Press, Inc., San Diego, California, USA, second edition, 1999.

[27] Mallat, S., and S. Zhong. Wavelet transform maxima and multiscale edges. In M. B. Ruskai, G. Beylkin, R. Coifman, I. Daubechies, S. Mallat, Y. Meyer, and L. Raphael, editor, *Wavelets and Their Applications*, pages 67–104. Jones and Bartlett Publishers, Boston, New York, USA, 1992.

[28] Massopust, P.R. *Fractal Functions, Fractal Surfaces, and Wavelets*. Academic Press, Inc., San Diego, California, USA, 1994.

[29] Meyer, Y. *Wavelets and operators*. Cambridge University Press, New York, USA, 1992.

[30] Phillips, O.M. *The Dynamics of the Upper Ocean*. Cambridge University Press, New York, USA, second edition, 1977.

[31] Press, W.H., S.A. Teukolsky, W.T. Vetterling, and B.P. Flennery. *Numerical Recipes in Fortran*. Cambridge University Press, New York, USA, second edition, 1992.

[32] Tennekes, H., and J.L. Lumley. *A First Course in Turbulence*. The MIT Press, Cambridge, Massachusetts, USA, 1972.

[33] Wickerhauser, M.V. Acoustic signal compression with wavelet packets. In C.K. Chui, editor, *Wavelets: A tutorial in Theory and Applications*, pages 679–700. Academic Press, Inc., San Diego, California, USA, 1992.

[34] Wickerhauser, M.V. Comparison of picture compression methods: wavelet, wavelet packet, and local cosine. In C.K. Chui, editor, *Wavelets: Theory, Algorithms, and*

Applications, pages 585–621. Academic Press, Inc., San Diego, California, USA, 1994.

[35] Zhang, X. Wavenumber spectrum of very short wind waves: An application of two dimensional Slepian windows to spectral estimation. *J. of Atmospheric and Oceanic Technology*, 11:489–505, 1994.

Appendix： Slide Sample

The Best Wavelet for Water Waves and Its Optimization — Wavelet Coherences versus Fourier Coherences

A basic research of IHMT (2019)

李勇榮

交通部運輸研究所
港灣技術研究中心
email: ronlee@ms4.hinet.net

Three main parts, Six theses, One backbone

The Best Wavelet, The Optimization, The Coherences

1. Comprehensive wavelet categories and characterizations ➲
2. The best discrete basis, inclusive entropy criteria, probability density distribution ➲
3. The phase distribution of wavelet characteristic function ➲
4. The counterpart best continuous wavelet ➲
5. The optimization for physics ➲
6. Wavelet coherences against Fourier coherences ➲

Backbone — The writing of codes, The workbench

Tested wavelet bases

- Orthonormal ➲
  - ∗ Daubechies most compactly supported wavelets (ONxxA) ➲
  - ∗ Daubechies least asymmetric wavelets (ONxxS) ➲
  - ∗ Coiflets (ONxxC) ➲
  - ∗ Meyer wavelet (Meyer) ➲
  - ∗ Battle and Lemarié wavelet (B&L) ➲
- Semi-orthogonal ➲
- Bi-orthogonal ➲
- Wavelet packet ➲
- Wavelet packet best basis ➲
- Wavelet packet best level ➲
- Fourier basis included ➲

13/113

回舊 回新 ◀◀ ▶▶ ◀ ▶ ❐ 再見

Conclusions

The last word in the best wavelet
. . . . . concerning water wave applications

- Discrete domain:
  The dual semi-orthogonal cardinal spline wavelet
- Continuous domain:
  The Morlet wavelet
- The adaptation for better modeling of water wave physics:
  Energy dissipation due to irrotational straining
- The absolute superiority of wavelet approach on coherences:
  Based on the best wavelet for water waves

106/113

回舊 回新 ◀◀ ▶▶ ◀ ▶ ❐ 再見